Lappeenranta-Lahti University of Technology LUT
LUT School of Energy Systems
Electrical Engineering
Master's Thesis
2021

Mikko Hämäläinen

MODELLING DIRECT TORQUE CONTROLLED INDUCTION MACHINE IN SIMULINK

Examiners: Professor Juha Pyrhönen
D.Sc. Lassi Aarniovuori
Supervisor: D.Sc. Lassi Aarniovuori
D.Sc. Markku Niemelä

Abstract

Mikko Hämäläinen
Modelling Direct Torque Controlled induction machine in Simulink
Master's Thesis 2021
Lappeenranta-Lahti University of Technology LUT
LUT School of Energy Systems
Electrical Engineering
Lappeenranta
61 pages, 35 Figures, 3 Tables

Examiners: Professor Juha Pyrhönen
D.Sc. Lassi Aarniovuori
Supervisor: D.Sc. Lassi Aarniovuori
D.Sc. Markku Niemelä

Keywords: Simulink, Matlab, DTC

In this thesis Direct Torque Control (DTC) of induction machine was studied to an extent that allowed building a DTC model with the Matlab® Simulink® software. The aim of the thesis was to create a DTC model that could be used in the education of the electrical drives.

In the Simulink Simscape™ Electrical™ library there are already blocks for the DTC and the induction machine. The purpose of this thesis, however, was to create corresponding models using just the basic Simulink blocks. This allows to understand better what happens withing the DTC.

With the model created the effect of different hysteresis band widths, different sampling periods, different motor conditions and different inductances were simulated. Increasing the hysteresis band widths and sampling period lead to lower average switching frequencies, which increases the harmonic content of the motor phase currents. Although lower switching frequency lowers the switching losses the motor losses increase as a result of increased harmonics. In addition, it was noticed that different motor load conditions have a big impact on the switching frequency.

Values of stator and rotor leakage inductances and the magnetizing inductance also had an impact on the switching frequency. Higher leakage inductances lowered the switching frequency. Phase currents also changed depending on the inductances. With lower leakage inductances the starting currents rised considerably. Steady-state currents got lower as the magnetizing inductance rose.

Tiivistelmä

Mikko Hämäläinen
Suoravääntösäädetyn induktiokoneen mallintaminen Simulinkillä
Diplomityö 2021
Lappeenrannan-Lahden teknillinen yliopisto LUT
LUT School of Energy Systems
Sähkötekniikka
Lappeenranta
61 sivua, 35 kuvaa, 3 taulukkoa

Työn tarkastajat:	Professori Juha Pyrhönen
	TkT Lassi Aarniovuori
Työn ohjaaja:	TkT Lassi Aarniovuori
	TkT Markku Niemelä

Avainsanat: Simulink, Matlab, DTC

Työssä tutkittiin, kuinka induktiokoneen suora vääntömomentin säätö (Direct Torque Control, DTC) toimii, sekä rakennettiin induktiokoneen ja DTC-säätimen simulointimallit Matlab® Simulink® ohjelmistolla. Tavoitteena oli, että suorasta vääntömomentin säädöstä ja sen simuloinnista saataisiin yhtenäinen kokonaisuus, jota voitaisiin käyttää apuna sähkökäyttöjen opetuksessa.

Induktiokoneelle ja DTC-säätimelle löytyy valmiit lohkot Simulinkin Simscape™ Electrical™ kirjastosta. Tässä työssä tehdyillä malleilla kuitenkin oli ehtona, että ne piti luoda ilman erillisiä Simulink kirjastoja. Tällä tavoin tehdyt mallit pystyttäisiin mitä todennäköisimmin luomaan vielä tulevaisuudenkin Simulink® versioiden kanssa. Lisäksi pienempinä paloina DTC-säädön toimintaperiaate on paremmin omaksuttavissa.

Tehtyjen Simulink mallien avulla havainnoitiin, miten hystereesirajojen tai näytteenottojakson muutokset sekä oikosulkumoottorin erilaiset kuormitustilanteet vaikuttavat suoran vääntömomentinsäädön kytkentätaajuuden keskiarvoon ja virran harmoniseen sisältöön.

Huomattiin, että kytkentätaajuuden keskiarvo laskee isommilla näytteenottojaksoilla ja hystereesirajoilla, sekä pienellä moottorin kuormituksella. Kytkentätaajuudeen laskiessa invertterin kytkentähäviöt pienenevät, mutta moottorille syötettävän virran harmoninen sisältö kasvaa, jolloin moottorin häviöt kasvavat.

Moottorin induktansseilla oli myös huomattava vaikutus invertterin kytkentätaajuuksiin, sekä moottorin ottovirtoihin. Hajainduktanssien kasvaessa kytkentätaajuus pieneni. Käynnistysvirroissa huomattiin sama ilmiö. Ilman kuormaa ja kuormitettuna jatkuvuustilan virrat laskivat magnetointi-induktanssin kasvaessa.

Preface

This thesis was done in Lappeenranta-Lahti University of Technology during 2020 and 2021.

I would like to thank D.Sc. Lassi Aarniovuori for the assistance throughout the process and the interesting topic that gave my little grey cells a good exercise. Also I would like to thank my examiner Professor Juha Pyrhönen and supervisor D.Sc. Markku Niemelä for their invaluable counsel.

In addition, I would like to express my gratitude to my family and friends for their support throughout the years and especially to Emilia for her immense support. Furthermore, a big thanks to all the friends I made during the years in the LUT for the unforgettable memories.

Mikko Hämäläinen
January 30, 2021
Lappeenranta

Contents

Nomenclature

Latin alphabet

A	State space model help variable
$\boldsymbol{a}$	Phase operator
B	State space model help variable
C	State space model help variable
D	State space model help variable
E	State space model help variable
F	State space model help variable
f	Frequency
f_{sw}	Switching frequency
G	State space model help variable
I	Current
$\boldsymbol{i}_{\mathrm{r}}$	Rotor current vector
$i_{\mathrm{r}\alpha}$	Rotor current vector α-component
$i_{\mathrm{r}\beta}$	Rotor current vector β-component
$\boldsymbol{i}_{\mathrm{s}}$	Stator current vector
$i_{\mathrm{s}\alpha}$	Stator current vector α-component
$i_{\mathrm{s}\beta}$	Stator current vector β-component
J	Inertia
L	Inductance
L_{m}	Magnetizing inductance
L_{r}	Rotor inductance
$L_{\mathrm{r}\sigma}$	Rotor leakage inductance
L_{s}	Stator inductance
$L_{\mathrm{s}\sigma}$	Stator leakage inductance
N_{w}	Number of switching events
n	Speed
n_{s}	Synchronous speed
n_{ref}	Speed reference
P	Power
P_{out}	Output power
p	Pole pairs
R	Resistance
R_{Fe}	Iron loss resistance
R_{r}	Rotor resistance
R_{s}	Stator resistance
S	Apparent power
$S_{\mathrm{U,V,W}}$	Phase U, V or W switch position
s	Slip
T	Temperature, Torque
T_{b}	Breakdown torque

T_e	Electromagnetic torque
$\boldsymbol{T}_\mathrm{e}$	Electromagnetic torque vector
T_err	Torque error
$T_\mathrm{e,est}$	Electromagnetic torque estimate
$T_\mathrm{e,ref}$	Electromagnetic torque reference
T_load	Load torque
T_n	Rated torque
t	Time
U	Voltage
U_DC	DC voltage
$U_\mathrm{U,V,W}$	Phase U, V or W voltage
$\boldsymbol{u}$	Voltage vector
$u_\mathrm{r\alpha}$	Rotor voltage vector α-component
$u_\mathrm{r\beta}$	Rotor voltage vector β-component
$\boldsymbol{u}_\mathrm{s}$	Stator voltage vector
$u_\mathrm{s\alpha}$	Stator voltage vector α-component
$u_\mathrm{s\beta}$	Stator voltage vector β-component
x	Variable, axis
y	Axis
Z	Impedance

Greek alphabet

α	α-axis, temperature coefficient
β	β-axis
Δ	Difference
ΔT	Torque hysteresis limit
Δt	Time frame
$\Delta\psi$	Stator flux linkage hysteresis limit
θ	Angle
κ	Sector
σ	Leakage
τ	Torque control signal
ϕ	Stator flux linkage control signal
ψ	Flux linkage
ψ_err	Stator flux linkage error
$\psi_\mathrm{r\alpha}$	Rotor flux linkage vector α-component
$\psi_\mathrm{r\beta}$	Rotor flux linkage vector β-component
$\psi_\mathrm{s\alpha}$	Stator flux linkage vector α-component
$\psi_\mathrm{s\beta}$	Stator flux linkage vector β-component
ψ_s	Absolute value of the stator flux linkage
$\psi_\mathrm{s,n}$	Nominal value of the stator flux linkage
$\psi_\mathrm{s,est}$	Absolute value of the stator flux linkage estimate vector
$\boldsymbol{\psi}_\mathrm{s,est}$	Stator flux linkage estimate vector
$\psi_\mathrm{s,ref}$	Stator flux linkage reference

ω	Angular velocity
ω_s	Stator electrical angular velocity
ω_r	Rotor electrical angular velocity
Ω_m	Mechanical angular velocity

Subscripts

base	Per-unit base value
d	Direct axis
e	Elecromagnetic
est	Estimate
m	Mechanical, Magnetizing
max	Maximum
n	Nominal, Rated
out	Output
p	Phase
q	Quadrature axis
r	Rotor
ref	Reference
s	Stator, Synchronous
U	Phase U
V	Phase V
W	Phase W

Abbreviations

AC	Alternating Current
DC	Direct Current
DFLC	Direct Flux Linkage Control
DTC	Direct Torque Control
EMF	Electromotive Force
FFT	Fast-Fourier Transform
FOC	Field Oriented Control
IM	Induction Machine
MMF	Magnetomotive Force
PWM	Pulse-Width Modulation
RMS	Root Mean Square
THD	Total Harmonic Distortion
VFD	Variable Frequency Drive
VSI	Voltage Source Inverter

1 Introduction

Rotating electrical machines are used everywhere. Their applications can range from turning a pump in industrial setting to turning the wheels of an electrical vehicle. Different Variable Frequency Drives (VFD) have become a viable way to implement a more sophisticated control for different applications and improve the efficiency of drives. There are two different schools of controlling electrical machines: scalar control or vector control.

Scalar control or commonly known as *U/f* control is quite a basic machine control topology. It is based on changing the motor's input voltage and frequency in a linear fashion which leads to a change in the machine's speed. *U/f* control is simple and easy to implement and works well with somewhat static loads like pumps and fans but it has its drawbacks. It is known that induction machine's speed is a function of the slip. When the load torque changes so does the machine's speed. Therefore, without proper sensors and feedback an *U/f* driven motor might have issues working in highly dynamic drives.

Vector control allows a more precise control of machine. Vector control is based on constantly calculating the machine's inner state with the help of the space vectors which allows a more straightforward presentation of the machine during the transients. The main problem with the traditional field oriented control (FOC) is that it needs angle measurement from the motor shaft which increases implementation costs. Sensorless FOC removes the need of a speed measurement as the rotor angle is numerically estimated.

Direct torque control (DTC) can solve the problems regarding rotor angle and the need of speed measurements as it is based solely on the stator reference frame space vectors. Motor phase currents and voltages are the only necessary measurements for the control of the machine. DTC is a further development of the Direct Flux Linkage Control (DFLC).

Although the Simulink itself has a library which has a ready-made DTC block it might not be easiest to use from the education standpoint. Creating a DTC model with basic blocks allows breaking the control system into smaller pieces which might allow understanding the working principles a bit better. There are publications where DTC has been realized in Simulink, so the created model is not the first of its kind (Alnasir and Almarhoon, 2012).

1.1 Research methods

Research methods used in this thesis mostly consists of relying on a different literature sources. The following research questions were used to create this thesis.

- How does DTC work?
- How to create Simulink model for DTC?
- How to create Simulink model for an IM?
- What kind of effects hysteresis band widths have?

- What kind of effects does different DTC sampling periods have?
- How do values of the inductances affect the DTC controlled machine?

2 Theory

Direct Torque Control is a type of vector control and the basics of the vector control lies in the space vector theory and different reference frame transformations. Vector presentation allows simplified calculations of the machine's inner state which in turn enables feedback to be use in control. In practice, vector control is realised with variable frequency drives. In this section the theory behind the space vectors, different vector transformations, induction machines, voltage source inverter (VSI) and DTC itself are studied.

2.1 Space vector theory

In a three-phase system representing machine dynamics with conventional means can become quite abstruse and complicated. The space vector theory was developed in 1950s by Kovácks and Rácz to represent three phase quantities in a more straightforward form (Károly Pál Kovács, 1954). Usually following basic assumptions are made when using the space vector theory (Park, 1929).

- Air gap flux density distribution is sinusoidal.
- Magnetizing circuit saturation is constant.
- Resistances R and inductances L are constant.
- There are no iron losses.
- Electric machine is treated as two-pole machine.

In reality, the air gap flux density is seldom sinusoidal. However, with the vector control exact waveform of the air gap flux density does not need to be known and only assumption that it is sinusoidal is good enough.

It is known that the inductance changes when the magnetizing circuit gets closer to the saturation. With the assumption of the constant magnetizing circuit saturation the inductances are considered as constants and updated with known values in known operating points. Magnetizing inductance changes also as a function of torque as the magnetomotive force (MMF) calculation needs to be done along longer flux lines than at no load.

In electrical machines, the winding resistance is a function of temperature.

$$R = R_{\mathrm{n}}(1 + \alpha(T - T_{\mathrm{n}})) \tag{2.1}$$

where R is the winding resistance at the temperature of T, R_{n} is the winding resistance at the temperature of T_{n} and α is temperature coefficient of the winding material. Even though the resistance is considered as constant its value should be updated through known operating points. Some drives employ thermal motor models to estimate operating temperature (Tiitinen, 1996).

The skin effect creates a non-uniform current density in the machine winding which results in a change of the winding AC resistance (Juha Pyrhönen, 2008). However the frequency's effect on resistance and inductance can be neglected if absolute accuracy is not required.

Problem with ignoring the iron losses of the machine is that it disallows evaluating the efficiency of the machine. This simplification does not really affect the control of the electrical machine. The assumption that the machine has only one pole pair also do not have impact on the usability of the space vectors. The number pole pairs just needs to be taken into account when working with machine's electrical and mechanical angular velocities and the torque equation.

2.1.1 Three-phase system space vectors

Three-phase system space vectors can be created with the help of the phase operator $\boldsymbol{a}$.

$$\boldsymbol{a} = e^{\mathrm{j}\frac{2\pi}{3}} \tag{2.2}$$

By raising the $\boldsymbol{a}$ into the power of 0,1 and 2 you get three magnetic axes 120° apart from each other. With the help of the phase operator $\boldsymbol{a}$ the general space vector transformation of three-phase quantities $x_{\mathrm{U,V,W}}(t)$ can be done with the following equation.

$$\boldsymbol{x}_{\mathrm{U,V,W}}(t) = \frac{2}{3}(\boldsymbol{a}^0 x_{\mathrm{U}}(t) + \boldsymbol{a}^1 x_{\mathrm{V}}(t) + \boldsymbol{a}^2 x_{\mathrm{W}}(t)) \tag{2.3}$$

This equation applies whether working with voltages, currents or other three-phase quantities. Consider a situation where there are three phase voltages $u_{\mathrm{U}}(t)$, $u_{\mathrm{V}}(t)$ and $u_{\mathrm{W}}(t)$ with amplitudes of 1 and frequency f of 50 Hz.

$$\begin{aligned} u_{\mathrm{U}}(t) &= \sin(2\pi f t) \\ u_{\mathrm{V}}(t) &= \sin(2\pi f t - \frac{2\pi}{3}) \\ u_{\mathrm{W}}(t) &= \sin(2\pi f t + \frac{2\pi}{3}) \end{aligned} \tag{2.4}$$

Voltages $u_{\mathrm{U,V,W}}(t)$ as a functions of time and their space vector counterparts at the moment of observation can be seen in Fig. 2.1.

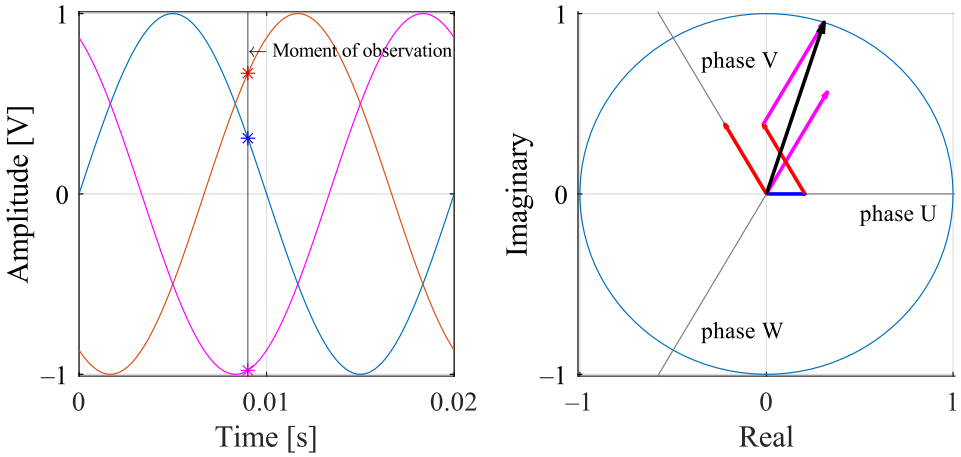

Figure 2.1: Three-phase voltages in time domain and space vector equivalent in the moment of observation. As the voltage vectors $\boldsymbol{u}_{\mathrm{U,V,W}}$ change in respect to time the black vector sum rotates around the origin.

In a three-phase system the different equations would have to be calculated separately for each phase which is undesirable when there are limited resources. Clarke's and Park transformations allow transforming three-phase quantities to a two-phase counterparts. Fewer variables leads to less computational power needed which in turn help to achieve quicker control methods.

2.1.2 Clarke's transformation

Clarke's transformation is used to transform three-phase quantities from stationary three axis reference frame to a stationary two axis reference frame (W.C. Duesterhoeft, 1951). Other name for the stationary two axis reference frame is a stator reference frame. Clarke's transformation is sometimes called as $\alpha\beta\gamma$-transformation. Usually the α-axis is aligned with the three-phase system U-axis and the three-phase components are balanced which leads to γ-component being a zero. Then the transformation can be called as $\alpha\beta0$-transformation. In some sources x-axis and y-axis are used instead of α-axis and β-axis (Juha Pyrhönen, 2016).

$\alpha\beta0$-transformation of the three-phase quantities $x_{\mathrm{U,V,W}}(t)$ can be done with the following equations.

$$x_\alpha(t) = \frac{2}{3}x_\mathrm{U}(t) - \frac{1}{3}x_\mathrm{V}(t) - \frac{1}{3}x_\mathrm{W}(t) \tag{2.5}$$

$$x_\beta(t) = \frac{\sqrt{3}}{3}x_\mathrm{V}(t) - \frac{\sqrt{3}}{3}x_\mathrm{W}(t) \tag{2.6}$$

$\alpha\beta0$-transformation of voltages shown in Eq. (2.4) is shown in Fig. 2.2.

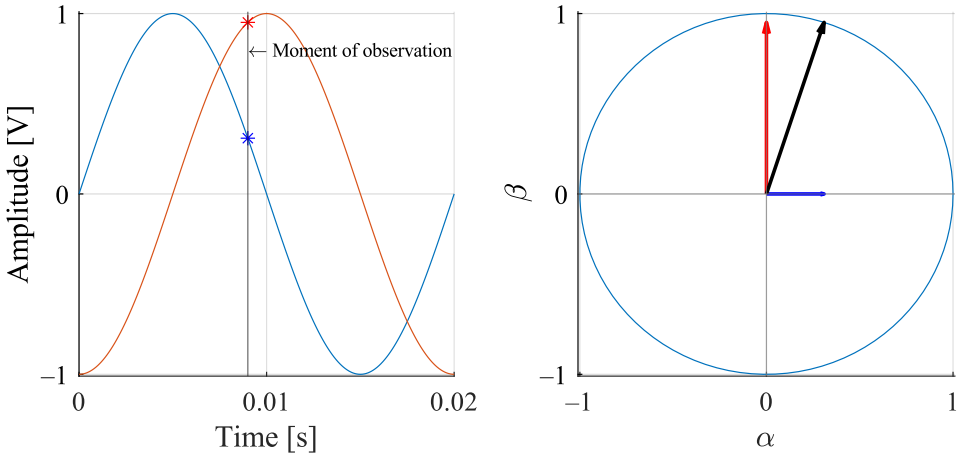

Figure 2.2: Voltage vectors in stationary reference frame. The moment of observation is same as with the three-phase space vectors.

Inverse Clarke transformation can be used to transform two-phase quantities from the stationary reference frame back to the three-phase system. Equations are as follows.

$$x_{\mathrm{U}}(t) = x_{\alpha}(t) \tag{2.7}$$

$$x_{\mathrm{V}}(t) = -\frac{1}{2}x_{\alpha}(t) + \frac{\sqrt{3}}{2}x_{\beta}(t) \tag{2.8}$$

$$x_{\mathrm{W}}(t) = -\frac{1}{2}x_{\alpha}(t) - \frac{\sqrt{3}}{2}x_{\beta}(t) \tag{2.9}$$

2.1.3 Park's transformation

Originally Park's transformation was created to transform three-phase stationary reference frame quantities to a rotating dq-reference frame and it was first introduced by R.H. Park in the 1920's (Park, 1929). Generally Park's transformation can be used with any arbitrary rotational speed but in the case with electric motors two quite common ones are synchronously rotating reference frame and rotor reference frame. With the synchronous rotating reference frame d-axis and q-axis rotates around the origin at the synchronous speed n_{s} and with the rotor reference frame at the mechanical angular velocity ω_{m}. Unlike the field oriented control, the DTC does not require a rotating reference frame for the motor control.

Park's transformation from the $\alpha\beta$-reference frame to dq-reference frame with generic variables can be done with the following equations.

$$x_{\mathrm{d}}(t) = \cos(\theta)x_{\alpha}(t) + \sin(\theta)x_{\beta}(t) \tag{2.10}$$

$$x_{\mathrm{q}}(t) = -\sin(\theta)x_{\alpha}(t) + \cos(\theta)x_{\beta}(t) \tag{2.11}$$

θ is the angle between the d-axis and α-axis at the time instant t.

Inverse park transformation can be used to transform two-phase quantities from the rotating reference frame back to the stationary two-phase reference frame.

$$x_\alpha(t) = \cos(\theta)x_\mathrm{d}(t) - \sin(\theta)x_\mathrm{q}(t) \tag{2.12}$$

$$x_\beta(t) = \sin(\theta)x_\mathrm{d}(t) + \cos(\theta)x_\mathrm{q}(t) \tag{2.13}$$

2.2 Induction machine

Induction machine (IM) is quite a common sight in the industry. Their robust nature and overall simplicity have made them a really desirable choice. Working principles of induction machine lies in the Faraday's law and Lorentz's law. Electric currents rushing through the stator windings creates rotating magnetic field which then 'cut' through the short-circuited squirrel cage embedded in the rotor. Electromotive force (EMF) is then induced in the rotor bars. According to Lenz's law induced EMF creates a current to the rotor bars that opposes the stator's changing magnetic flux. The rotor currents react with the common air gap flux and creates forces according the Lorentz force which results in torque. In a steady-state, induction machine is always rotating a bit slower than the synchronous speed n_s in motoring mode. At synchronous speed there would be no changing magnetic flux affecting the rotor bars and therefore there would be no electromotive force generated which is why the induction machines are often called an asynchronous machines. Common form for induction machines speed is as follows.

$$n = (1 - s)n_\mathrm{s} \tag{2.14}$$

where n is rotor speed, s is the slip and n_s synchronous speed. Induction motor speed goes hand in hand with the value of the slip. As the value of the slip increases the rotor speed drops down. In general, the purpose of an electrical machine is to produce torque. Typical curve for an electromagnetic torque as a function of a slip is shown in Fig. 2.3.

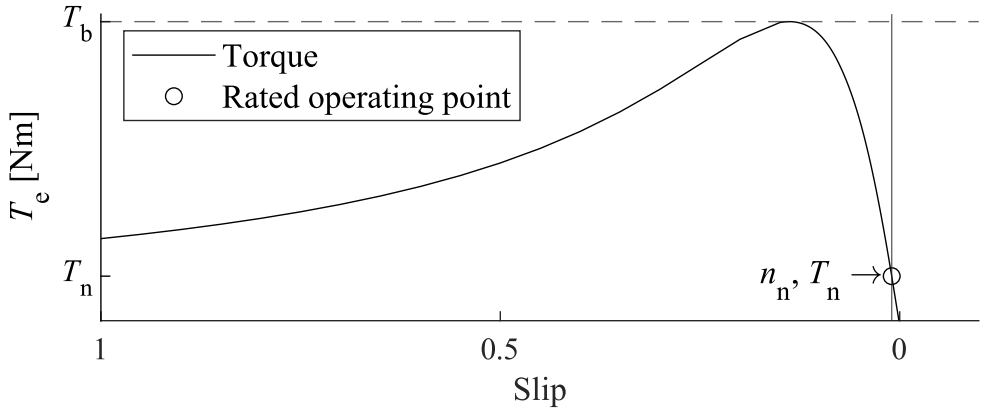

Figure 2.3: Induction machine's torque as a function of a slip.

In the figure it can be seen that the torque generated by an induction machine depends on the slip value. The value of the slip increases when more load is introduced to the motor. If the load torque rises above the breakdown torque T_b motor stall is inevitable. The rated point of an induction motor is usually achieved with quite small slip values.

2.2.1 Single-phase phasor T-equivalent circuit

Often the electrical machines are expressed with equivalent circuits since they allow quite straightforward presentation of the machine. Single-phase phasor equivalent circuit is a powerful utility when working with an electrical machine in a steady-state. During the transients the single-phase phasor equivalent circuit does not work. Induction motor single-phase phasor equivalent circuit is shown in Fig. 2.4.

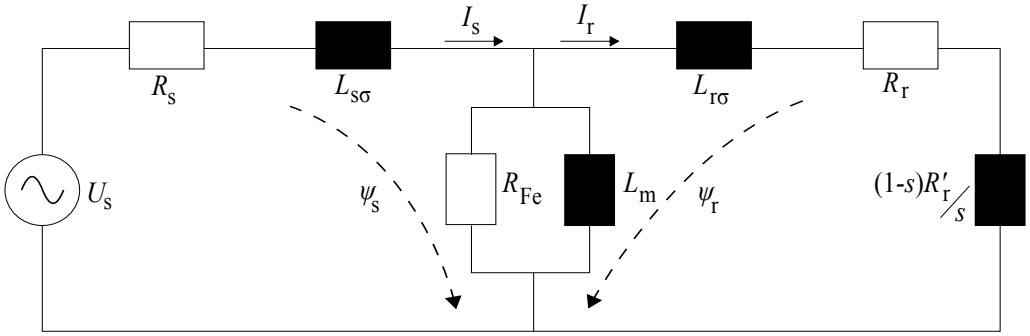

Figure 2.4: Induction machine single-phase phasor T-equivalent circuit, where rotor components are referred to the stator.

Equivalent circuit of an induction machine contains stator and rotor leakage inductances $L_{\mathrm{s}\sigma,\mathrm{r}\sigma}$ and phase resistances $R_{\mathrm{s,r}}$, voltage source, magnetizing inductance L_m and iron loss resistance R_Fe. Usually different equivalent circuit parameters are given by the motor's manufacturer. If this is not possible parameters can be extracted with a no-load test and short-circuit test. These however, does not represent equivalent circuit parameters accurately in the rated point.

2.2.2 Equivalent circuit in stator reference frame

Since the single-phase phasor equivalent circuits only work in the steady-state the dynamic modeling of an induction motor is often done with space vector equivalent circuit in a stator reference frame. The space vector equivalent circuit is also a single-phase circuit but it now contains space vector quantities. These space vectors can be described with their components. In this two-phase presentation induction machine equivalent circuit is broken down to α- and β-components. Two-phase space vector equivalent circuits can be seen in Fig. 2.5.

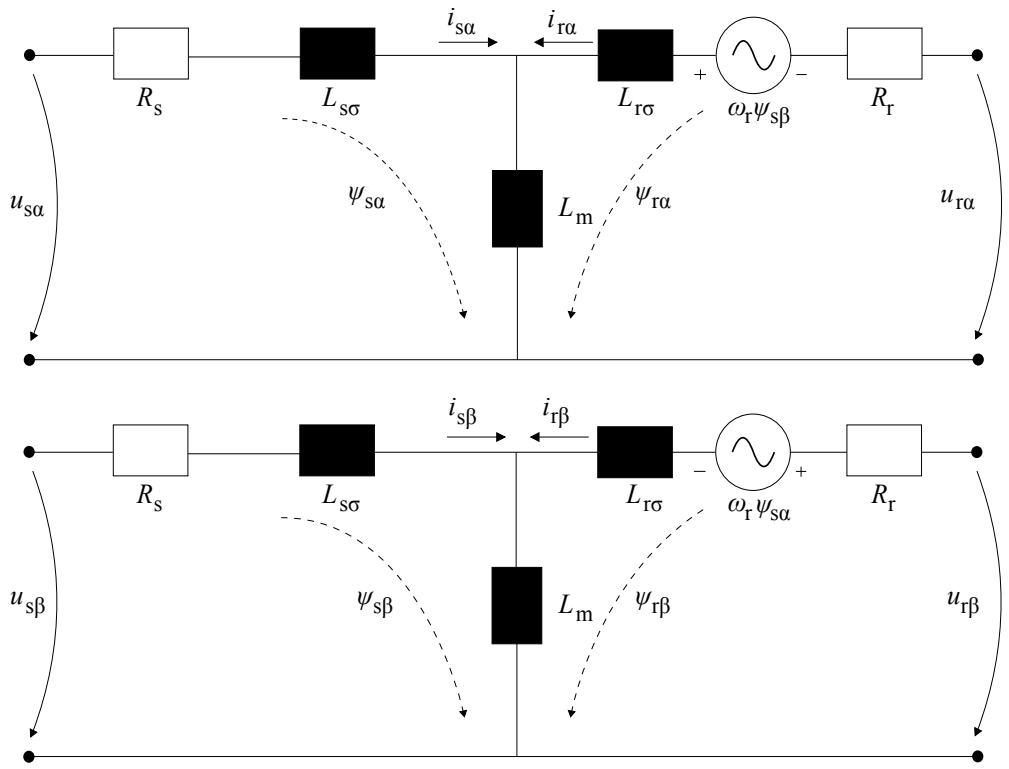

Figure 2.5: Induction machine space vector T-equivalent circuits in stator reference frame. Iron loss resistance R_{Fe} is neglected.

Stator and rotor inductances can be represented with the magnetizing inductance L_{m} and stator and rotor leakage inductances.

$$L_{\mathrm{s}} = L_{\mathrm{s}\sigma} + L_{\mathrm{m}} \tag{2.15}$$

$$L_{\mathrm{r}} = L_{\mathrm{r}\sigma} + L_{\mathrm{m}} \tag{2.16}$$

Stator side voltage equations based on the equivalent circuits in Fig. 2.5 are following.

$$u_{\mathrm{s}\alpha} = R_{\mathrm{s}} i_{\mathrm{s}\alpha} + \frac{\mathrm{d}}{\mathrm{d}t}\psi_{\mathrm{s}\alpha} \tag{2.17}$$

$$u_{\mathrm{s}\beta} = R_{\mathrm{s}} i_{\mathrm{s}\beta} + \frac{\mathrm{d}}{\mathrm{d}t}\psi_{\mathrm{s}\beta} \tag{2.18}$$

Stator side flux linkage equations are following.

$$\psi_{\mathrm{s}\alpha} = i_{\mathrm{s}\alpha} L_s + i_{\mathrm{r}\alpha} L_{\mathrm{m}} \tag{2.19}$$

$$\psi_{\mathrm{s}\beta} = i_{\mathrm{s}\beta} L_s + i_{\mathrm{r}\beta} L_{\mathrm{m}} \tag{2.20}$$

In a similar fashion the rotor side voltage and rotor flux equations can be derived.

$$u_{\mathrm{r}\alpha} = R_{\mathrm{r}} i_{\mathrm{r}\alpha} + \frac{\mathrm{d}}{\mathrm{d}t}\psi_{\mathrm{r}\alpha} - \omega_{\mathrm{r}}\psi_{\mathrm{r}\beta} \tag{2.21}$$

$$u_{\mathrm{r}\beta} = R_{\mathrm{r}} i_{\mathrm{r}\beta} + \frac{\mathrm{d}}{\mathrm{d}t}\psi_{\mathrm{r}\beta} + \omega_{\mathrm{r}}\psi_{\mathrm{r}\alpha} \tag{2.22}$$

$$\psi_{\mathrm{r}\alpha} = i_{\mathrm{r}\alpha} L_{\mathrm{r}} + i_{\mathrm{s}\alpha} L_{\mathrm{m}} \tag{2.23}$$

$$\psi_{\mathrm{r}\beta} = i_{\mathrm{r}\beta} L_r + i_{\mathrm{s}\beta} L_{\mathrm{m}} \tag{2.24}$$

2.2.3 State space model

Simulating the induction machine can be done in a different ways. There are literature about the dynamic modelling of an induction machine (Bose, 2001) (Ong, 1998). The induction machine model used in this thesis is based on the models used by Tarkiainen in his thesis (Tarkiainen, 1999) and by Aarniovuori in his paper regarding FOC vector control (Lassi Aarniovuori, 2018). To realise the induction machine model Tarkiainen and Aarnivuori used the induction machine state space model in stationary $\alpha\beta$-reference frame, which is derived from the equations (2.15) - (2.24).

$$\begin{bmatrix} \frac{\mathrm{d}}{\mathrm{d}t}\psi_{\mathrm{s}\alpha} \\ \frac{\mathrm{d}}{\mathrm{d}t}\psi_{\mathrm{s}\beta} \\ \frac{\mathrm{d}}{\mathrm{d}t}\psi_{\mathrm{r}\alpha} \\ \frac{\mathrm{d}}{\mathrm{d}t}\psi_{\mathrm{r}\beta} \end{bmatrix} = \begin{bmatrix} -A & 0 & C & 0 \\ 0 & -A & 0 & C \\ D & 0 & -B & -\omega_{\mathrm{r}} \\ 0 & D & \omega_{\mathrm{r}} & -B \end{bmatrix} \begin{bmatrix} \psi_{\mathrm{s}\alpha} \\ \psi_{\mathrm{s}\beta} \\ \psi_{\mathrm{r}\alpha} \\ \psi_{\mathrm{r}\beta} \end{bmatrix} + \begin{bmatrix} 1 & 0 \\ 0 & 1 \\ 0 & 0 \\ 0 & 0 \end{bmatrix} \begin{bmatrix} u_\alpha \\ u_\beta \end{bmatrix}$$

where A, B, C and D are parameters containing the stator and rotor resistances $R_{\mathrm{s,r}}$ and stator, rotor and magnetizing inductances $L_{\mathrm{s,r,m}}$. Parameters E, F and G are used in solving the stator and rotor current equations $i_{\mathrm{s}\alpha,\mathrm{s}\beta}$ and $i_{\mathrm{r}\alpha,\mathrm{r}\beta}$.

$$A = \frac{R_{\mathrm{s}} L_{\mathrm{r}}}{L_{\mathrm{s}} L_{\mathrm{r}} - L_{\mathrm{m}}^2} \qquad B = \frac{R_{\mathrm{r}} L_{\mathrm{s}}}{L_{\mathrm{s}} L_{\mathrm{r}} - L_{\mathrm{m}}^2} \qquad C = \frac{R_{\mathrm{s}} L_{\mathrm{m}}}{L_{\mathrm{s}} L_{\mathrm{r}} - L_{\mathrm{m}}^2} \tag{2.25}$$

$$D = \frac{R_{\mathrm{r}} L_{\mathrm{m}}}{L_{\mathrm{s}} L_{\mathrm{r}} - L_{\mathrm{m}}^2} \qquad E = \frac{L_{\mathrm{r}}}{L_{\mathrm{s}} L_{\mathrm{r}} - L_{\mathrm{m}}^2} \qquad F = \frac{L_{\mathrm{m}}}{L_{\mathrm{s}} L_{\mathrm{r}} - L_{\mathrm{m}}^2} \tag{2.26}$$

$$G = \frac{L_{\mathrm{s}}}{L_{\mathrm{s}} L_{\mathrm{r}} - L_{\mathrm{m}}^2} \tag{2.27}$$

Solving the state space model matrices gives the following equations for the magnetic flux linkage components.

$$\psi_{s\alpha} = \int (u_\alpha - A\psi_{s\alpha} + C\psi_{r\alpha})\mathrm{d}t \tag{2.28}$$

$$\psi_{s\beta} = \int (u_\beta - A\psi_{s\beta} + C\psi_{r\beta})\mathrm{d}t \tag{2.29}$$

$$\psi_{r\alpha} = \int (-B\psi_{r\alpha} + D\psi_{s\alpha} - \omega_r\psi_{r\beta})\mathrm{d}t \tag{2.30}$$

$$\psi_{r\beta} = \int (-B\psi_{r\beta} + D\psi_{s\beta} + \omega_r\psi_{r\alpha})\mathrm{d}t \tag{2.31}$$

Stator and rotor currents can be solved from the following equations.

$$i_{s\alpha} = E\psi_{s\alpha} - F\psi_{r\alpha} \tag{2.32}$$

$$i_{s\beta} = E\psi_{s\beta} - F\psi_{r\beta} \tag{2.33}$$

$$i_{r\alpha} = G\psi_{r\alpha} - F\psi_{s\alpha} \tag{2.34}$$

$$i_{r\beta} = G\psi_{r\beta} - F\psi_{s\beta} \tag{2.35}$$

Generated electromagnetic torque can be calculated with the stator currents $\boldsymbol{i}_{s\alpha,s\beta}$ and the stator magnetic fluxes $\boldsymbol{\psi}_{s\alpha,s\beta}$.

$$T_e = \frac{3}{2}p(\psi_{s\alpha}i_{s\beta} - \psi_{s\beta}i_{s\alpha}) \tag{2.36}$$

2.2.4 IM mechanical model

Rotor electrical angular velocity is required in the rotor flux linkage equations (2.30) and (2.31). It can be solved with a mechanical model which is following.

$$T_e = J\frac{\mathrm{d}}{\mathrm{d}t}\Omega_m + T_{load} \tag{2.37}$$

where T_e is the electromagnetic torque, J is rotor inertia, Ω_m mechanical angular velocity and T_{load} is the load torque. Solving the mechanical angular velocity leads to following equation.

$$\Omega_m = \int \frac{T_e - T_{load}}{J}\mathrm{d}t \tag{2.38}$$

Rotor electrical angular velocity can be solved with the mechanical angular velocity by multiplying mechanical velocity with the number of motor pole pairs.

$$\omega_r = p\Omega_m \tag{2.39}$$

where ω_r is rotor electrical angular velocity and p is the number of motor pole pairs.

2.2.5 Field weakening

When running an induction motor over its rated speed, field weakening must be used. The torque of an induction motor is a function of stator currents and flux linkages as shown in Eq. (2.36). Without adjusting the stator flux linkage, an induction motor output power could be quite easily exceeded, which could lead to problems with the thermal limits of the machine. Output power or shaft power of an electrical machine can be expressed as a function of rotor angular velocity and electromagnetic torque.

$$P_{\text{out}} = T_{\text{e}}\Omega_{\text{m}} \tag{2.40}$$

In other words when increasing the rotor angular velocity Ω_{m} over the rated value the available torque should be decreased.

It is quite simple to adjust the value of the stator flux linkage as it is one of the controlled variables with the DTC. Basic concept of the field weakening is that stator flux linkage is kept constant below the rated frequency and when the field weakening region has been reached the stator flux linkage value is updated either dynamically or with predetermined values.

In reality, with a frequency converter with diode-bridge rectifier the inverter modulator will not be capable of producing the same voltage that is supplied to the diode bridge unless overmodulation is used. In many converters the maximum output is limited to about 90 % of the input voltage and therefore the motor goes to field weakening in practice at 45 Hz in case of a 50 Hz motor. Stator flux linkage can be expressed as a function of input voltage and its frequency.

$$\psi_{\text{s}} = \frac{\sqrt{2}U_{\text{p}}}{2\pi f} \tag{2.41}$$

where the U_{p} is root mean square (RMS) phase voltage.

2.3 Variable Frequency Drive (VFD)

Variable frequency drive is used to transform electrical power to mechanical power. Usually the input of the VFD is a grid voltage which is manipulated with rectifier and inverter circuits to achieve output voltage at a desired frequency that is used to drive the motor. This is usually achieved by Pulse-Width Modulating (PWM) the voltage which results in an approximate sine wave current waveform output.

There are many different converter topologies but two quite common ones are voltage source inverters (VSI) and current source inverters (CSI). Most notable difference between the two is that a VSI uses capacitor in the DC link while CSI uses an inductor.

DTC modulates inverter a bit differently. Voltage is not modulated by the means of sine-triangle modulation or space vector modulation, because with DTC switch positions are

determined solely by the outputs of hysteresis controllers and stator flux linkage sector selector. The pulse patterns in DTC still quite much resemble space vector modulated PWM.

2.3.1 Voltage source inverter (VSI)

Voltage source inverter circuit is a combination of three different sections. The rectifier circuit, DC link and inverter circuit. Rectifier circuit is usually made with six diodes to create a slightly varying DC voltage for the DC link. DC link capacitor is used to filter possible noises in the input grid voltage waveform and to smooth out the rectified DC voltage. Inverter circuit uses six semiconductor switches to create output AC voltage. Output frequency can be controlled by switching the switches in a suitable manner. Generic schematic of a VSI is shown in Fig. 2.6.

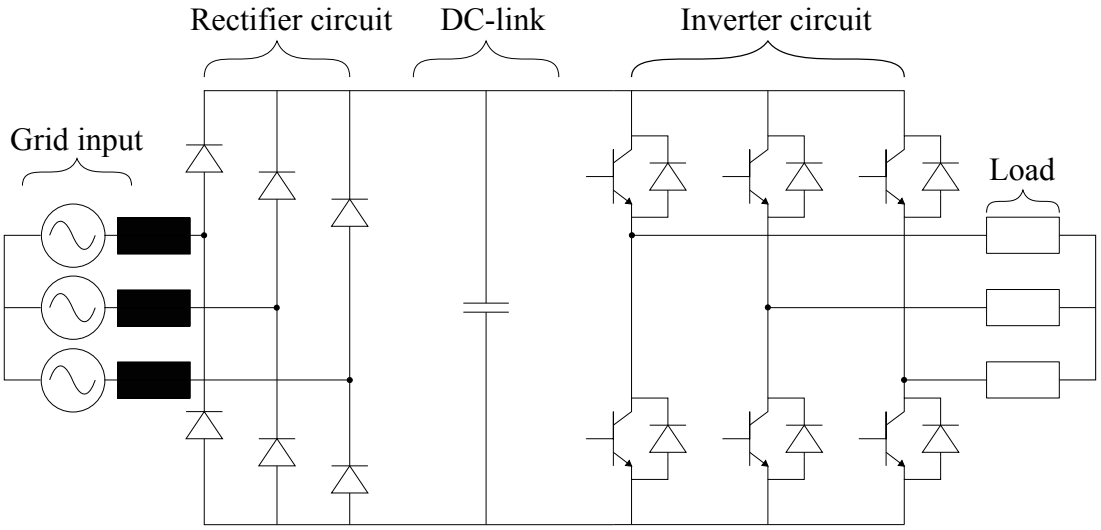

Figure 2.6: Voltage source inverter circuit.

2.3.2 VSI non-ideal characteristics

Ideal semiconductor switch would have instantaneous on/off switching, large current conducting ability, zero current when turned off, no voltage drop when turned on and no power losses. (Ned Mohan, 1995) However, these characteristics are not possible to achieve in real-life applications.

There are two kinds of losses with the IGBT switches: on-state losses and the switching losses. On-state losses are created by small voltage drop U_{on} across the switch when it is conducting current. Switching losses are generated during the switches turn-on and turn-off phases as the voltage over the switch does not drop down to U_{on} and the current I_{o} through the switch does not rise up instantaneously.

2.4 Direct Torque Control

Basic direct torque control concept was originally proposed by Depenbrock in 1985 (Depenbrock, 1985). Also a year later Takahashi and Noguchi in 1986 published their paper about the principles of DTC (Isao Takahashi, 1986). The basic concept behind the DTC is that with the stator current and voltage measurements electrical machine's stator flux linkage and torque can be estimated. Machine flux linkage and torque control is performed with hysteresis controllers and an optimal switching table. As the stator side variables can be easily solved in the stator reference frame, there is no need of rotor position measurements.

With the DTC electrical machine's stator flux linkage and torque are estimated atleast once in every control cycle. Common control cycle or sampling period of a DTC system is 25 µs. (Tiitinen, 1996) The stator flux linkage $\boldsymbol{\psi}_\mathrm{s}$ can be solved with the 'current model' or the 'voltage model'. The current model is the following.

$$\boldsymbol{\psi}_\mathrm{s} = L_\mathrm{s}\boldsymbol{i}_\mathrm{s} + L_\mathrm{m}\boldsymbol{i}_\mathrm{r} \tag{2.42}$$

where $\boldsymbol{i}_\mathrm{s}$ is stator current space vector, $\boldsymbol{i}_\mathrm{r}$ rotor current space vector, L_s stator winding total inductance and L_m magnetizing inductance. A problem with the current model is that acceptable rotor current approximation can be difficult. Also the accuracy of the current model is highly depended on inductances which have been assumed to be constants when working with space vectors. (Kaukonen, 1999) Even though the current model has its problems it can be effectively used in the stator flux linkage correction. The stator flux linkage estimate is mainly solved with the voltage model.

$$\boldsymbol{\psi}_\mathrm{s} = \int (\boldsymbol{u}_\mathrm{s} - R_\mathrm{s}\boldsymbol{i}_\mathrm{s})\mathrm{d}t \tag{2.43}$$

where $\boldsymbol{u}_\mathrm{s}$ is the stator voltage space vector, R_s is the stator winding resistance and $\boldsymbol{i}_\mathrm{s}$ is the stator current space vector. Advantage of the voltage model is that it only needs the stator variables, which can be quite straightforwardly measured from the machine. Though in real-life problems can arise with the voltage drop $-R_\mathrm{s}\boldsymbol{i}_\mathrm{s}$ as the stator resistance R_s is a function of temperature and frequency.

The electromagnetic torque of the induction machine is the cross product of the magnetic flux linkage $\boldsymbol{\psi}_\mathrm{s}$ and the stator current $\boldsymbol{i}_\mathrm{s}$ space vectors. Equation for the electromagnetic torque is the following.

$$\boldsymbol{T}_\mathrm{e} = \frac{3}{2}p\boldsymbol{\psi}_\mathrm{s} \times \boldsymbol{i}_\mathrm{s} \tag{2.44}$$

where p is the number of the pole pairs and T_e is the electromagnetic torque. In Eq. (2.44) $\boldsymbol{T}_\mathrm{e}$ is a vector. However, scalar values of the torque are used in control and positive torque is assumed to rotate the machine in mathematically positive direction, i.e. counterclockwise, and negative torque in negative one, i.e. clockwise.

2.4.1 Hysteresis controllers

Hysteresis controllers are used to give control signals for the optimal switching table. There are two hysteresis controllers used in basic DTC. One is for the absolute value of the stator flux linkage vector ψ_s and the other one is for the electromagnetic torque T_e. The stator flux linkage is either increased or decreased with a two-level hysteresis controller. Error, or the difference between the stator flux linkage reference and its estimated value is calculated with the following equation.

$$\psi_{\text{err}} = \psi_{\text{s,ref}} - \psi_{\text{s,est}} \tag{2.45}$$

The aim is to keep the value of the stator flux linkage estimate between the hysteresis limits. The stator flux linkage control scheme is shown in Fig. 2.7.

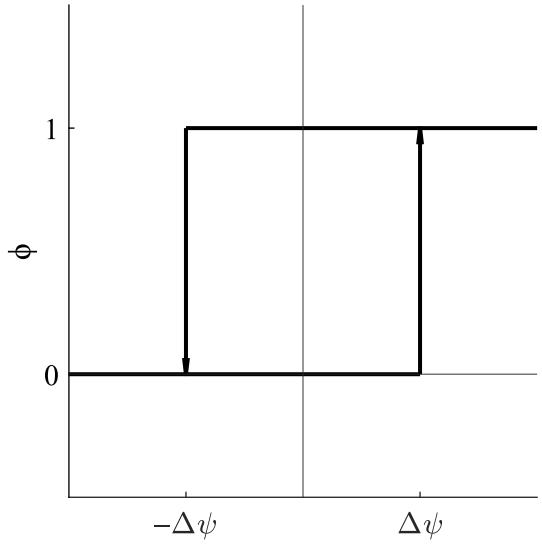

Figure 2.7: Two-level hysteresis controller for the stator flux linkage

If the error ψ_{err} between the stator flux linkage absolute value reference and its estimated value is higher than the allowed limit $\Delta\psi$ the hysteresis controller outputs 1 and if the ψ_{err} is smaller than the allowed limit $-\Delta\psi$ the controller outputs 0. Absolute value of the stator flux linkage is increased when $\phi = 1$ and decreased when $\phi = 0$.

Torque is controlled with a three-level hysteresis controller. The torque error, or the difference T_{err} is calculated with the reference torque $T_{\text{e,ref}}$ and estimated torque $T_{\text{e,est}}$.

$$T_{\text{err}} = T_{\text{e,ref}} - T_{\text{e,est}} \tag{2.46}$$

Based on the estimated torque difference T_{err} motor's electromagnetic torque is either increased, decreased or kept the same. Controller outputs either $\tau = -1$, 0 or 1. $\tau = 1$ is used to increase torque to the positive rotation direction and $\tau = -1$ to the negative

direction. $\tau = 0$ is used when no change in the torque is required. Torque controller scheme is shown in Fig. 2.8.

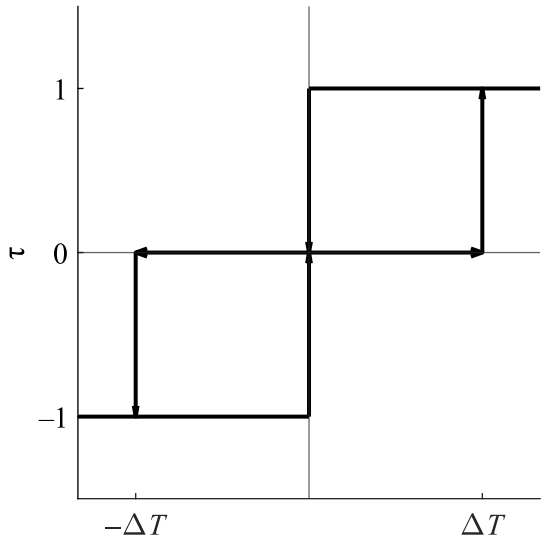

Figure 2.8: Three-level hysteresis controller for the torque control.

If the controller output is at 0 and the T_{err} rises above the positive torque limit ΔT the controller output switches to 1 and when the T_{err} has been decreased below the zero the controller outputs zero again. The same principle applies vice versa. If T_{err} reaches the lower torque limit $-\Delta T$ the controller output switches to -1 and stays there until the torque difference rises back above the zero.

2.4.2 Stator flux linkage vector sector table

As the stator flux linkage estimate vector rotates around the origin it is necessary to know in which sector the stator flux linkage vector is at any instant. This allows selecting right states for the inverter switches as each of the six sectors has specified switch positions that adjust the stator flux linkage vector and torque. $\alpha\beta$-plane is divided into six regions 60° apart from each other. The sector limits are shown in table 2.1 and the sectors are shown in Fig. 2.9.

Table 2.1: Sector limits

$\kappa(1)$	$\kappa(2)$	$\kappa(3)$	$\kappa(4)$	$\kappa(5)$	$\kappa(6)$
$[\frac{11\pi}{6}, \frac{\pi}{6}]$	$[\frac{\pi}{6}, \frac{\pi}{2}]$	$[\frac{\pi}{2}, \frac{5\pi}{6}]$	$[\frac{5\pi}{6}, \frac{7\pi}{6}]$	$[\frac{7\pi}{6}, \frac{3\pi}{2}]$	$[\frac{3\pi}{2}, \frac{11\pi}{6}]$

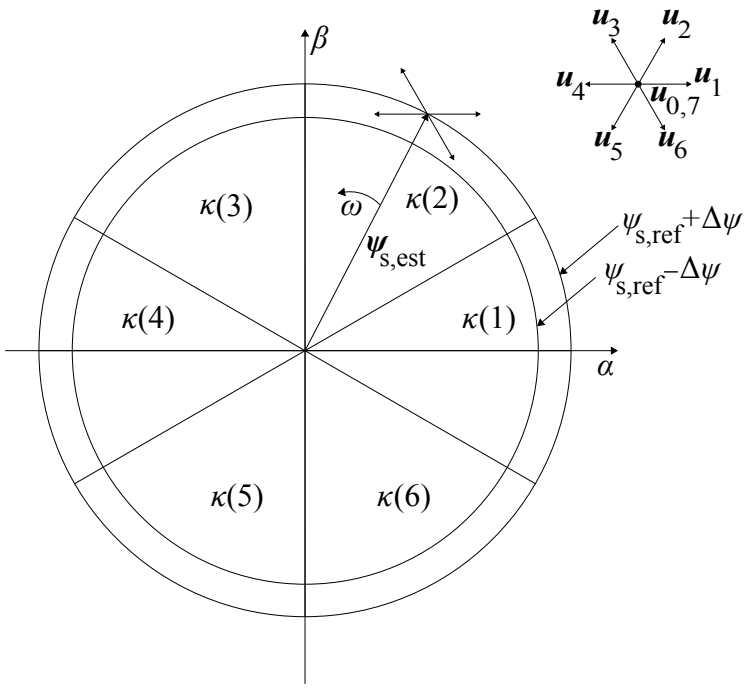

Figure 2.9: Flux linkage circle is divided into six equal sectors. Stator flux linkage hysteresis limits are shown in the figure. In this case the stator flux linkage vector has reached the upper hysteresis limit which means that the absolute value of stator flux linkage needs to be decreased. The correct voltage vectors that could decrease the stator flux linkage are $\boldsymbol{u}_4$, $\boldsymbol{u}_6$ or zero vectors $\boldsymbol{u}_{0,7}$. Selection between these four voltage vectors is done based on the output of the torque hysteresis controller.

2.4.3 Optimal Switching Table

Switching logic is based on the outputs of the hysteresis controllers and sector table. The optimal switching table consists of six different switch position combinations for each of the six sectors. Switch states are based on eight voltage vectors $\boldsymbol{u}_0 - \boldsymbol{u}_7$, where $\boldsymbol{u}_0$ and $\boldsymbol{u}_7$ are zero vectors. These voltage vectors can be seen in Fig. 2.9. Optimal switching table is shown in table 2.2.

Table 2.2: Optimal switching table for VSI switches (Isao Takahashi, 1986)

ϕ	τ	$\kappa = 1$	$\kappa = 2$	$\kappa = 3$	$\kappa = 4$	$\kappa = 5$	$\kappa = 6$
$\phi = 1$	$\tau = 1$	S(1,1,0)	S(0,1,0)	S(0,1,1)	S(0,0,1)	S(1,0,1)	S(1,0,0)
	$\tau = 0$	S(0,0,0)	S(1,1,1)	S(0,0,0)	S(1,1,1)	S(0,0,0)	S(1,1,1)
	$\tau = -1$	S(1,0,1)	S(1,0,0)	S(1,1,0)	S(0,1,0)	S(0,1,1)	S(0,0,1)
$\phi = 0$	$\tau = 1$	S(0,1,0)	S(0,1,1)	S(0,0,1)	S(1,0,1)	S(1,0,0)	S(1,1,0)
	$\tau = 0$	S(0,0,0)	S(1,1,1)	S(0,0,0)	S(1,1,1)	S(0,0,0)	S(1,1,1)
	$\tau = -1$	S(0,0,1)	S(1,0,1)	S(1,0,0)	S(1,1,0)	S(0,1,0)	S(0,1,1)

Considering the case in Fig. 2.9 the stator flux linkage vector has reached the upper limit and lets decide that the torque needs to be increased into the direction of rotation ω. In

this case the stator flux linkage hysteresis controller output is $\phi = 0$, torque hysteresis controller output is $\tau = 1$ and sector table output is $\kappa = 2$. This means that voltage vector $\boldsymbol{u}_4$ is chosen which corresponds with switch position S(0,1,1).

2.4.4 Switching frequency

DTC switching frequency is not constant. It is tied to the sampling time of the DTC system and the widths of the hysteresis bands as every switching event is a wanted one by the hysteresis controllers and sector logic. Since the switching frequency is not constant one way to estimate the switching frequency is to calculate average switching frequency over some time frame. This can be done by dividing the total sum of the switching events N_w with the corresponding time frame Δt.

$$f_{\mathrm{sw,average}} = \frac{\frac{1}{6}N_\mathrm{w}}{\Delta t} \tag{2.47}$$

Total sum of the switching events N_w has to be multiplied with the factor of $\frac{1}{6}$ in the case of inverter with six semiconductor switches. This way the average switching frequency from the point of view of one semiconductor switch can be calculated.

On high sampling times the stator flux linkage and torque has a longer time to travel based on the voltage vector used. Combining high sampling time with too tight hysteresis bands would lead to overshoot of the controlled variable because the inverter switch positions could not be updated in time. With a lower sampling time voltage vectors can be changed more often which in turn allows tighter hysteresis bands. However, the lower sampling time can come with a disadvantage. If the lower sampling time is accompanied by tighter hysteresis bands the switching losses increase as more switching operations takes place. These losses can lead to problems regarding the thermal limits of the inverter.

2.4.5 Stator flux linkage drifting

Stator flux linkage estimate is highly depended on the accuracy of the voltage and current measurements and stator resistance and inverter voltage drop estimates. Any uncertainty in the measurements and estimates are integrated with the voltage model Eq. (2.43), which leads to a cumulative error in the stator flux linkage estimate. As the motor is controlled with inaccurate control signals the real motor stator flux linkage vector can become eccentric even though the stator flux linkage estimate operates as desired. (Juha Pyrhönen, 2016) Effect of inaccurate voltage measurement to the real stator flux linkage vector is shown in Fig. 2.10.

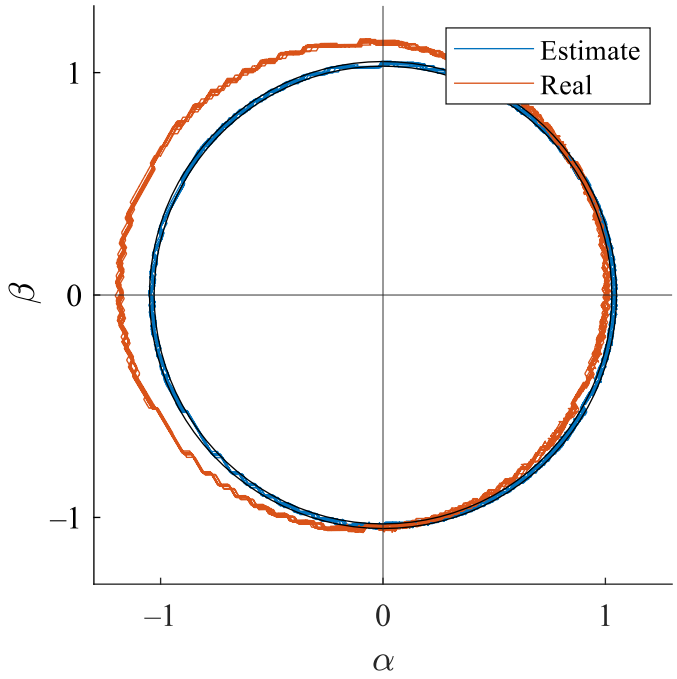

Figure 2.10: Real motor stator flux linkage vector tip path drifts away from an origin centered path when some error is introduced in the voltage measurement.

2.4.6 Adaptive motor model

Advantage of DTC system is that it only requires voltage and current measurements for the control of the machine. Adaptive motor model takes these as inputs and uses them to create stator flux linkage and torque estimates with Eqs. (2.43) and (2.44). In practice, phase voltages can be derived from DC-link voltage measurement and the states of the switches. However, the voltage drop across the inverter switches should be taken into account. Otherwise the accuracies of the stator flux and torque estimates suffer (Juha Pyrhönen, 2016).

Adaptive motor model needs the stator winding resistance R_s value as it is used in the voltage model equation. Therefore, during the commissioning stator resistance must be identified since stator resistances vary between the different machines. To achieve a more accurate stator flux linkage estimate some thermodynamical modeling should be applied in the motor model since the resistance is a function of a temperature. Also the inductance values are updated in the adaptive motor model to take the magnetic circuit saturation into account. Usually adaptive motor model is also used in the speed estimation and current model stator flux linkage estimation. (Tiitinen, 1996)

2.4.7 Stator current limitation method

Starting currents of an induction machine can be quite high without any current optimization or limiting methods. During the start the DTC inherently supplies a DC voltage for a short amount of time to the machine so the stator flux linkage can be established. After this, hysteresis controllers start to output necessary control signals to achieve the desired flux linkage and torque. In the startup process it means that rated magnetizing current is needed to magnetize the rotor before the stator flux linkage vector starts rotating. As a standing motor has no back emf the voltage pulses easily lead to very high starting currents. A current limit must be established.

Chapuis and Roye present in their conference paper a simple way to limit the startup currents of a DTC drive (Chapuis and Roye, 1998). Their method of current limitation involves two parts. First part is that when the absolute value of the stator current vector $\boldsymbol{i}_\mathrm{s}$ reaches a predetermined upper limit i_max zero voltage vector $\boldsymbol{u}_{0,7}$ is applied and the default DTC optimal switching logic is overriden. Second part is that during the startup the torque reference is delayed until the desired stator flux linkage is fully reached. This allows to properly magnetize the machine before any torque is produced. Torque delaying can be achieved by applying any non-zero voltage vector $\boldsymbol{u}_{1,6}$ until the stator flux linkage reaches the predetermined limit.

2.5 Per-unit system

With the electrical machines different variables are often expressed with the per-unit values. The main advantage of the per-unit system is that per-unit values of different machines can be directly compared to the each other. The basic concept of the per-unit system is that variables are divided with the base value of the variable in question. Per-unit values are dimensionless. Voltage base value is calculated with the rated line voltage.

$$U_\mathrm{base} = \frac{\sqrt{2}U_\mathrm{n}}{\sqrt{3}} \tag{2.48}$$

The base value of angular electrical velocity is calculated with the rated frequency.

$$\omega_\mathrm{base} = 2\pi f_\mathrm{n} \tag{2.49}$$

The current base value is the peak value of rated RMS current.

$$I_\mathrm{base} = \sqrt{2}I_\mathrm{n} \tag{2.50}$$

The impedance base value can be calculated by dividing the base voltage value with the base current value.

$$Z_\mathrm{base} = \frac{U_\mathrm{base}}{I_\mathrm{base}} \tag{2.51}$$

The inductance base value can be calculated with the base values of the impedance and electrical angular velocity.

$$L_{\text{base}} = \frac{Z_{\text{base}}}{\omega_{\text{base}}} \tag{2.52}$$

The stator flux linkage base value is calculated with the base values of voltage and electrical angular velocity.

$$\psi_{\text{base}} = \frac{U_{\text{base}}}{\omega_{\text{base}}} \tag{2.53}$$

The apparent power base value is calculated with the base values of voltage and current.

$$S_{\text{base}} = U_{\text{base}} I_{\text{base}} \tag{2.54}$$

Base value of the torque is calculated with the base values of apparent power and electrical angular velocity.

$$T_{\text{base}} = \frac{3}{2} p (\frac{S_{\text{base}}}{\omega_{\text{base}}}) \tag{2.55}$$

It must be noted that the base value of the torque is not equal to the rated torque. The base value of motor inertia is calculated with the number of pole pairs and by dividing the torque base value with the electrical angular velocity squared.

$$J_{\text{base}} = p \frac{T_{\text{base}}}{\omega_{\text{base}}^2} \tag{2.56}$$

When converting real valued quantity to per-units the real value is simply divided with corresponding base value. As an example consider a situation where motor's rated RMS current is I_{n} = 100 A and some current measurement shows i = 80 A. In the per-unit conversion first the base value is calculated with Eq. (2.50) which would mean that the I_{base} is about 141 A. After that the current measurement i is simply divided with the base value and the current measurement in per-units would be about 0.57 pu.

3 Simulink model

The Simulink DTC-model system created is made of three main parts: the DTC model, inverter model and induction motor model in stator reference frame. Each of these are made of necessary subsystems to further simplify the overall models. The system also includes step function sources for the speed reference and load torque.

Basically the reference signals are supplied to the DTC model which starts to output appropriate switch states for the inverter. Then the inverter supplies voltage to the induction motor model. In real life, voltage and current measurements are the only necessary measurement feedbacks from the motor to the DTC core as the other variables could be attained with the adaptive motor model. However, for the simulation purposes the 'real' motor and adaptive motor model are the same now. This leads to that the rotor currents and speed are measured too from the motor model. In practice, rotor currents can not be measured and thus they have to be always estimated if needed.

Some simplifications were done with the model. Stator flux vector drifting is not really a problem with this Simulink model since the real motor and the adaptive motor model are the same. The motor 'real' stator flux linkage and stator flux linkage estimates are essentially calculated with the same parameters in motor model and the DTC model. Consequently, the stator flux linkage correction measures are not necessary. Some error could be introduced to the current and voltage measurements with simple multiplications. Also the motor inductances were constant for the whole operating range, so magnetic circuit saturations were not considered with the simulation model at all. Furthermore, there is no thermodynamical modeling in the Simulink model, so the resistances also stay constants.

In the Simulink model some features could be toggled on or off through the initialization m-file. Toggleable features are: stator current limiter, field weakening, per-unit mode, current model correction, average switching frequency control and speed controller feedforward loop. Implementation of these features and different Simulink subsystems are more extensively explained with figures in the appendices.

Implemented per-unit mode closely resembles the implementation that Aarniovuori presented in his vector control paper (Lassi Aarniovuori, 2018). In the per-unit mode the base values Eqs. (2.48)-(2.56) are initialized in the m-file. These base values are then used to convert different motor and control variables to the per-unit system. With the similar gain help variables as Aarniovuori presented in his paper switching between the real values and per-units is quite straightforward.

Block diagram that gives a broad overview of the Simulink model is shown in Fig. 3.1.

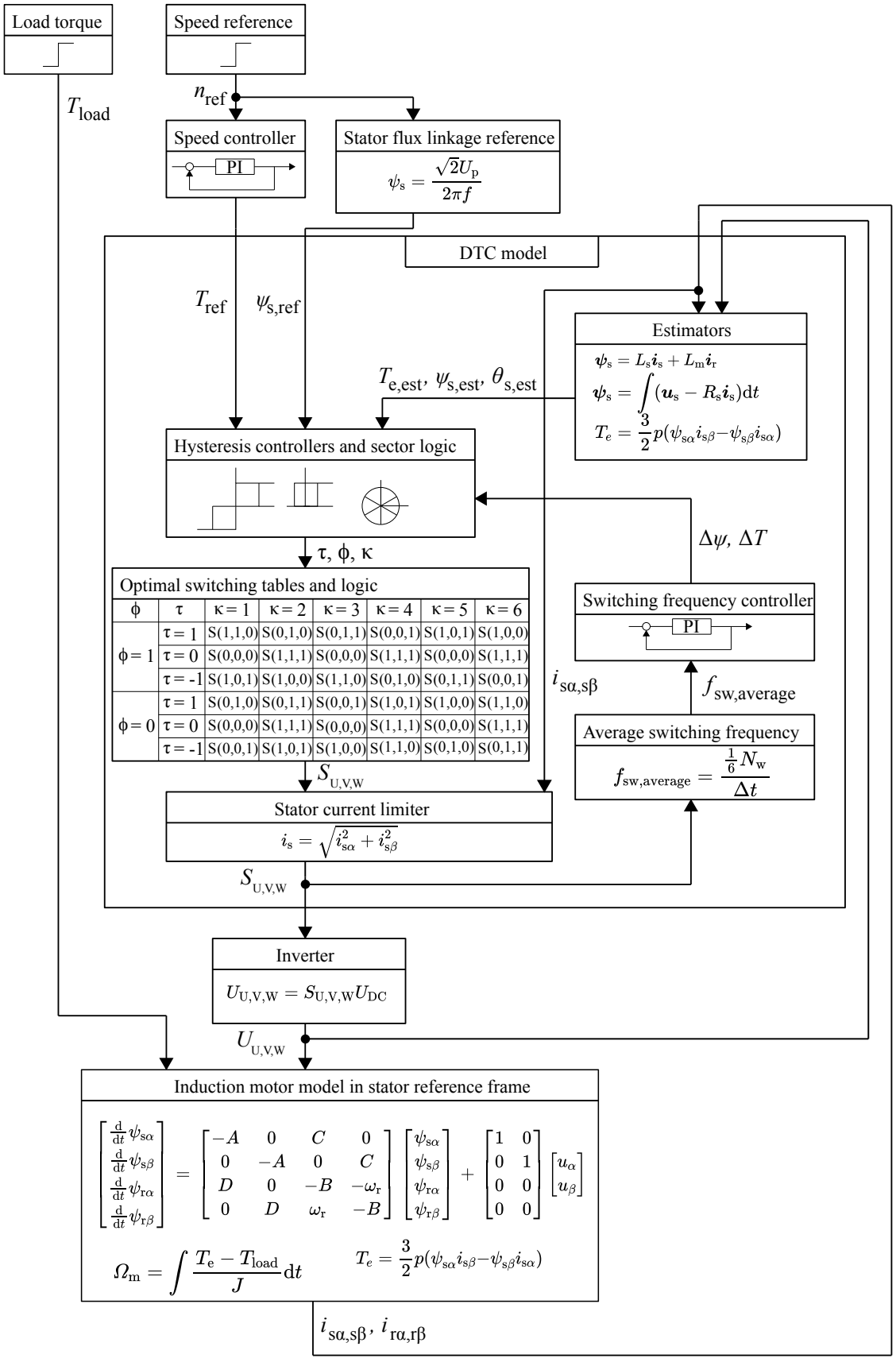

ϕ	τ	κ = 1	κ = 2	κ = 3	κ = 4	κ = 5	κ = 6
ϕ = 1	τ = 1	S(1,1,0)	S(0,1,0)	S(0,1,1)	S(0,0,1)	S(1,0,1)	S(1,0,0)
	τ = 0	S(0,0,0)	S(1,1,1)	S(0,0,0)	S(1,1,1)	S(0,0,0)	S(1,1,1)
	τ = -1	S(1,0,1)	S(1,0,0)	S(1,1,0)	S(0,1,0)	S(0,1,1)	S(0,0,1)
ϕ = 0	τ = 1	S(0,1,0)	S(0,1,1)	S(0,0,1)	S(1,0,1)	S(1,0,0)	S(1,1,0)
	τ = 0	S(0,0,0)	S(1,1,1)	S(0,0,0)	S(1,1,1)	S(0,0,0)	S(1,1,1)
	τ = -1	S(0,0,1)	S(1,0,1)	S(1,0,0)	S(1,1,0)	S(0,1,0)	S(0,1,1)

$$\begin{bmatrix} \frac{\text{d}}{\text{d}t}\psi_{\text{s}\alpha} \\ \frac{\text{d}}{\text{d}t}\psi_{\text{s}\beta} \\ \frac{\text{d}}{\text{d}t}\psi_{\text{r}\alpha} \\ \frac{\text{d}}{\text{d}t}\psi_{\text{r}\beta} \end{bmatrix} = \begin{bmatrix} -A & 0 & C & 0 \\ 0 & -A & 0 & C \\ D & 0 & -B & -\omega_{\text{r}} \\ 0 & D & \omega_{\text{r}} & -B \end{bmatrix} \begin{bmatrix} \psi_{\text{s}\alpha} \\ \psi_{\text{s}\beta} \\ \psi_{\text{r}\alpha} \\ \psi_{\text{r}\beta} \end{bmatrix} + \begin{bmatrix} 1 & 0 \\ 0 & 1 \\ 0 & 0 \\ 0 & 0 \end{bmatrix} \begin{bmatrix} u_\alpha \\ u_\beta \end{bmatrix}$$

Figure 3.1: Block diagram of the created Simulink DTC model. Note that all subsystems are not shown in this block diagram.

Stator flux linkage reference block implements Eq. (2.41). Below 45 Hz speed reference the stator flux linkage reference is kept constant and above 45 Hz speed the motor reaches the field weakening region and the block input n_{ref} is used to create new output stator flux linkage reference. Further explanation of the block is presented in Appendix D.1, fig. D.1.

Estimators block includes the current model Eq. (2.42), voltage model Eq. (2.43) and the torque Eq. (2.36) which are used to create the stator flux linkage estimates and torque estimate, respectively. α- and β-components are estimated separately. Essential block inputs are voltage measurements and stator and rotor current measurements. Block outputs stator flux linkage estimate, stator flux linkage angle and torque estimate. The absolute value of the stator flux linkage ψ_{s} can be calculated from α- and β-components with the following equation.

$$\psi_{\text{s}} = \sqrt{{\psi_{\text{s}\alpha}}^2 + {\psi_{\text{s}\beta}}^2} \tag{3.1}$$

Angle of the stator flux linkage vector is calculated with variation of tan function called atan2 that can give angle between $[-\pi \leq \theta < \pi]$.

$$\text{atan2}(\psi_{\text{s}\beta}, \psi_{\text{s}\alpha}) = \begin{cases} \arctan(\frac{\psi_{\text{s}\beta}}{\psi_{\text{s}\alpha}}) & \text{if } \psi_{\text{s}\alpha} > 0 \\ \arctan(\frac{\psi_{s\beta}}{\psi_{\text{s}\alpha}}) + \pi & \text{if } \psi_{\text{s}\alpha} < 0 \text{ and } \psi_{\text{s}\beta} \geq 0 \\ \arctan(\frac{\psi_{\text{s}\beta}}{\psi_{\text{s}\alpha}}) - \pi & \text{if } \psi_{\text{s}\alpha} < 0 \text{ and } \psi_{\text{s}\beta} < 0 \\ \frac{\pi}{2} & \text{if } \psi_{\text{s}\alpha} = 0 \text{ and } \psi_{\text{s}\beta} > 0 \\ \frac{\pi}{2} & \text{if } \psi_{\text{s}\alpha} = 0 \text{ and } \psi_{\text{s}\beta} < 0 \\ \text{undefined} & \text{if } \psi_{\text{s}\alpha} = 0 \text{ and } \psi_{\text{s}\beta} = 0 \end{cases} \tag{3.2}$$

Since the atan2 gives angles from $[-\pi \leq \theta < \pi]$ sector limits given in Table 2.1 are modified to accompany this change. The Simulink implementation is shown in Appendix C.2, Fig. C.2.

Hysteresis controllers and sector logic block contains the control logic of the DTC. In the Simulink these subsystems are triggered every 25 µs. Stator flux linkage estimate and reference, torque reference and estimate and stator flux linkage angle estimate are inputs of this block. Based on the inputs the controller and sector logic outputs τ, ϕ and κ are determined. More detailed information about the Simulink implementations can be found in Appendices C.3, C.4 and C.5, Figs. C.3 - C.6.

Optimal switching tables and logic contains optimal switching tables for each of the inverter switches and a subsystem that contains combinational logic that chooses right table row based on the hysteresis controller outputs. In Simulink, these blocks are triggered every 25 µs. Inputs are τ, ϕ and κ and block outputs right switch positions to create optimal voltage vectors. The Simulink implementation can be found in Appendix C.6, Fig C.7.

Stator current limiter block implements current limitation for the DTC. Absolute value of the stator current measurement is calculated in the stator reference frame with the

following equation.

$$i_{\mathrm{s}} = \sqrt{{i_{\mathrm{s}\alpha}}^2 + {i_{\mathrm{s}\beta}}^2} \tag{3.3}$$

Absolute value of the stator current is compared to the maximum current given in the m-file. If the maximum value is exceeded normal DTC operation is ignored. More detailed explanation can be found in Appendix C.7 and figure of the Simulink implementation in Fig. C.8.

Induction motor model in the stator reference frame block contains the motor model and motor's mechanical model. Inputs of this block are phase voltages from the inverter. Outputs are speed, stator and rotor currents. Equations (2.25) - (2.36) are realized in the motor model and Eq. (2.38) in the motor's mechanical model. The Simulink implementation is presented in Appendix B, Fig. B.1.

Average switching frequency and switching frequency controller blocks are used to control the inverter switching frequency, because without any control methods the switching frequency can rise too high. Average switching frequency block takes switch states $S_{\mathrm{U,V,W}}$ as inputs and outputs the value of the average switching frequency every 5 ms. The Simulink implementation is shown in Appendix C.8, Fig. C.9.

Switching frequency controller block adjusts the hysteresis limits with a PI-controller and else-if ladder. In short, if switching frequency is higher than desired the hysteresis band widths are increased and if switching frequency is lower than desired hysteresis band widths are decreased. More detailed explanation can be found in Appendix C.8 and the Simulink implementation in Fig. C.10.

4 Simulations

Simulations were carried out with a fixed step solver with a time step of 5 µs. One phase current I_{U}, absolute value of the stator flux linkage $\psi_{\mathrm{s,est}}$, angle of stator flux linkage vector θ, estimated electromagnetic torque $T_{\mathrm{e,est}}$, rotor speed n and switch states $S_{\mathrm{U,V,W}}$ were logged and used to calculate current harmonic content, see how the stator flux linkage vector behaves, estimate steady-state torque ripple and calculate average switching frequency, respectively. A Matlab scripts that allowed to run multiple simulations with different parameters automatically was created. This allowed to do a quite comprehensive simulations how change of the parameters affected the DTC.

The current limiter and the speed control feedforward loop were disabled during the hysteresis band width, sampling period, different speed and load conditions and inductance simulations. Although disabling the current limiter is quite unrealistic as the real inverters can not output unlimited amount of current, the simulations without the current limiter and feedforward loop had less changing variables and the effect of the studied parameter could be more easily identified based on the simulation data.

Simulated machine was a 75 kW 4-pole 400 V induction motor with the rated torque of 480 Nm. Its rated speed is 1486 rpm and the rated current 133 A. Equivalent circuit parameters are shown in table 4.1.

Table 4.1: 75 kW motor equivalent circuit parameters.

R_{s}	R_{r}	$L_{\mathrm{s}\sigma}$	$L_{\mathrm{r}\sigma}$	L_{m}	J
0.024 Ω	0.018 Ω	0.64 mH	0.40 mH	14 mH	1.4 kgm^2

4.1 Effects of hysteresis band widths

The hysteresis band simulations were carried out with ten different values for the stator flux linkage hysteresis band width $\Delta\psi$ and the torque hysteresis band width ΔT. In total, 100 different three second long simulations were executed. Rated load torque was activated after 1.5 seconds had passed to ensure that the motor could reach the desired speed first. Speed controller tried to adjust the motor speed to 1200 rpm. In the simulations $\Delta\psi$ and ΔT were incremented in $0.5\%\psi_{\mathrm{s,n}}$ and $0.5\%T_{\mathrm{n}}$ steps.

4.1.1 Average switching frequency

Based on the simulation results average switching frequency was calculated with Eq. (2.47). Average switching frequencies as a functions of hysteresis band widths $\Delta\psi$ and ΔT are shown in Fig. 2.47.

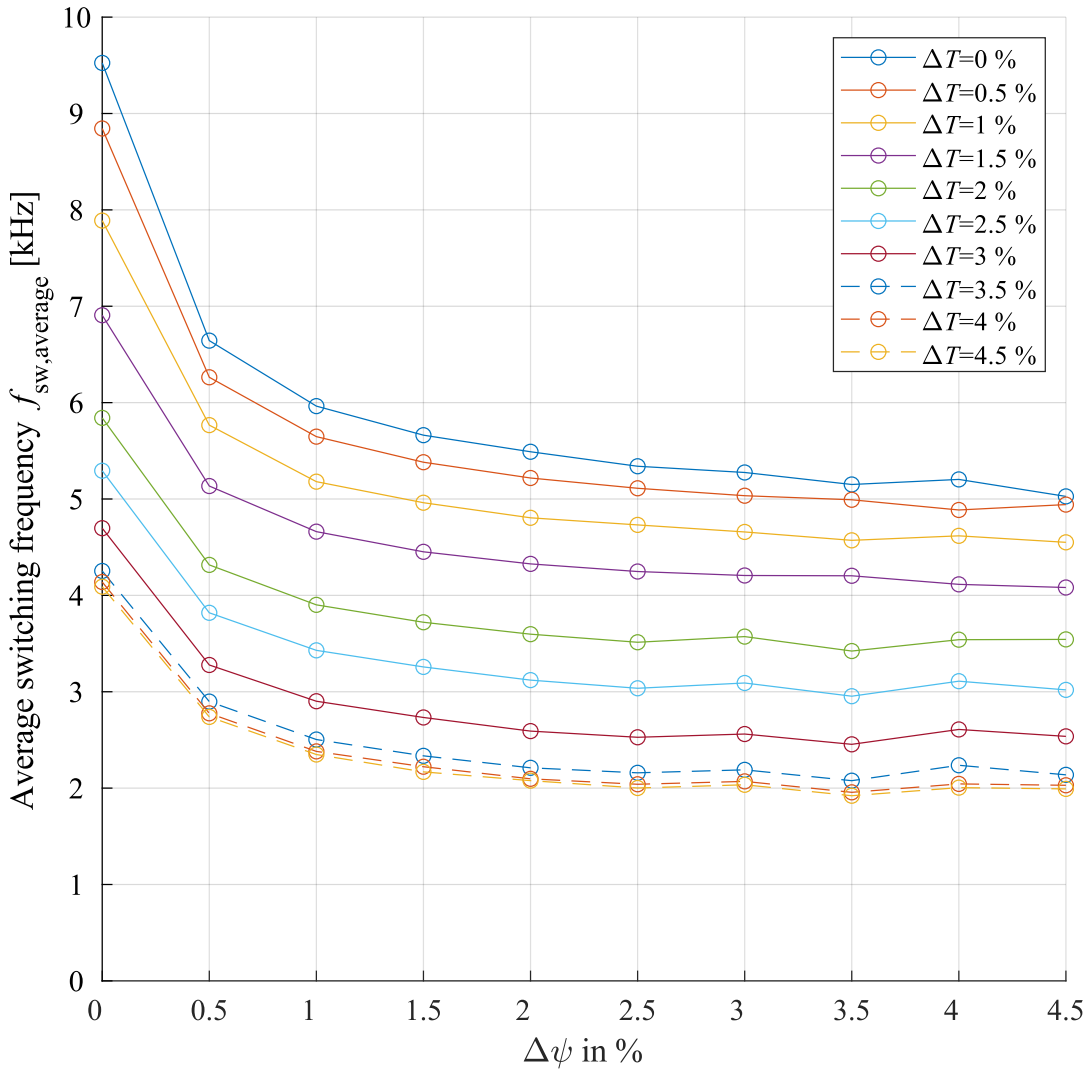

Figure 4.1: Time frame used to calculate the switching frequency is the whole simulation time of 3 s. Increasing the $\Delta\psi$ and ΔT lowers the average switching frequency.

Basically overall average switching frequency changes in respect to the hysteresis band widths. A wider hysteresis band gives the stator flux linkage and the torque more time to move and reach the hysteresis limits. Especially the wider hysteresis bands are more favourable when considering the losses of the inverter as its switching losses decrease with lower switching frequencies. Also it must noted that the value of the average switching frequency is highly depended on the calculation time frame Δt. This can be quite well seen in the Fig. 4.2, where the switching frequency is calculated every Δt = 0.005 s.

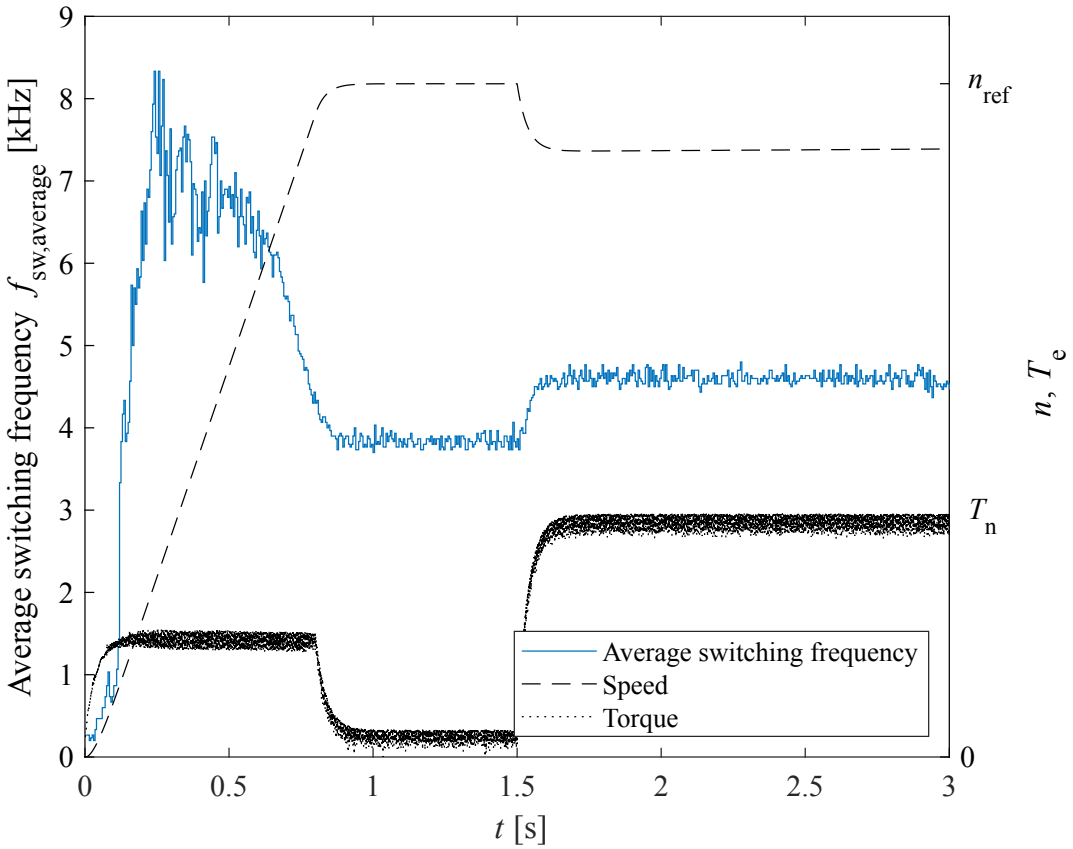

Figure 4.2: Hysteresis controller bands are $\Delta\psi = 1\%$ and $\Delta T = 1.5\%$. All of the hysteresis band simulations were conducted in a similar way. Startup is done without a load and rated load torque activates at 1.5 s. Speed reference n_{ref} was 1200 rpm.

During the startup speed controller and stator flux linkage reference system outputs reference signals which the DTC controllers starts to respond. The torque estimate rises quickly to the reference value compared to the the stator flux linkage and this leads to lower switching frequencies at the start. For a short duration during the startup the voltage vectors are changing solely based on the output of the torque hysteresis controller and sector changes. This behaviour is further shown in Fig. 4.3

When the torque reference settles to somewhat steady acceleration value and the stator flux linkage estimate gets within its hysteresis band more switching events starts to occur. Average switching frequency drops down when the steady-state without load has been reached. Partly the reason for this is that the torque reference stops changing as the desired speed has been achieved and the rotor stops accelerating. When the load torque is introduced the motor speed drops down and speed controller starts to output higher torque reference. However, the speed PI-controller coefficients are rather gentle, so the controller does not output high enough torque reference that the rotor could accelerate back to or

stay at the desired speed and therefore there is a constant error between the rotor speed and desired speed when there is a load. When the load torque is introduced the average switching frequency grows, because the torque hysteresis controller has to ask for more torque more often as the torque estimate drops down more aggressively.

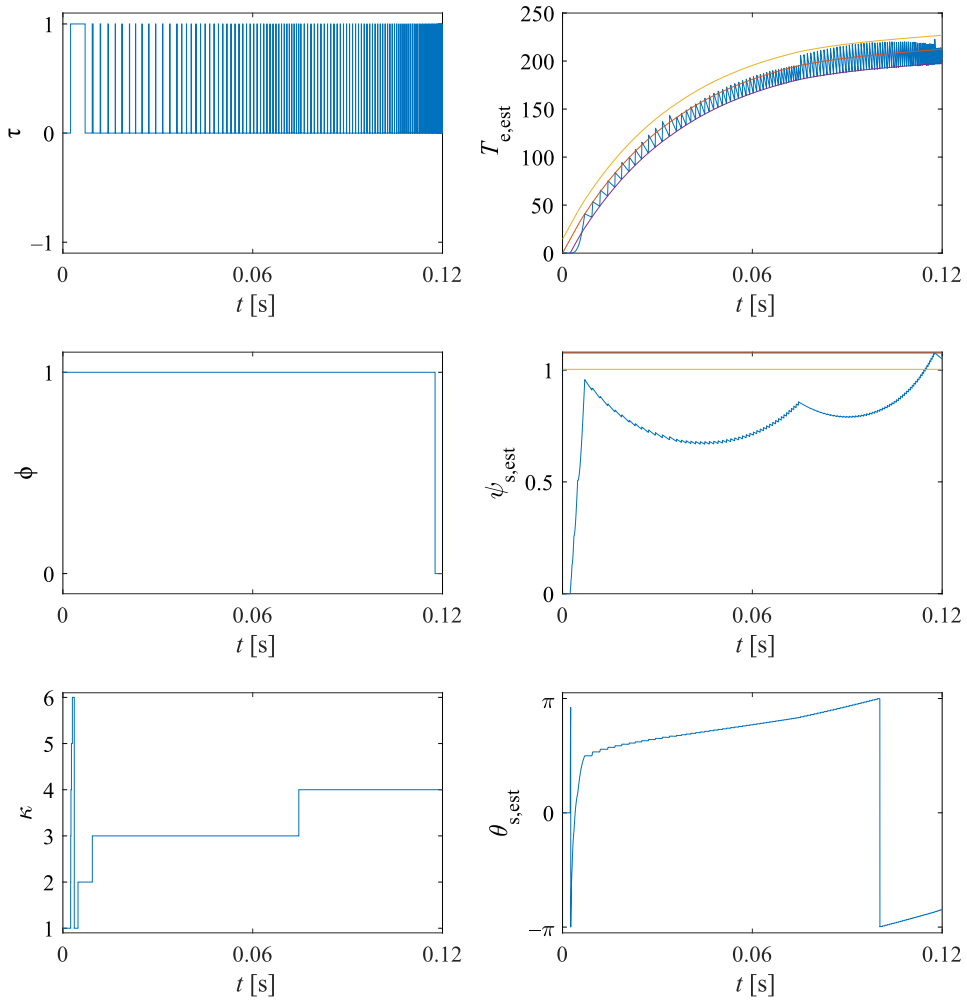

Figure 4.3: Hysteresis controller bands are $\Delta\psi = 1\%$ and $\Delta T = 1.5\%$. During the startup the stator flux linkage control bit ϕ stays at 1 until the estimate reaches the hysteresis band. The voltage vectors during this time is chosen solely on the torque hysteresis controller output and sector logic.

4.1.2 Phase current harmonic content

Effect of the different hysteresis band widths $\Delta\psi$ and ΔT to the current harmonic content was also studied with the simulations. Phase current Fast Fourier Transform (FFT) spectra were created and total harmonic distortions (THD) were calculated. In the THD calculations the first 40 harmonics were used. Effects of the different hysteresis limits $\Delta\psi$ and ΔT to the THD are shown in Fig 4.4.

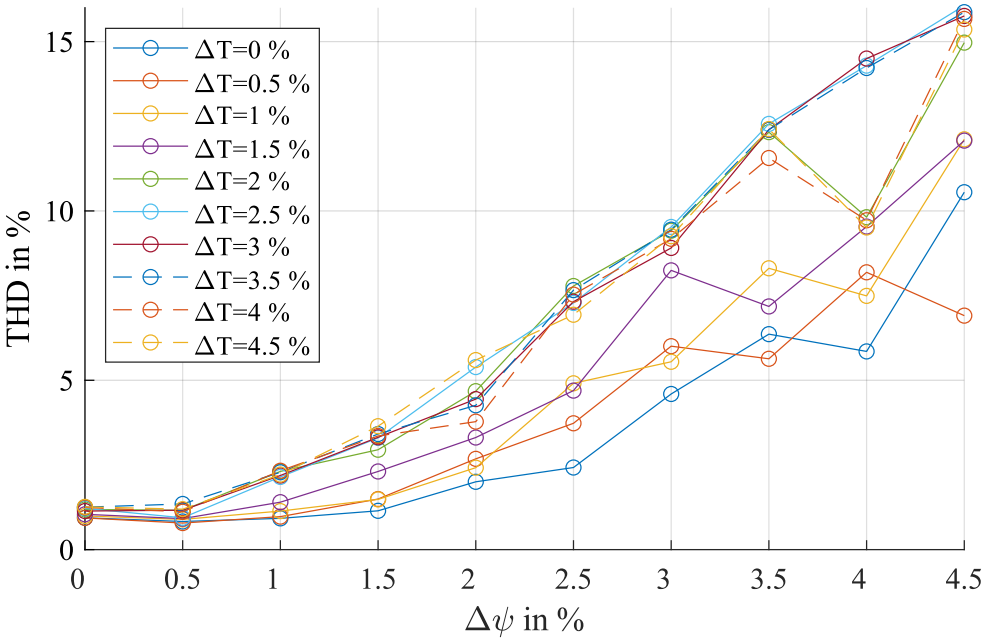

Figure 4.4: Current THD increases as the $\Delta\psi$ hysteresis band width increases since lower switching frequency creates more harmonics in the current.

Lower switching frequency due to growing hysteresis bands $\Delta\psi$ and ΔT deteriorates the current waveform and thus the current THD increases. Increase in the harmonic content of the phase current increases the motor losses, so from the motors point of view larger hysteresis band widths are not so favourable as from the inverters point of view. THD power per harmonic for the first 10 harmonics and single sided FFT spectra are shown in Fig. 4.5.

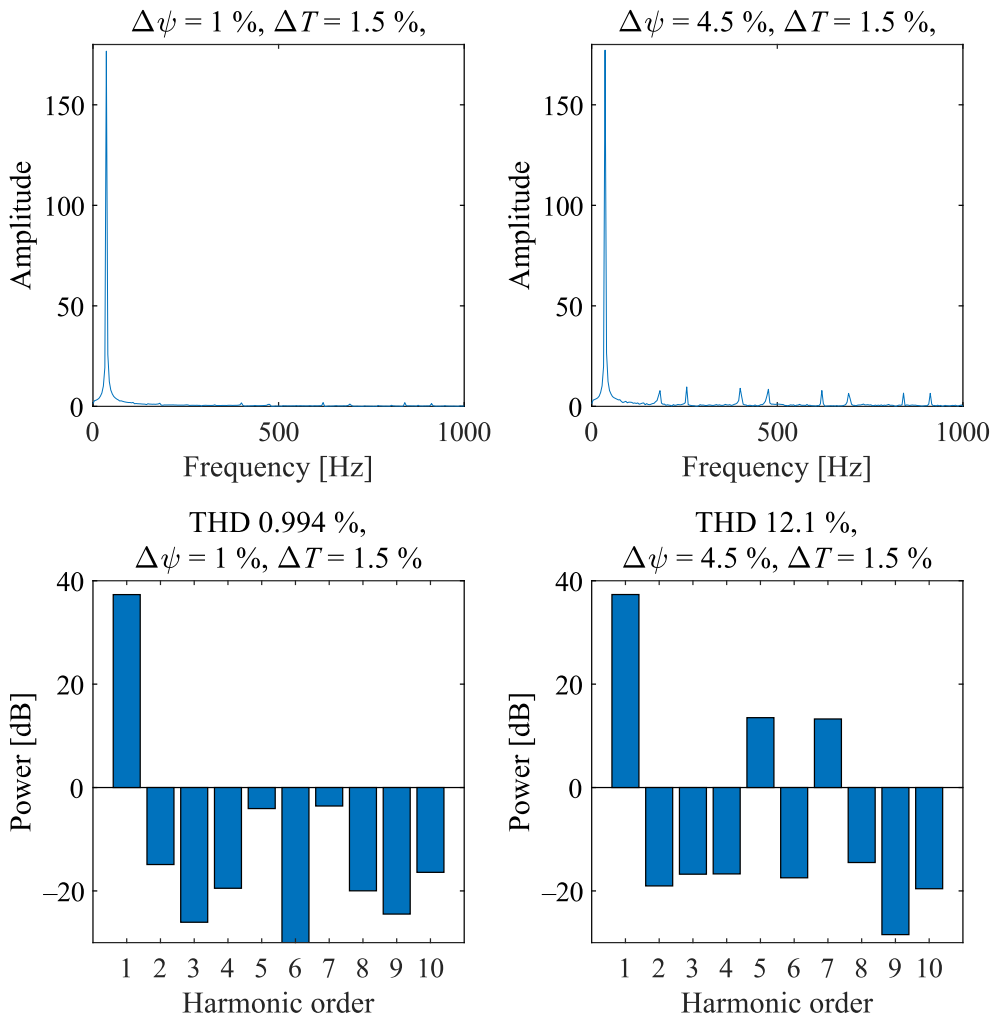

Figure 4.5: Phase current single sided FFT spectra and THD with two different stator flux linkage hysteresis band widths. ΔT is a constant 1.5% T_{n}.

From the FFT spectra it can be seen that more harmonic frequencies are present with higher $\Delta\psi$. First two harmonic spikes seen in the FFT with $\Delta\psi$ = 4.5 % are 5th and 7th harmonic frequencies. These harmonics can be clearly seen in THD bar graph. FFTs were calculated when the load torque was active. In the FFT spectra current amplitude at the fundamental frequency is about 177 A, which corresponds with RMS current of 125 A.

4.1.3 Stator flux linkage vector

Behaviour of the stator flux linkage estimate vector in $\alpha\beta$-plane and as a function of time was also examined with the simulations. Simulation results with two different ψ hysteresis bands widths are shown in Fig. 4.6.

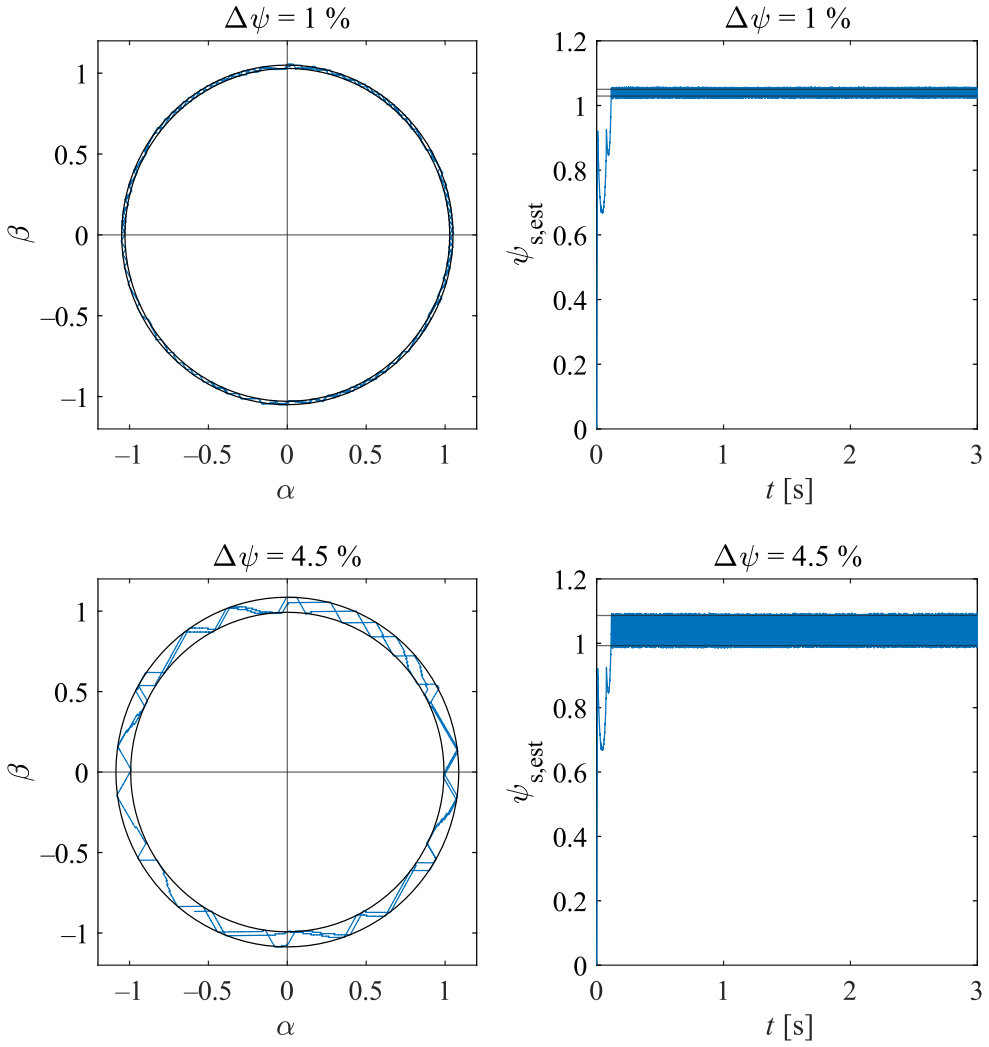

Figure 4.6: Only 10 ms time frame is plotted in the $\alpha\beta$-plane figures. As the $\Delta\psi$ increases the $\boldsymbol{\psi}_{\text{s,est}}$ has more room to move, which leads to choppier waveform. Time domain figures contain whole simulation data.

The stator flux linkage hysteresis controller tries to keep the absolute value of the stator flux linkage between the values of $\psi_{\text{s,ref}} + \Delta\psi$ and $\psi_{\text{s,ref}} - \Delta\psi$ which are represented in the figures with black circles and black parallel lines. Essentially, the increase in the stator flux linkage hysteresis band width leads to choppier stator flux linkage vector tip waveform in $\alpha\beta$-plane. This is because the stator flux linkage estimate takes more time to

reach the controller hysteresis limits and the same voltage vector can be held for a longer time. From the time domain figures it can be seen that the absolute value of the stator flux linkage estimate $\psi_{s,est}$ stays quite well between the hysteresis limits regardless of the hysteresis band width.

4.1.4 Steady-state torque ripple

Rough estimates of torque ripples were examined with different hysteresis bands in a steady-state without load and with rated load. Torque ripple is calculated by subtracting maximum torque estimate from minimum torque estimate between the simulation time frames of 1.1 s - 1.4 s and 1.7 s - 3 s. The time frames were chosen in a way that ensured the transients had already diminished and the motor speed stayed somewhat constant. Torque ripples as function of hysteresis bands are shown in Figs. 4.7 and 4.8.

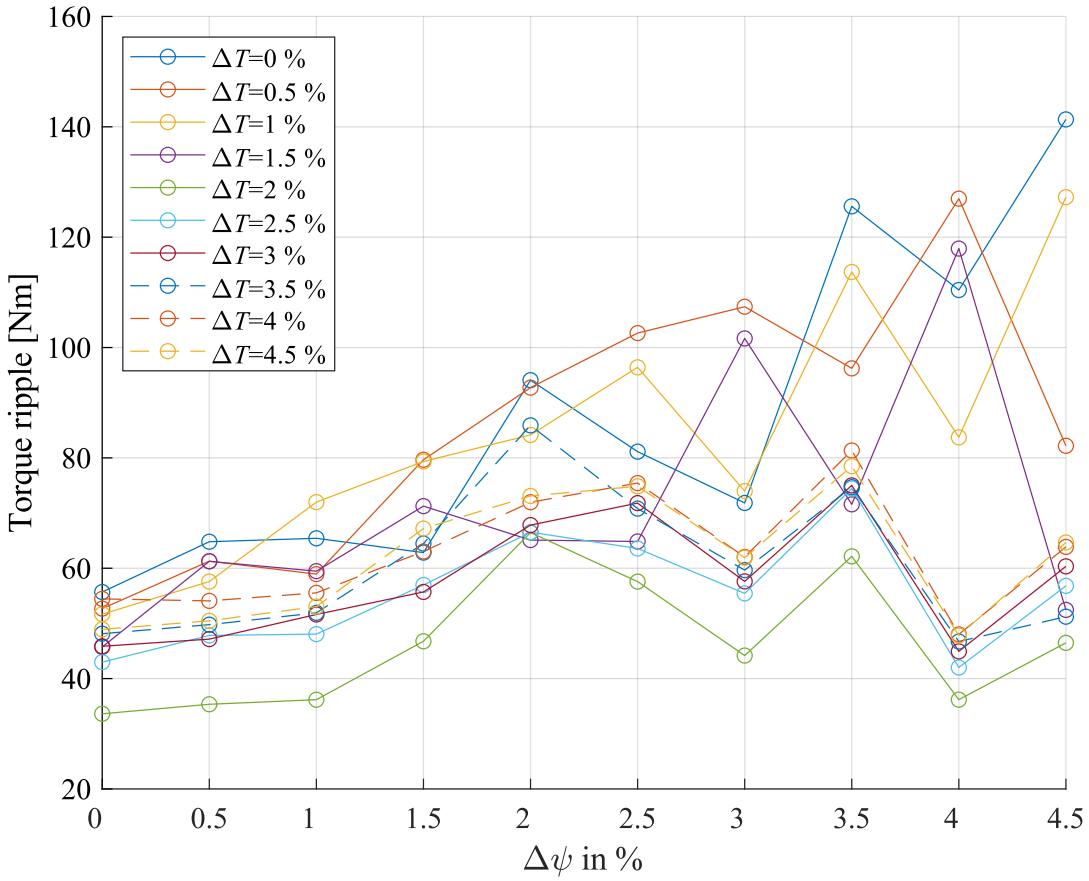

Figure 4.7: Torque ripple in steady-state without load.

Both hysteresis band widths has an effect on the torque ripple. Torque ripple is a inherent property of the DTC and its behaviour with different hysteresis bands seems to be quite coincidental with the chosen hysteresis band widths.

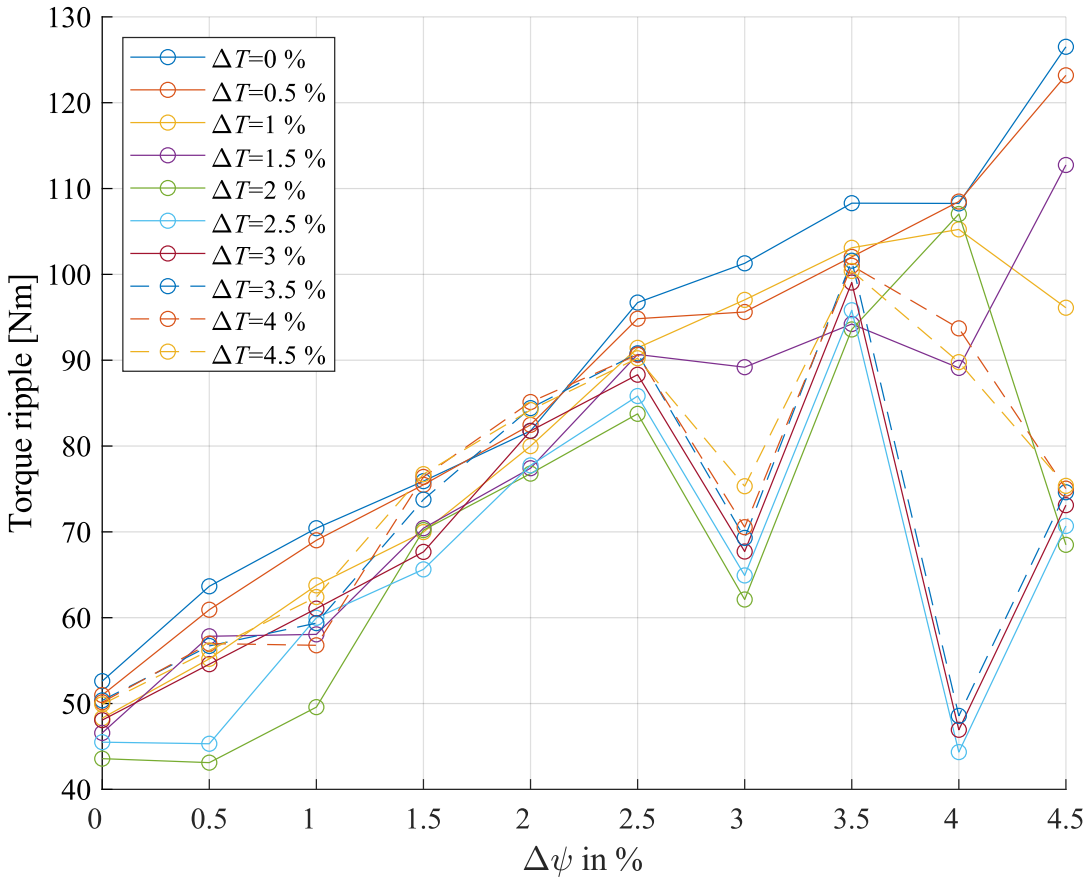

Figure 4.8: Torque ripple in steady-state with rated load torque.

More deviation in the torque ripple with different hysteresis bands widths can be observed when the load torque is active. Just like without the load the torque ripple with smaller torque hysteresis bands shows the highest ripples.

With some of the hysteresis band width combinations horrendous torque ripples were observed. Reason for this lies in the stator flux linkage hysteresis control and sector logic. Largest torque ripples happened when the hysteresis limits and the speed reference were chosen in a way that the stator flux linkage vector changed sector while its length was decreasing $\phi = 0$ and simultaneously torque had to be increased $\tau = 1$. Even though, the next chosen voltage vector was the right one according to the optimal switching table this next voltage vector could not effectively increase the torque until the stator flux linkage bit ϕ changed to 1. This problematic behaviour can be seen in the Fig. 4.9.

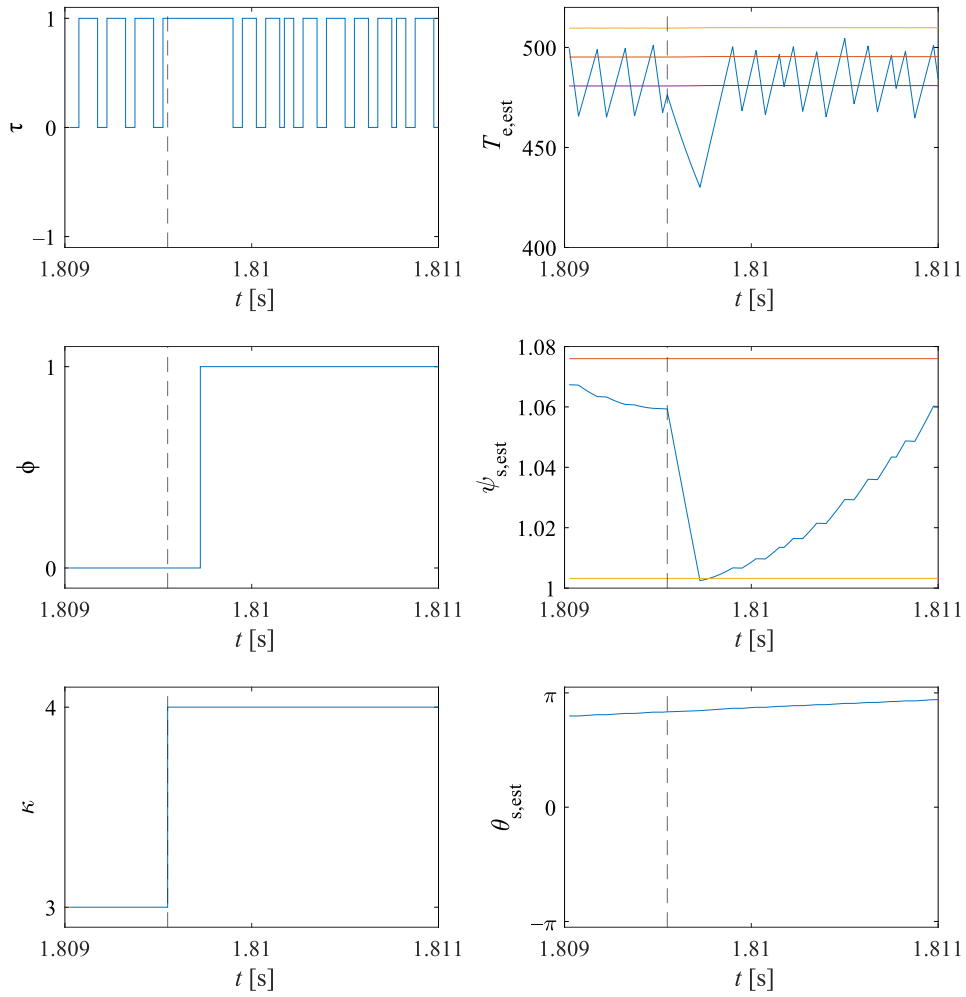

Figure 4.9: Hysteresis limits used were $\Delta\psi$ = 3.5 % and ΔT = 3 %. Torque ripple in this figure is about 70 Nm. Dashed line parallel to the y-axis represents the time instant that the stator flux linkage changes sector κ from 3 to 4.

As the stator flux linkage sector changes its sector a new voltage vector is selected. The new voltage vector starts to decrease the length of the stator flux linkage more aggressively. Meanwhile, the torque hysteresis controller output stays at $\tau = 1$ this new voltage vector could not increase the torque until the stator flux linkage vector length starts to increase with $\phi = 1$.

4.2 Effects of DTC sampling period

DTC sampling period simulations were conducted with four different sampling periods of 25 µs, 50 µs, 75 µs and 100 µs and hysteresis band widths were incremented in 0.5% steps from 0% to 2%. In total, 100 different simulations were executed with different hysteresis band widths and sampling period combinations. Simulations were 3 seconds long and load torque was activated at 2 s. Average switching frequencies with different hysteresis limits and sampling periods are shown in Figs. 4.10 and 4.11.

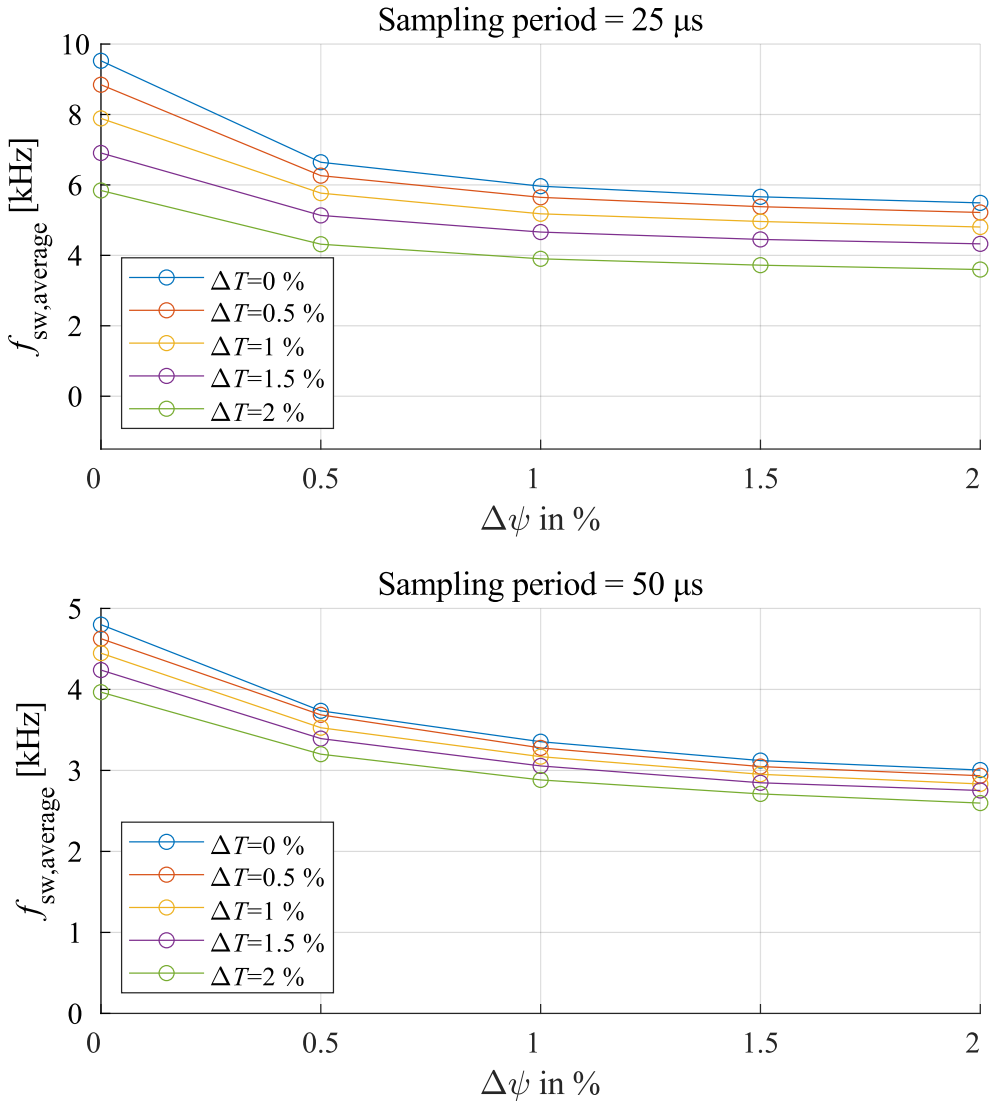

Figure 4.10: Average switching frequency as a functions of ΔT and $\Delta\psi$ with the DTC sampling periods of 25 µs and 50 µs. Time frame Δt used in the switching frequency calculation was 3 s. With the 25µs sampling period the average switching frequencies are the same as in the Fig. 4.1.

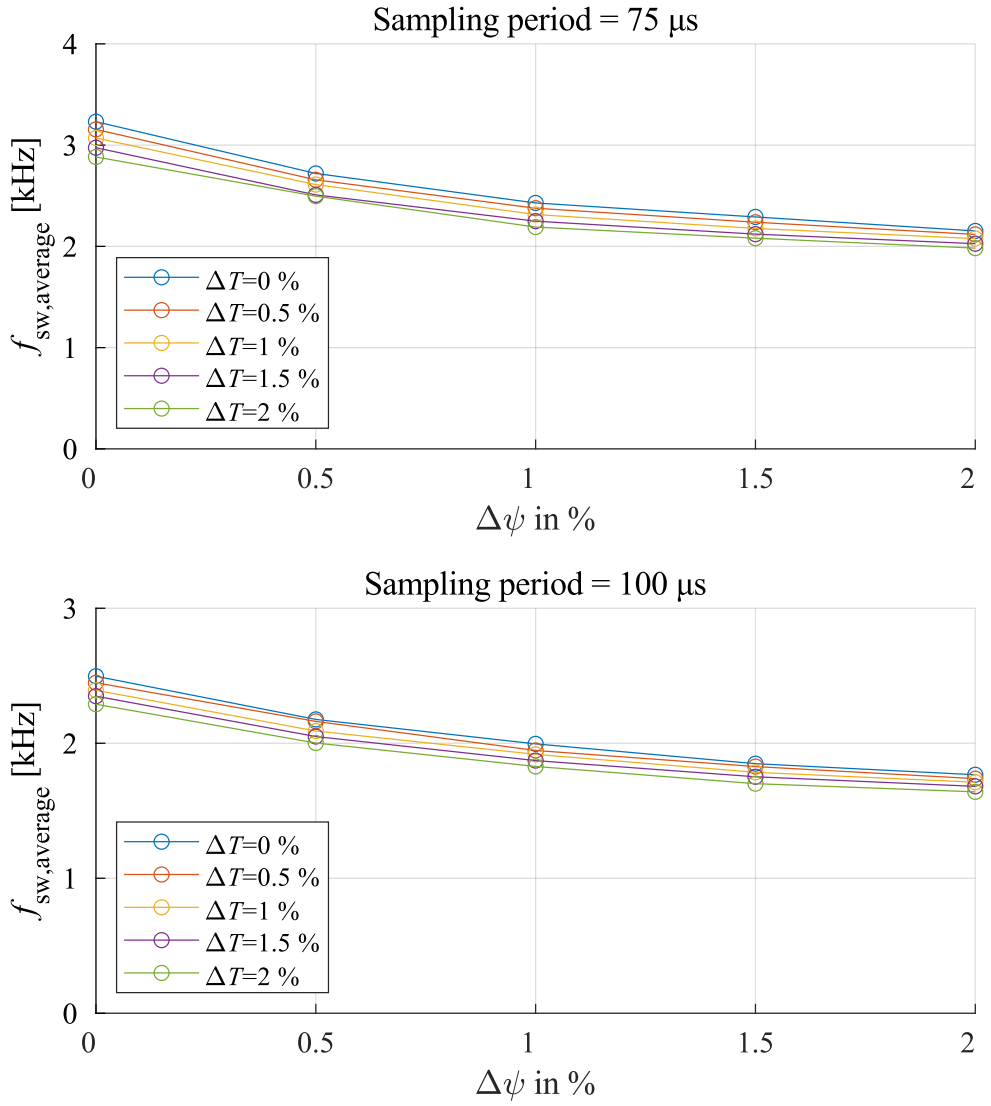

Figure 4.11: Average switching frequency as a functions of ΔT and $\Delta\psi$ with the DTC sampling periods of 75 µs and 100 µs. Time frame Δt used in the switching frequency calculation was 3 s.

Overall the DTC sampling period had a big impact on the average switching frequency. When the sampling period got longer the estimates and hysteresis controller states were updated more seldomly and thus the average switching frequency got lower. On the 100 µs sampling period the switching frequency plummeted even more and the differences between the different torque hysteresis limits vanished. Torque control was way too slow and the torque estimate constantly overshot the hysteresis limit regardless of the limit. Effect of the sampling period to the speed and torque can be seen in Fig. 4.12.

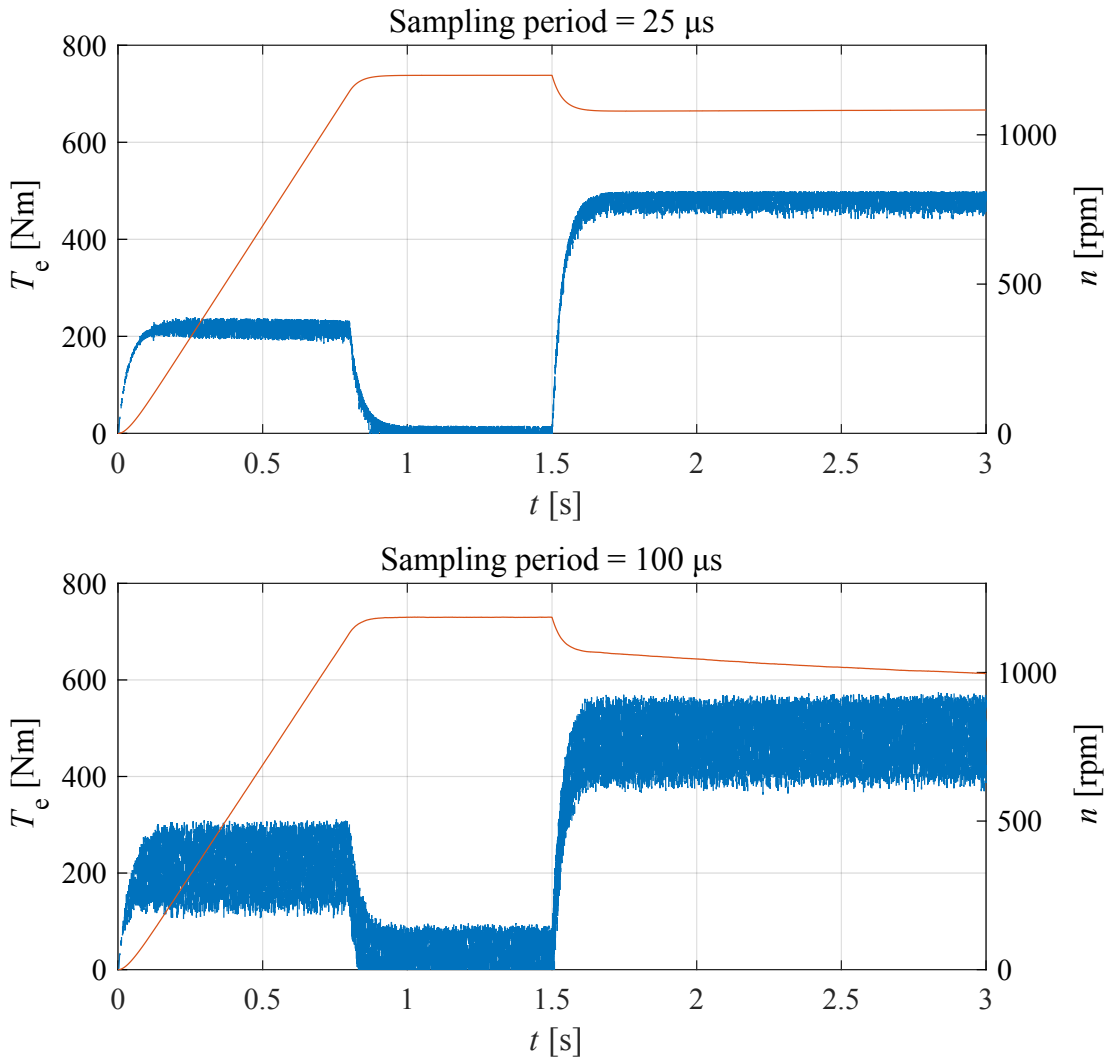

Figure 4.12: Torque and speed data of two simulations with 25 µs and 100 µs sampling periods. Hysteresis limits were ΔT = 1.5 % and $\Delta\psi$ = 1 %.

Even with the usual sampling period of 25 µs there were some torque ripple as the torque hysteresis controller had some issues to keep the torque estimate within the hysteresis limits. Raising the DTC sampling period made the torque ripple issue much worse. The optimal voltage vectors were updated too seldomly and thus the torque constantly overshot the hysteresis limits. In addition, with the 100 µs sampling period the system had problems in achieving acceptable speeds. When the load was introduced the motor speed started to drop down and it gradually descended to a value of 880 rpm.

4.3 Effects of different motor speed and load conditions

Effect of different loading conditions and speed references on the average switching frequency were also studied with simulations. Speed references went well into field weakening region with 12.5% steps from 25% to 200%n_s. Load torques went with 25% steps from 25% - 100%T_n and they were activated at simulation time 2 s. In total, 64 different simulations were executed with different combinations of motor and load conditions. Hysteresis band widths were constant $\Delta T = 1.5\%T_n$ and $\Delta\psi = 1\%\psi_{s,n}$. Average switching frequencies as a functions of rotor speed references are shown in Fig. 4.13.

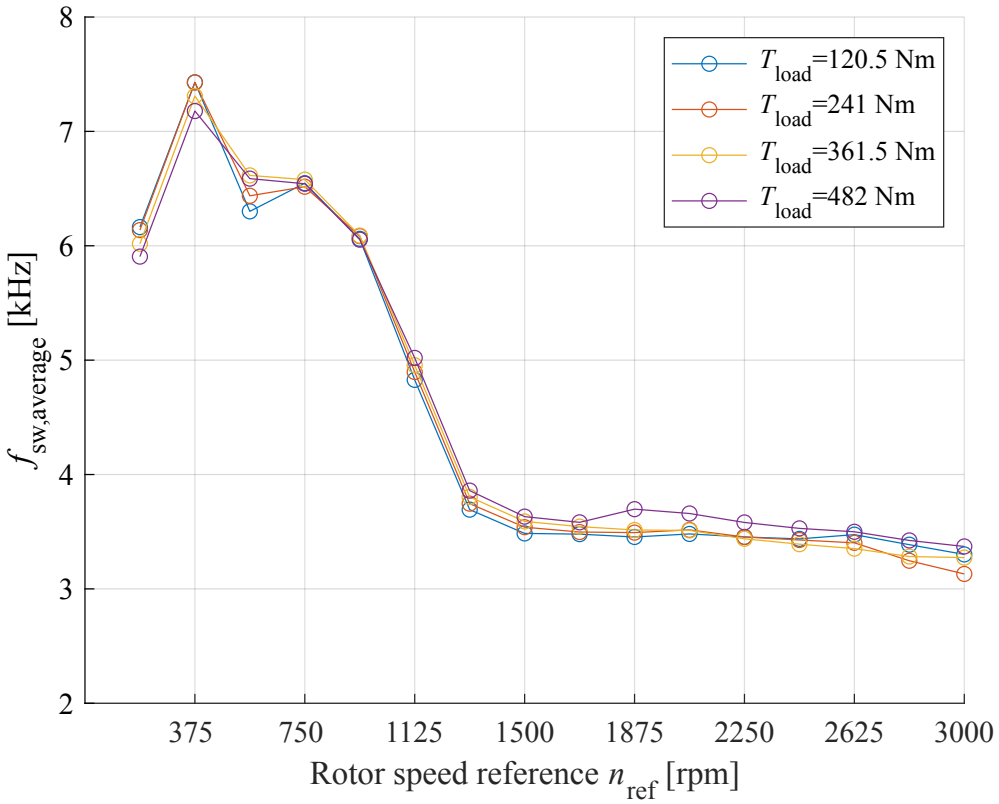

Figure 4.13: Time frame Δt used in $f_{sw,average}$ calculations were 3 s.

Average switching frequency as a function of rotor speed behaved quite counterintuitively. Switching frequency drops down as the rotor speed reference increases. Faster progression of the stator flux linkage vector around the $\alpha\beta$-plane origin resulted in less switching events. However, the average switching frequency did not drop down as aggressively anymore when the field weakening region had been reached even though the stator flux progression was faster around the $\alpha\beta$-plane. Reason for this lies in the fact that the circumference of the stator flux linkage reference circles in the $\alpha\beta$-plane got smaller as the stator flux linkage reference diminished.

It must be noted that in some simulations with the field weakening and higher load torques

the motor could not produce enough torque to maintain stable operation. This was due to the torque reference output in the Simulink model was saturated to ensure that the motors output power stays in somewhat realistic levels.

At lower speed references the average switching frequency was quite high. Without any switching frequency control the inverter could encounter issues in keeping up with the DTC system. Effect of the field weakening on the stator flux linkage estimate can be seen in Fig. 4.14.

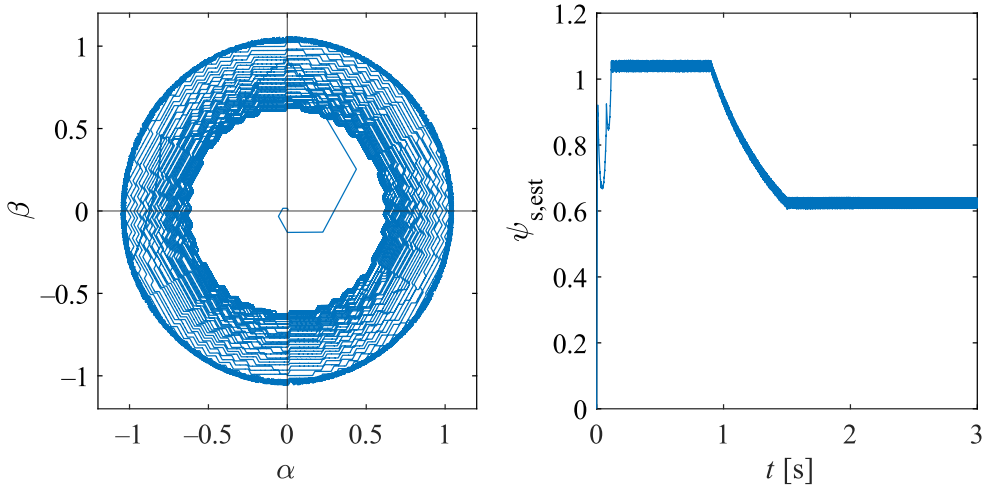

Figure 4.14: Stator flux linkage estimate $\psi_{\text{s,est}}$ in a $\alpha\beta$-plane and as a function of time with the load torque T_{load} = 241 Nm and the speed reference n_{ref} = 2250 rpm.

As the rotor speed increased above the 45 Hz speed the field weakening activated and the value of the stator flux linkage reference started to decrease. The stator flux linkage estimate followed the decreasing reference until the desired speed reference had been reached.

4.4 Effects of the different inductances

The effects of the inductances were also simulated with the DTC model. Stator leakage inductance, rotor leakage inductance and magnetizing inductance were all varied from 80 % to the 120 % of the nominal values in 10 % steps. In total, there were 125 different inductance combinations simulated. The DTC sampling period was 25 µs and the hysteresis band widths were constant $\Delta T = 1.5\%T_\mathrm{n}$ and $\Delta\psi = 1\%\psi_\mathrm{s,n}$. Speed reference was 1200 rpm, simulation time was 2 s and the rated load torque was activated at 1.5 s.

Based on the simulations the phase current RMS characteristics in startup, without a load and with the rated load torque were analyzed. Also the effects of inductances on the motor startup times and average switching frequencies were examined.

In the inductance simulations the current limiter and the speed reference ramp were disabled. As the speed reference was given as a step signal a higher torque references could be reached in the startup. Speed and torque curves with nominal inductances can be seen in Fig. 4.15.

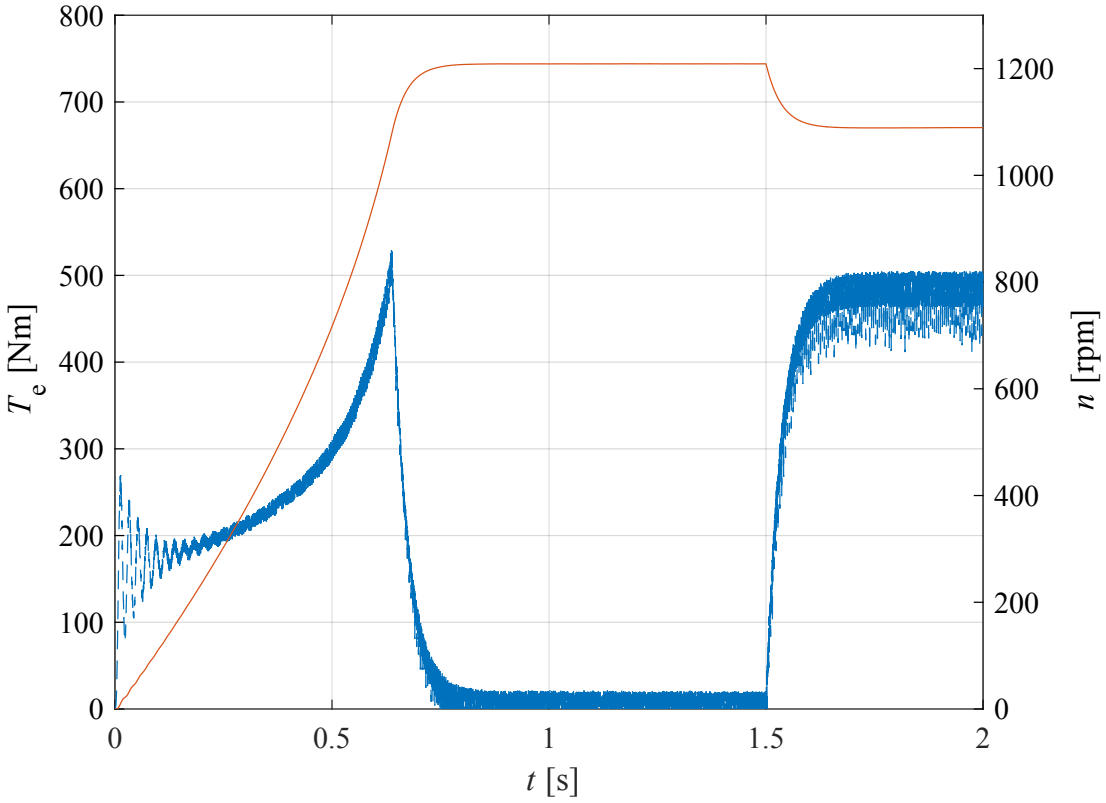

Figure 4.15: All of the inductance simulations were performed in a similar way. First the motor was started without load and at 1.5 s load torque was introduced.

4.4.1 Current characteristics

Simulation results of the RMS current characteristics with varying inductances in the startup are shown in Fig. 4.16. The motor was considered to be started when the rotor speed exceeded 1200 rpm.

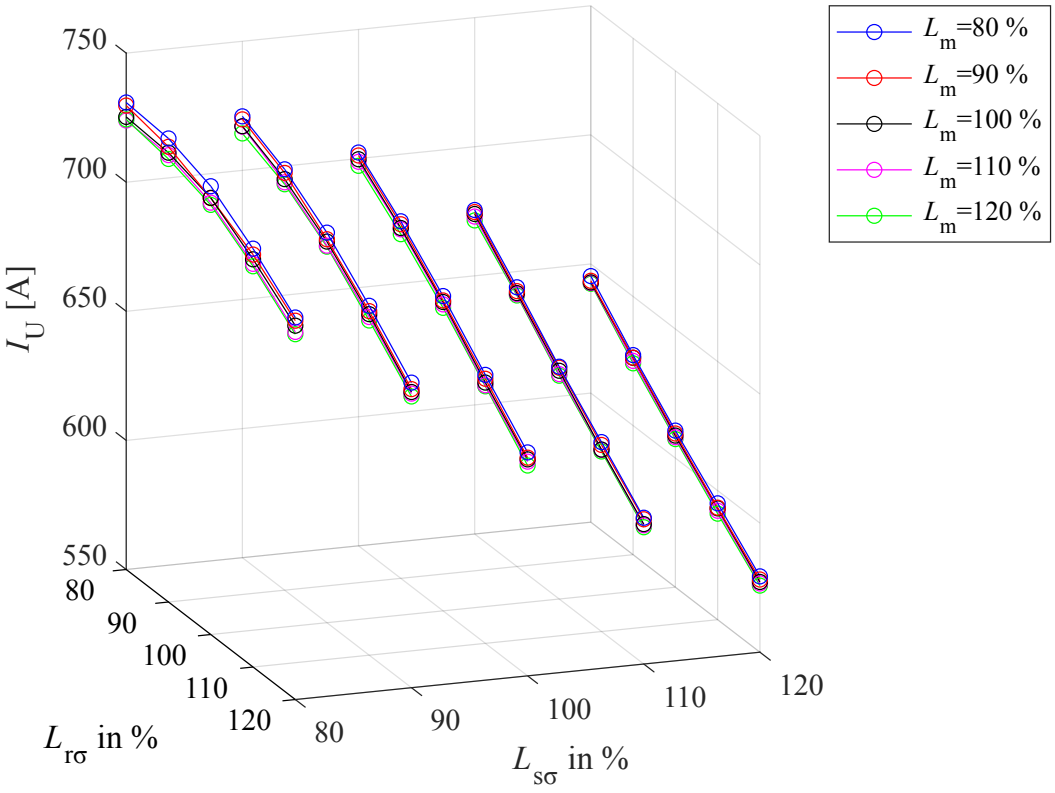

Figure 4.16: RMS currents during the startup without current or torque limitations.

Calculated RMS current values are in close proximity to each other with different values of magnetizing inductance. This shows that the startup currents are mostly affected by the stator and rotor leakage inductances. Increase in both leakage inductances lead to decrease in the startup stator currents. The figure also shows that the current drawn during the start can be 4-5 times the rated current if current limitation methods are not used, which is why the stator currents must be regulated in practice. In steady-states situation changes and it can be seen from the simulation results shown in Fig. 4.17.

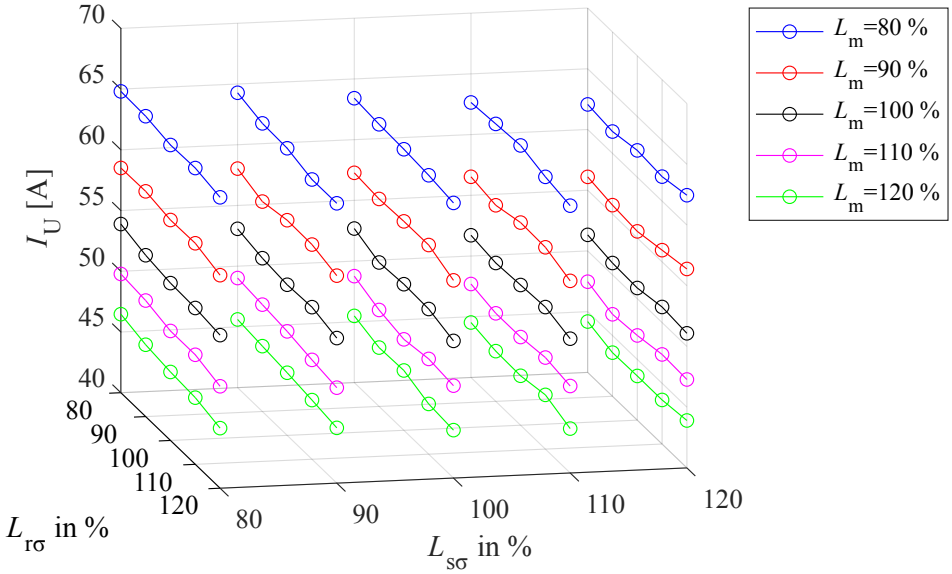

(a) Steady-state without load torque.

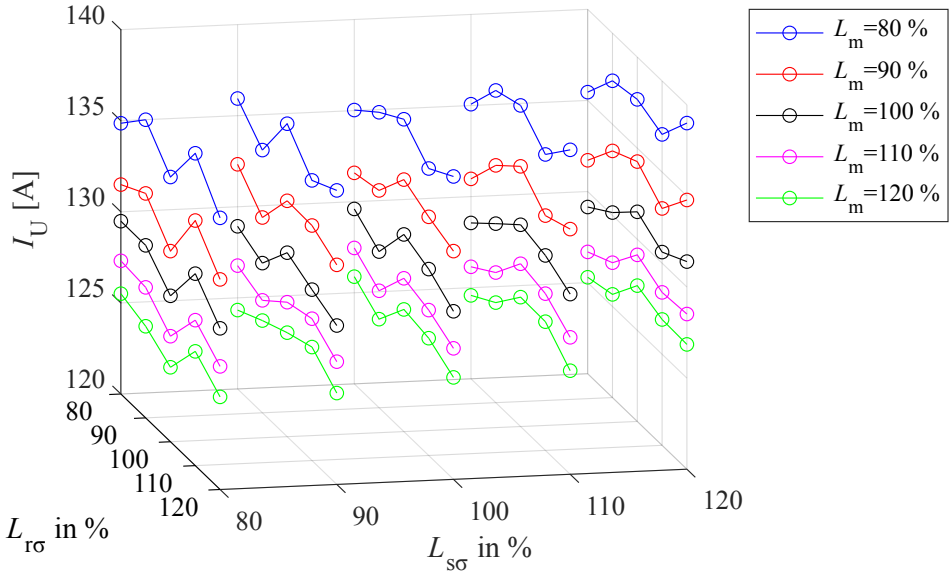

(b) Steady-state with rated load torque.

Figure 4.17: In a steady-state the leakage inductances do not have a large impact on the current drawn. Notable differences can be observed with different magnetizing inductance values.

4.4.2 Motor startup and torque rise time

Motor startup and torque rise times were also examined with different inductance values. Startup was considered performed when the rotor speed reached 1200 rpm. With a high torque reference and without current limitation there was small oscillation in the produced torque as seen in Fig. 4.15. So torque rise times tell how fast the torque reached the value T_e = 350 Nm after the torque oscillations had attenuated. This value was chosen because with some inductance values the speed reference was reached before the torque had enough time to rise to the rated value. Simulation results are shown in Fig. 4.18.

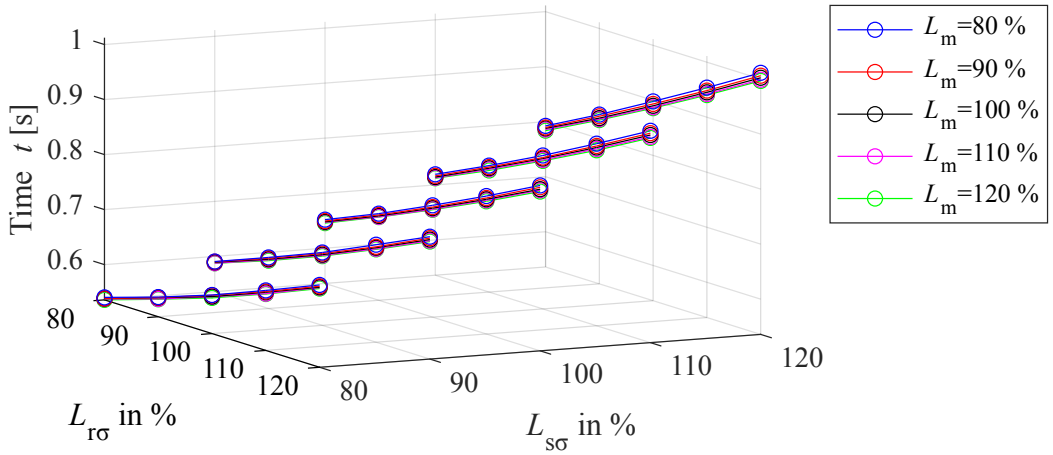

(a) Startup times.

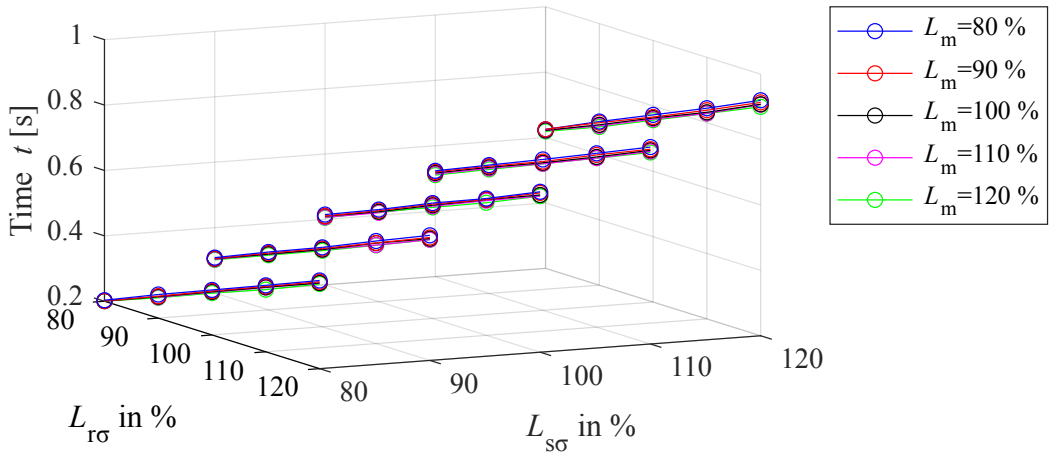

(b) Torque rise times.

Figure 4.18: Motor startup times and torque rise times as a functions of inductances.

With lower leakage inductances motor startup and torque rise takes less time as higher amount of the created flux participates in torque production. Varying the magnetizing inductance does not show any significant difference in the motor startup and torque rise times.

4.4.3 Average switching frequency

Average switching frequencies were also calculated with different inductance values. Calculation time frames were 2 s and the results are shown in Fig. 4.19.

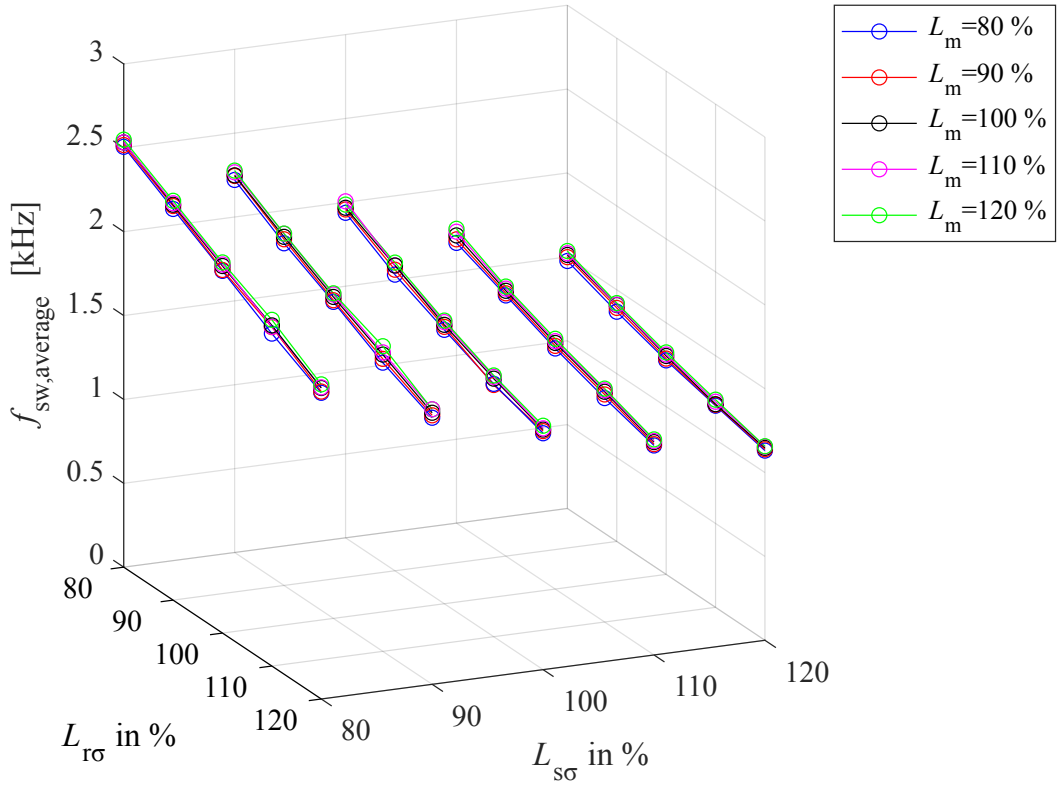

Figure 4.19: Average switching frequencies with different inductance values.

Different magnetizing inductances had barely no effect to the average switching frequency. Notable differences comes from the leakage inductances as the switching frequency diminished with higher leakage inductances. Higher switching frequencies with lower leakage inductances show that with lower leakage inductance values the stator flux linkage and the torque responds more quickly to the applied voltage vectors.

Reason that the switching frequencies differs so much from the switching frequencies in the hysteresis band and different speed and load simulations is that there is no speed ramp for the speed controller. This leads to high torque reference at the startup and the produced torque does not rise up to the reference instantly from the standstill. Consequently, the torque hysteresis controller output does not change as often.

4.5 Current limiting

Current limitation method was also briefly tested with the Simulink model. Simulations were 2 s long and the rated load torque was activated at 1.5 s. DTC sampling period was 25 µs and hysteresis band widths were constant $\Delta T = 1.5\%T_\mathrm{n}$ and $\Delta\psi = 1\%\psi_\mathrm{s,n}$. Current limit were 207 A, which is the peak value of the 146 A RMS current. Simulation results with current limiter off are shown in Fig. 4.20.

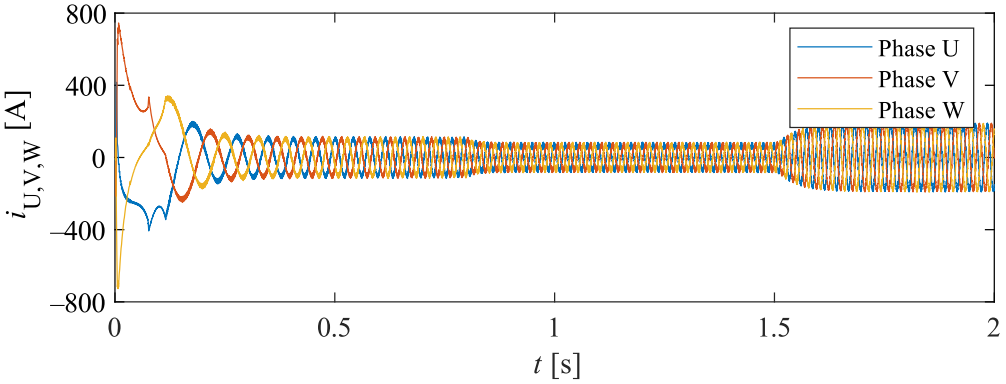

(a) Phase U, V and W current measurements with current limiter off.

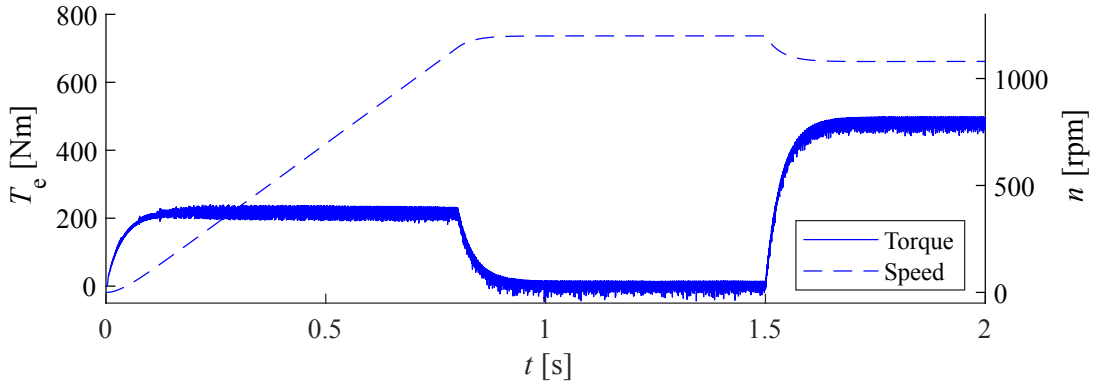

(b) Speed and torque with current limiter off.

Figure 4.20: RMS currents and speed and torque curves where the current limiter was disabled.

In the inductance simulations high startup currents were observed. This was because the speed reference was a step signal and therefore the torque reference at the startup was much higher. In this simulation the speed reference was created with a ramp and consequently PI-controller torque reference output was more restrained. However, phase V and W startup current peaks still reached almost 800 A which is about four times the peak amplitude of the rated current. Simulation results with current limiter on are shown in Fig. 4.21.

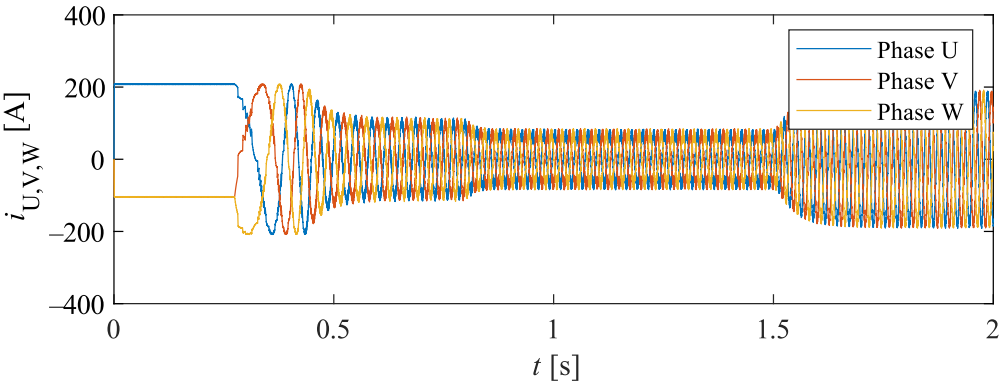

(a) Phase U, V and W current measurements with current limiter on.

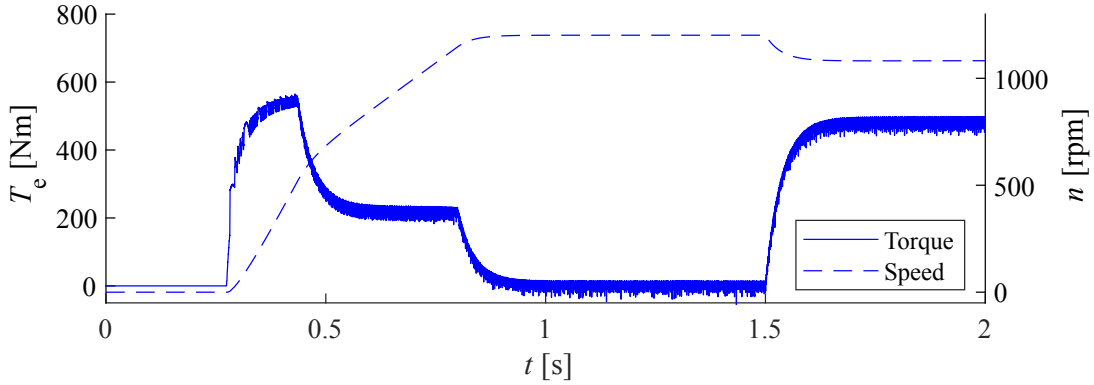

(b) Speed and torque with current limiter on.

Figure 4.21: RMS currents and speed and torque curves where the current limiter was enabled.

With the stator current limiter phase U, V and W startup currents were much lower. Phase U reached highest amplitude peak which was only a bit over 200 A during the torque delay. However, this stator current limiter implementation came with a downside of a longer startup time and therefore a relatively high DC magnetizing currents had to be supplied for a longer time.

4.6 Torque response

Torque response of the DTC system is often recalled as one of the fastest available. Earlier simulations had the speed controller feedforward loop disabled and because of this and modest PI-controller coefficients the torque references rose really calmly. To show the swiftness of the DTC system one simulation were executed where the speed controller feedforward loop was active. Speed reference was 1200 rpm, hysteresis controller limits were constant $\Delta T = 1.5\%T_\mathrm{n}$ and $\Delta\psi = 1\%\psi_\mathrm{s,n}$ and the rated load torque was activated at 1.5 s. Simulation results are shown in Fig. 4.22.

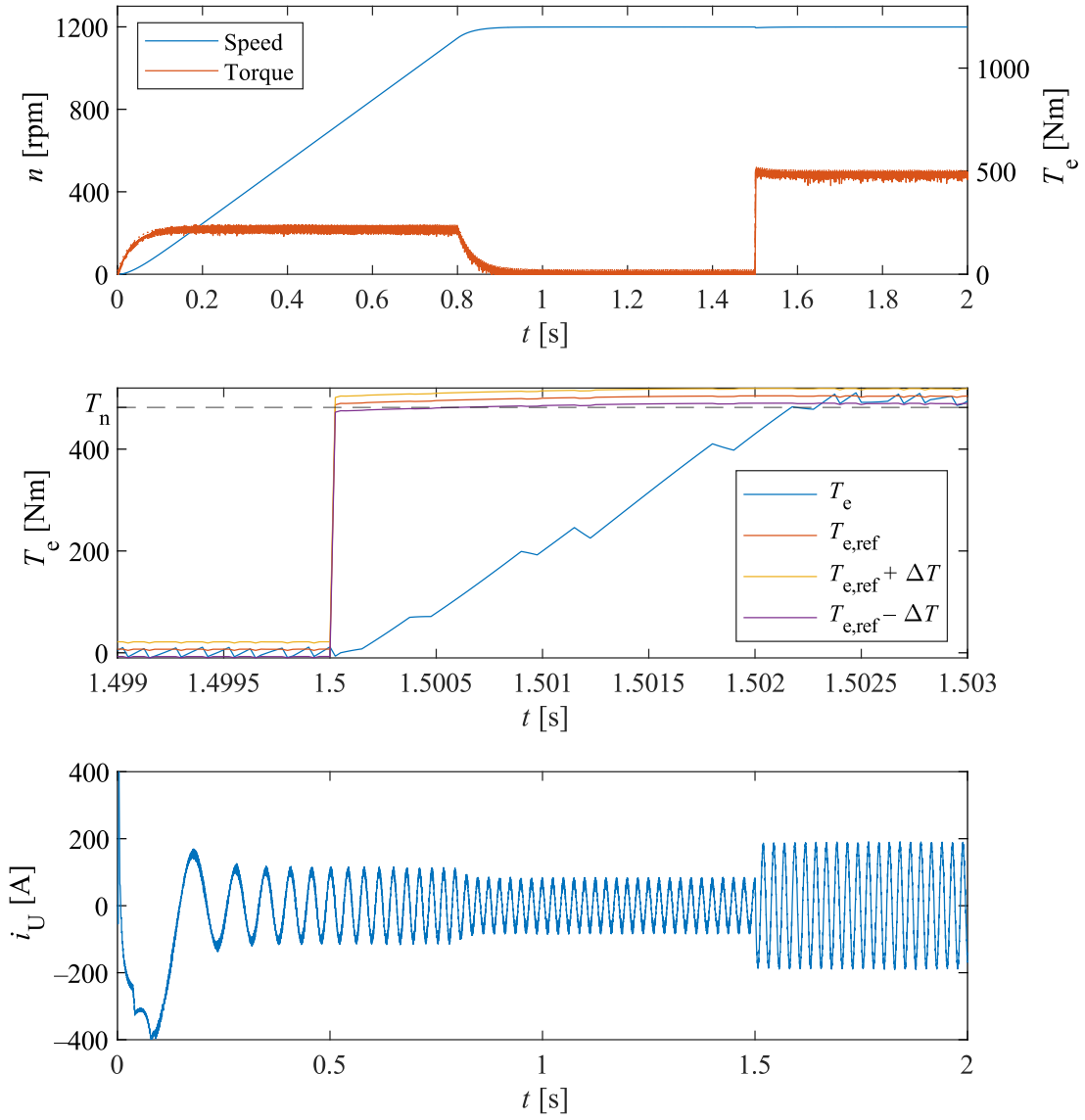

Figure 4.22: Speed, produced torque and phase U current when the speed controller feedforward loop was active.

From the figure it can be seen that when the the speed controller feedforwad loop was enabled the speed did not drop down when the load torque activated. Additionally, the torque responded really fast to the aggressive torque reference as the torque rise time is just a few milliseconds. Phase U current rose cleanly and swiftly to respond to a new torque demand.

5 Summary

In this thesis theory of the induction motor, space vectors, inverters and the DTC were reviewed in chapter two to an extent that was necessary for the creation of Simulink models. In chapter three a broad overview of the Simulink model was given and more detailed explanations were gathered to the appendices. With the DTC Simulink model multiple simulations were carried out to show how different parameters affected the control system. Simulations and simulation results were shown in chapter four.

The aim of this thesis was to create a DTC model in the Simulink by utilizing only the basic Simulink blocks. The motor model was done based on the induction motor state space model in the stator reference frame, which was supplied with a simplified inverter. Inverter modulation was done with the DTC subsystem. The DTC subsystem contains essential parts of the DTC: the two-level hysteresis controller for the stator flux linkage, three-level hysteresis controller for the torque, stator flux linkage estimator, torque estimator and the optimal switching logic.

On top of the DTC essentials a speed PI-controller, stator flux linkage reference subsystem, average switching frequency controller and stator current limiter were implemented. The speed PI-controller was used to give a torque reference for the torque hysteresis controller. The stator flux linkage reference subsystem gives a stator flux linkage reference for the stator flux linkage hysteresis controller. With the stator flux linkage reference subsystem it was possible to drive the motor in the field weakening region. Average switching frequency controller was used to adjust the stator flux linkage and torque hysteresis controller limits to achieve the desired switching frequency.

Stator current limiter was used to override the normal control logic if the stator current amplitude rose too high. Even though, the startup currents were more restrained with this stator current limiter implementation a better alternatives could have been sought. One simple way to limit the startup currents would have been more calm torque references at the startup by using a rate change limiter of the torque reference.

In the simulations, effects of the DTC sampling period, hysteresis limits, inductances and different speed and load conditions were studied. It was found out that higher sampling periods had a deteriorating effect on the operability of the DTC as the stator flux linkage and the torque estimates were updated and controlled more seldomly. Hysteresis band width simulations showed that the switching frequency is affected by the widths of the hysteresis bands and that it was highly varying during the simulations. With constant hysteresis band widths the highest switching frequencies were observed at the startup. Inductance simulations showed that with lower leakage inductances the motor reacted faster to the DTC. This is natural. In DTC control the motor leakage inductances are finally the limiting factors to torque changes. This makes the DTC the fastest torque controller, in principle.

Inherent property of the DTC as any PWM supply is a torque ripple and it was clearly shown in the hysteresis band width simulations. The torque ripples were calculated and it was found out that with some of the hysteresis limit combinations the torque ripple growed to horrendous proportions. Thus the hysteresis limits should be selected with care to minimize problems with the torque ripple. Other possible solution could be modifying the sector and stator flux linkage hysteresis logics in a way that shown problematic behaviour could be avoided.

The Simulink model does not take into consideration different operating points of the machine at all, which means that inductances and resistances are constant through the whole operating range. Even though the Simulink model had some simplifications it worked as expected. Future work regarding the models could consist of implementing realistic errors in the measurements to examine stator flux linkage drifting, modifying the inverter model further to correspond better with a real counterpart, implementing some kind of a thermal model to the motor model to take the varying resistances into account and some saturation modeling for the different inductances.

References

Alnasir, Z. and Almarhoon, A. (2012). Design of Direct Torque Controller of Induction Motor (DTC). *International Journal of Engineering and Technology*, 4, pp. 54–70.

Bose, B. (2001). *Modern Power Electronics And AC Drives*. Prentice Hall PTR. ISBN 0-13-016743-6.

Chapuis, Y. and Roye, D. (1998). Direct Torque Control and Current Limitation Method in Start up of an Induction Machine. pp. 451–455.

Depenbrock, M. (1985). Direkte Selbstregelung (DSR) für hochdynamische Drehfeldantriebe mit Stromrichterspeisung. *etzArchiv*, Bd 7, Heft 7, pp. 211–218.

Isao Takahashi, T.N. (1986). A New Quick-Response and High-Efficiency Control Strategy of an Induction Motor. *IEEE Transactions on industry applications*, 1A-22(5), pp. 820–827.

Juha Pyrhönen, Valéria Hrabovcová, R.S.S. (2016). *Electrical Machine Drives Control - An Introduction*. John Wiley & Sons Ltd. ISBN 9781119260455.

Juha Pyrhönen, Tapani Jokinen, V.H. (2008). *Design Of Rotating Electrical Machines*. John Wiley & Sons Ltd. ISBN 978-0-470-69516-6.

Kaukonen, J. (1999). *Salient Pole Synchronous Machine Modelling in an Industrial Direct Torque Controlled Drive Application*. Dissertation. Lappeenranta University of Technology. ISBN 951-764-305-5, ISSN 1455-4491.

Károly Pál Kovács, I.R. (1954). *Transiente Vorgänge in Wechselstrommaschinen*. Verlag der ungarischen Akademie.

Lassi Aarniovuori, Hannu Kärkkäinen, M.N. (2018). Modelling a Vector Controlled Induction Motor in Simulink.

Ned Mohan, Tore M. Undeland, W.P.R. (1995). *Power Electronics: Converters, Applications and Design*. John Wiley & Sons, inc. ISBN 0-471-58408-8.

Ong, C.M. (1998). *Dynamic Simulation of Electric Machinery using Matlab/Simulink*. Prentice Hall PTS. ISBN 0-13-723785-5.

Park, R.H. (1929). Two-Reaction Theory of Synchronous Machines, Generalized Method of Analysis - Part I. *AIEE Transactions*, 48, pp. 716–727. doi:10.1109/T-AIEE.1929.5055275.

Tarkiainen, A. (1999). *Sähkökäyttöjen kaapelivärähtelyt*. Master's thesis. Lappeenrannan teknillinen yliopisto. url: `https://lutpub.lut.fi/handle/10024/35200`.

Tiitinen, P. (1996). The Next Generation Motor Control Method, DTC Direct Torque Control.

W.C. Duesterhoeft, Max W. Schulz, E.C. (1951). Determination of Instantaneous Currents and Voltages by Means of Alpha, Beta and Zero Components. *AIEE Transactions*, 70, pp. 1248–1255. doi:10.1109/T-AIEE.1951.5060554.

A Appendix Simulink base model

The Simulink base model consists of three main subsystems: DTC model, inverter and induction motor model in stator reference frame. DTC model includes all of the control logic related to the DTC and it is further explained in Appendix C.

Inverter is heavily simplified so it only contains a binary multiplication with the switch states $S_{\mathrm{U,V,W}}$ and DC-link voltage U_{DC}. Induction motor model in stator reference frame contains motor model derived from the state space model. Load torque is brought to the base system with a step function. Speed reference and stator flux linkage reference has their own subsystems and their Simulink implementations are shown in Appendix D. The Simulink base model is shown in Fig. A.1.

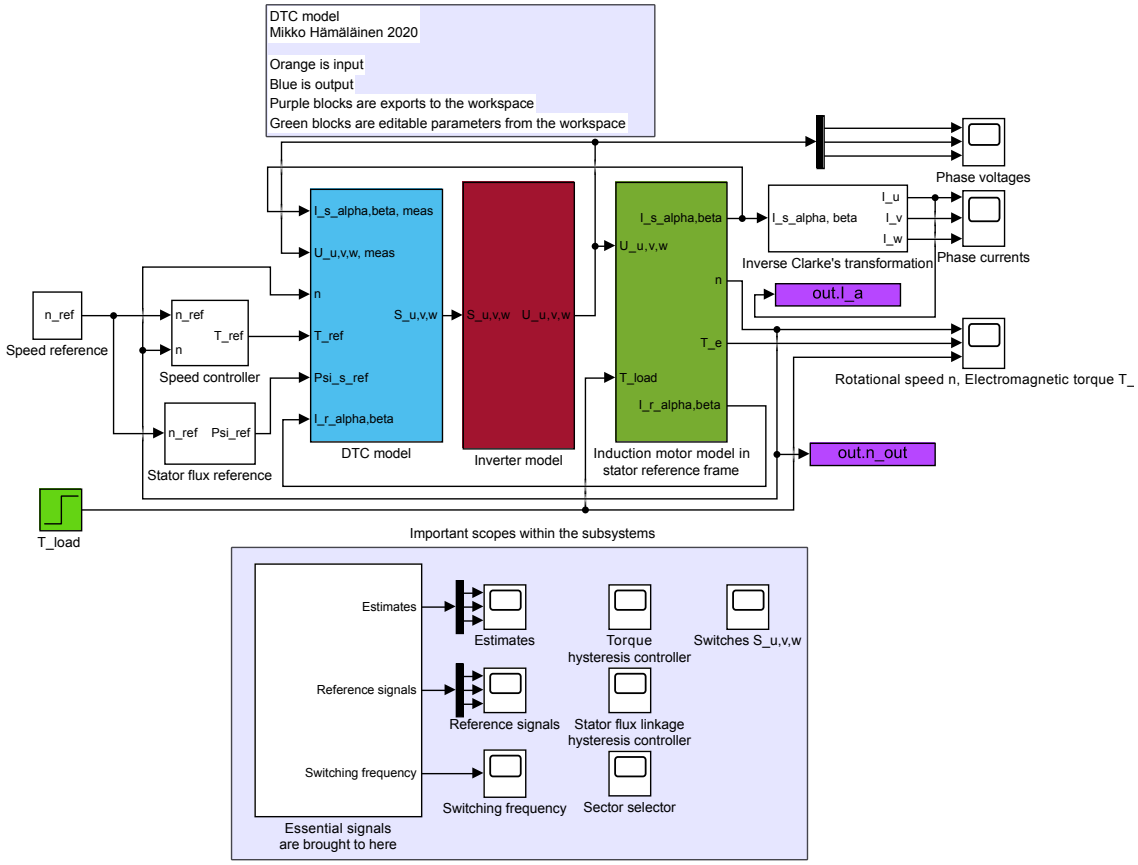

Figure A.1: Simulink base system model.

B Appendix Induction motor Model

Induction motor model derived from the state space model is shown in Fig. B.1.

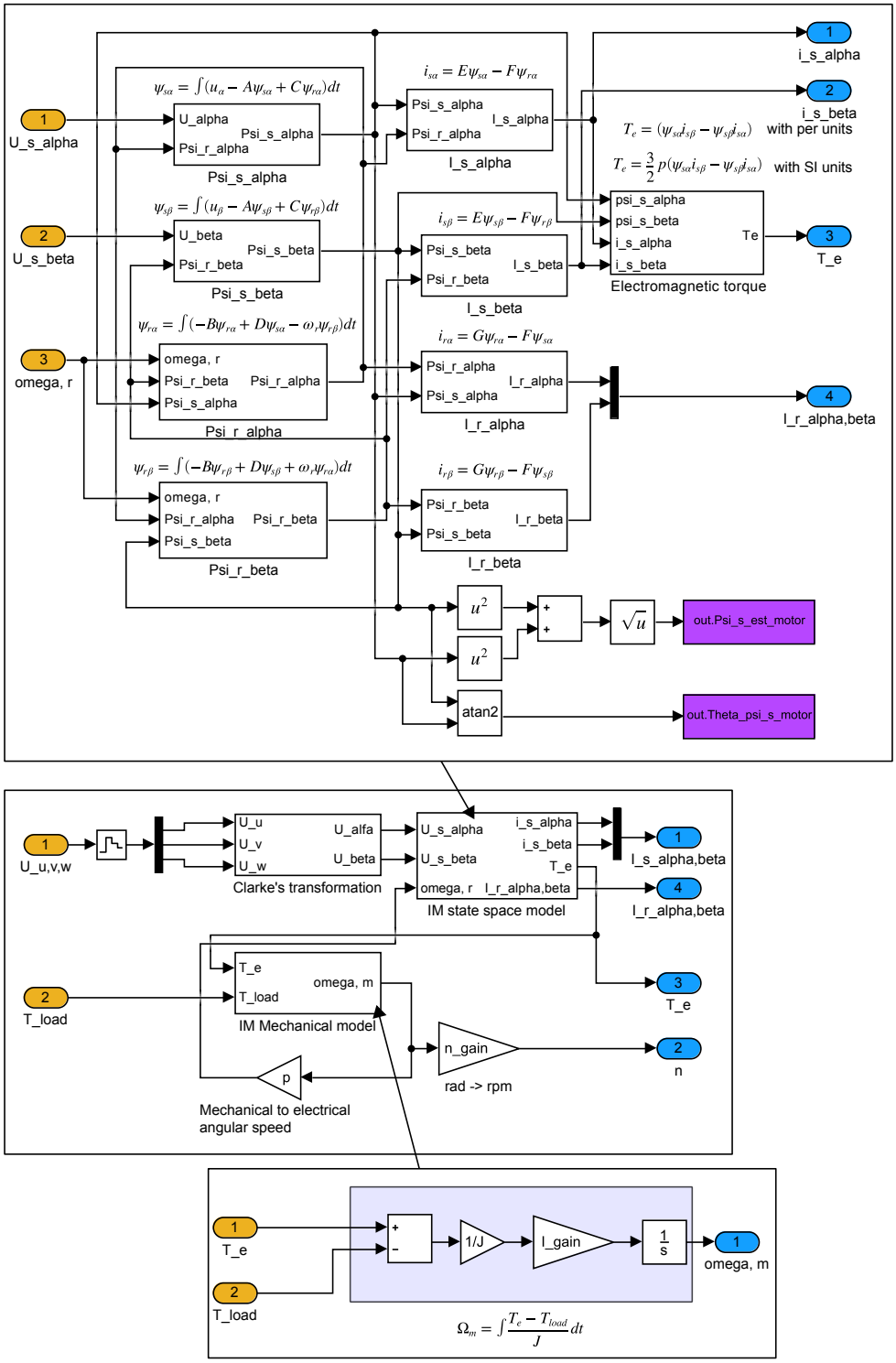

Figure B.1: Induction motor model subsystem.

C Appendix DTC Model

Created Simulink DTC model subsystem and its subsystems are explained in following subsections.

C.1 DTC model

In the DTC model subsystem there are seven subsystems: Speed controller feedforward component, DTC estimators, DTC controllers, Optimal switching table, Stator current limiter, Average switching frequency calculator and Hysteresis limits controller. DTC model inputs are voltage, stator and rotor currents, speed and reference signals. Output is switch states $S_{\mathrm{U,V,W}}$. Simulink DTC model subsystem is shown in Fig. C.1.

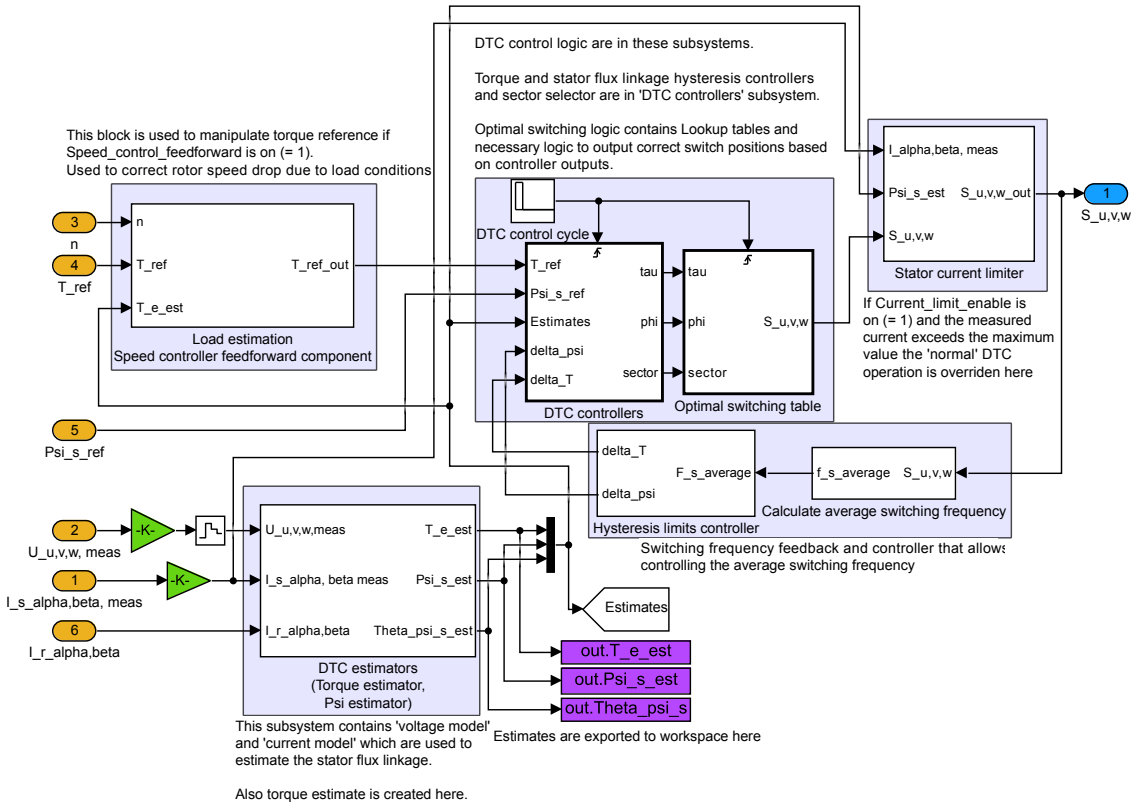

Figure C.1: DTC model subsystem holds most of the necessary calculations and logic for the DTC.

C.2 DTC Estimates

DTC estimators uses motor voltage and current measurements in stator reference frame as inputs and outputs the estimated absolute value of the stator flux linkage, torque and the stator flux linkage vector angle. Psi estimators within the DTC estimators subsystem creates stator flux linkage estimates with the voltage model Eq. (2.43) and the current model Eq. (2.42). A stator flux linkage estimate is calculated with the voltage model in every simulation step, which is every 5 µs, and with the current model every 1 ms. Current model correction can be toggled on or off from the created m-file. Torque estimator realizes the Eq. (2.36) to produce torque estimate with the stator flux linkage estimate. DTC estimators Simulink implementation is shown in Fig. C.2.

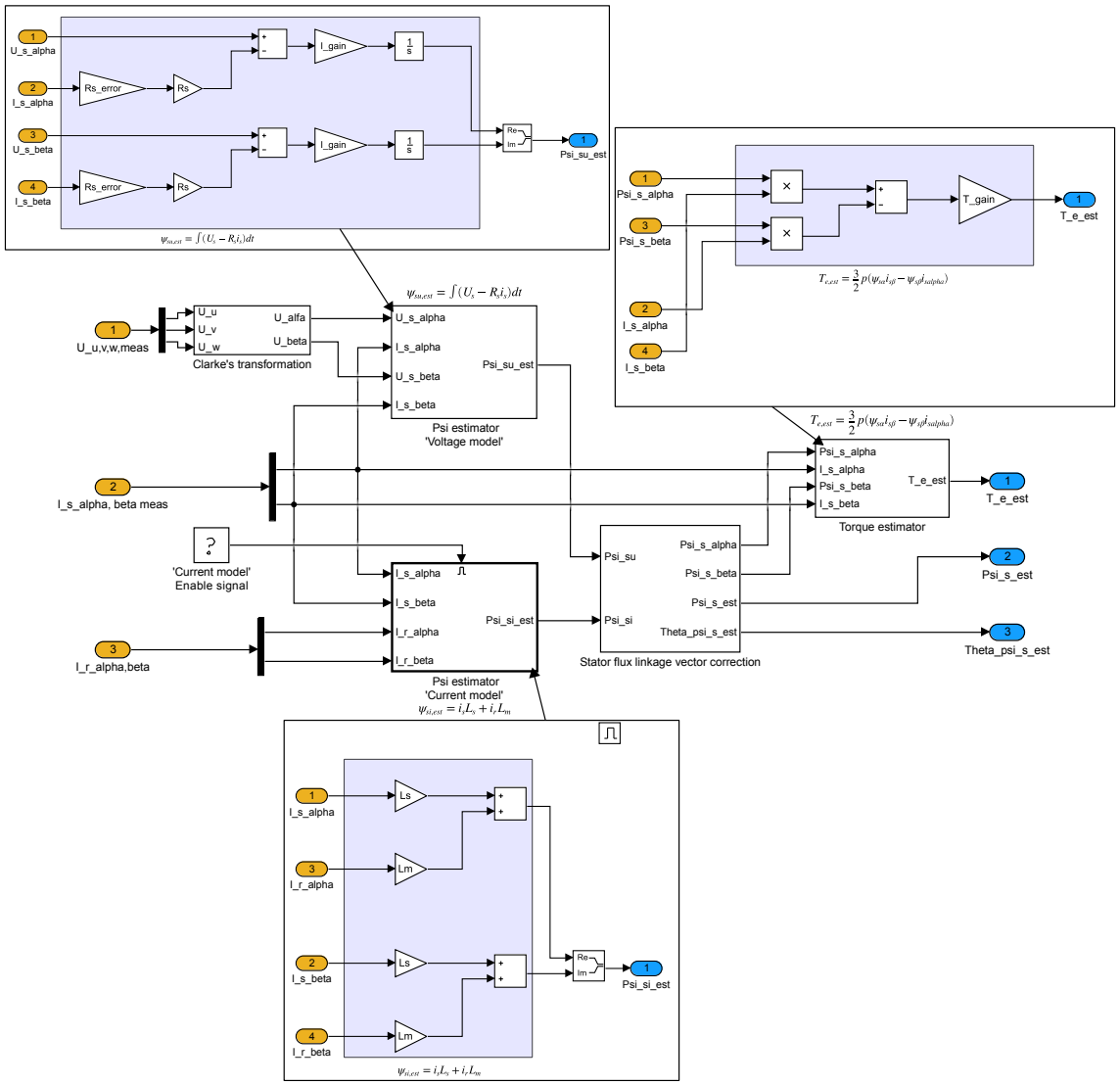

Figure C.2: Within the DTC estimators subsystem the torque estimate, the voltage model and current model equations are realized.

C.3 DTC controllers

DTC controllers subsystem includes stator flux linkage and torque hysteresis controllers and sector logic. This subsystem is triggered every 25 µs. The stator flux linkage and torque reference and estimate signals are brought as inputs here and supplied to the controllers. Subsystem outputs the control signals τ, ϕ and κ.

Depending on the value of the Switching_frequency_control_enable variable the switching frequency control is either on or off. When switching frequency control is off the hysteresis limits are constants which are initialized in the m-file. Switching frequency control is enabled or disabled in the m-file. DTC controllers Simulink implementation is shown in Fig. C.3.

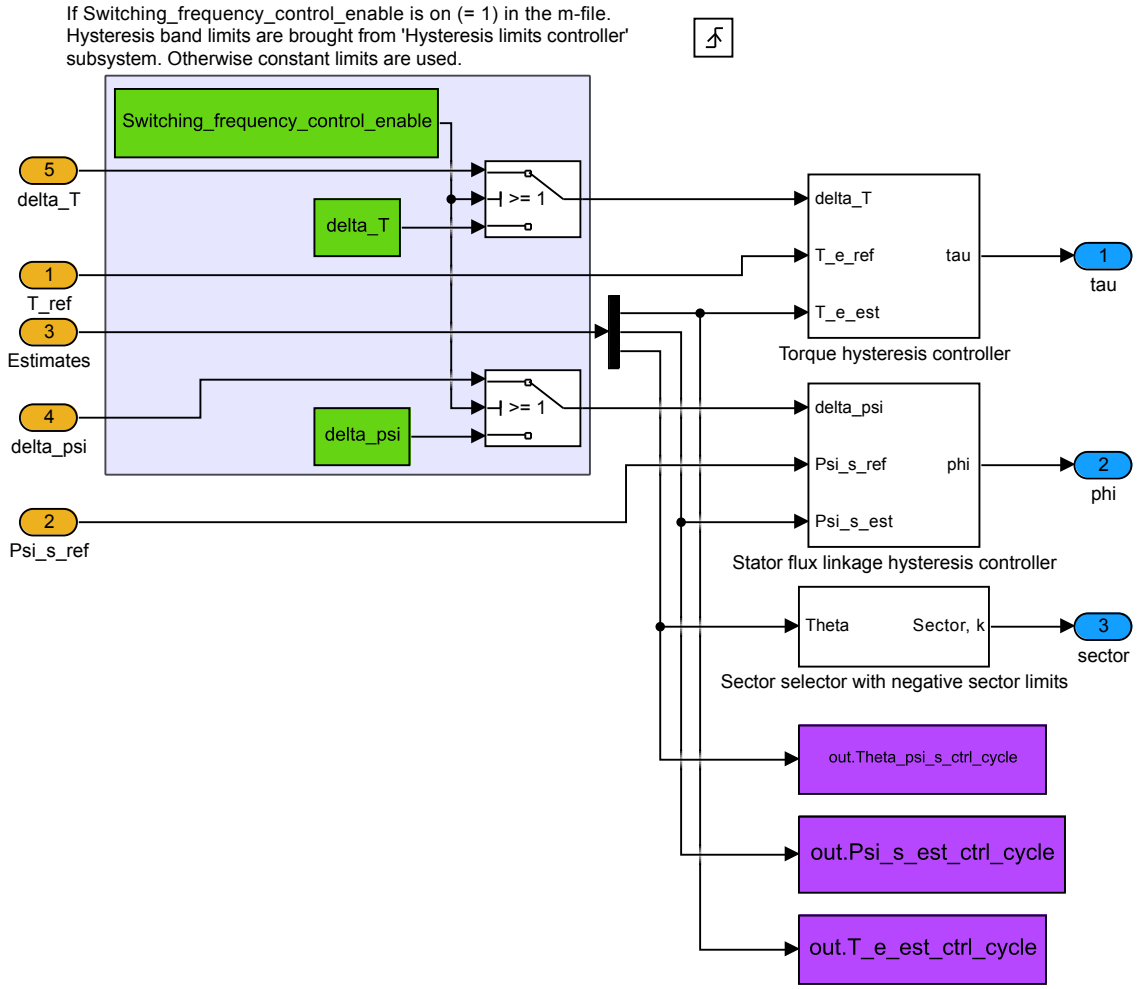

Figure C.3: DTC controllers subsystem includes hysteresis controllers and sector logic.

C.4 Hysteresis controllers

Three-level hysteresis controller for the torque was realized with an else-if ladder. First the error T_{err} between the reference and estimate signals is calculated with a sum block. Then the controller output is updated to a new value by comparing the error to the hysteresis limits and the last controller state stored in the memory block. Torque hysteresis controller Simulink implementation is shown in Fig. C.4.

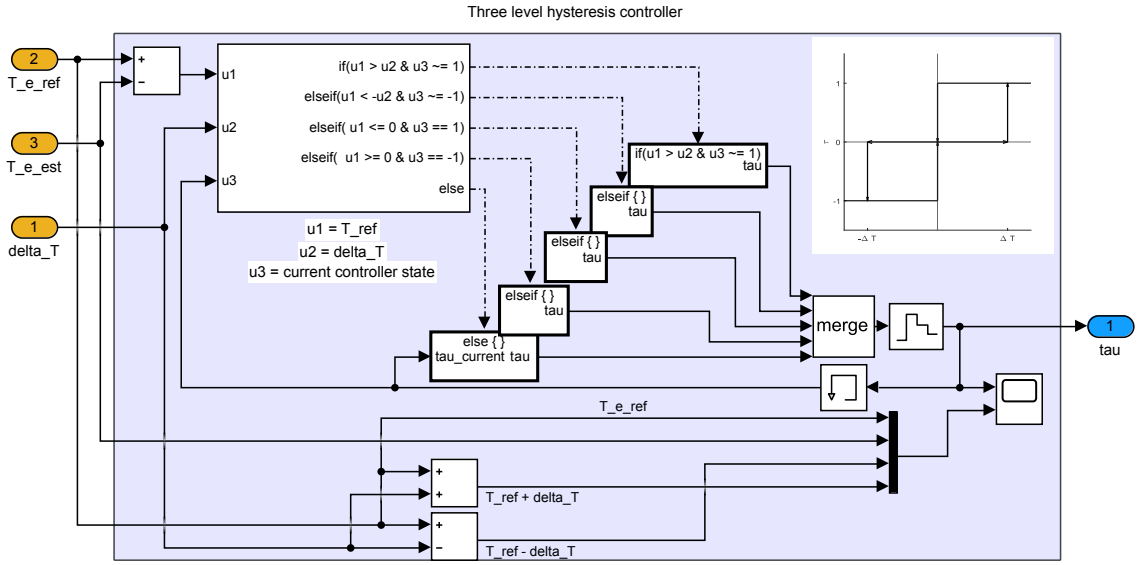

Figure C.4: Three-level hysteresis controller subsystem for the torque.

Two-level hysteresis controller for the stator flux linkage was realized with a controllable switch, two relational operators and memory block. The error ψ_{err} between the reference and estimate signal is calculated with a sum block and the difference is compared to the hysteresis limit. Controllable switch input port is depended on the memory block output. Stator flux linkage hysteresis controller Simulink implementation is shown in Fig. C.5.

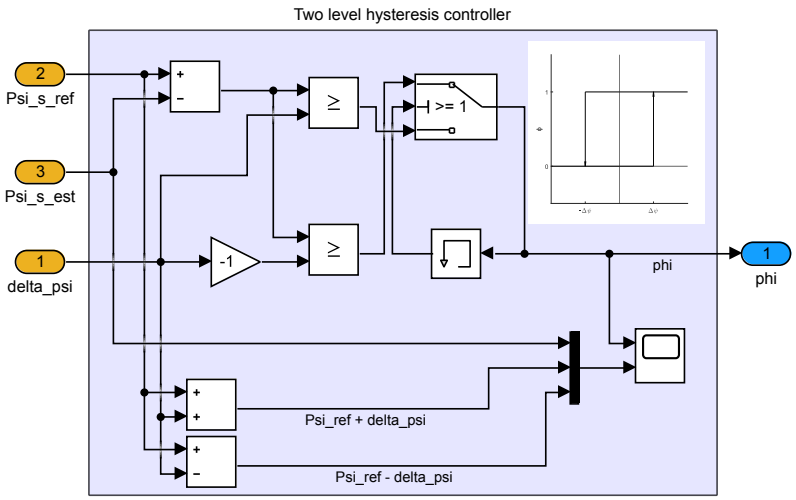

Figure C.5: Two-level hysteresis controller subsystem for the stator flux linkage.

If the state stored in the memory block is 0 the switch input port three is active. When switch input three becomes true as the upper hysteresis limit is reached, the memory block state changes to 1 and switch input port one activates. Now the output of the hysteresis controller is the state of the lower relational operator. Output stays at 1 and the input port one stays active until the error drops below or is equal to the lower hysteresis limit. When lower hysteresis limit is reached the controller output changes to 0 and input port three activates.

C.5 Sector logic

Sector selector utilizes combinational logic to determine in which sector the stator flux linkage vector currently is at. The subsystem input stator flux linkage vector angle θ is compared to the sector limits and if the angle is between the certain limits the corresponding sector number is outputted. Sector limit angles given in table 2.1 are from 0 to 2π. As the atan2 outputs angles from -π to π the sector limits were modified to accompany this change. New modified limits are shown in table C.1 and the sector logic Simulink implementation is shown in Fig. C.6.

Table C.1: Modified sector limits

$\kappa(1)$	$\kappa(2)$	$\kappa(3)$	$\kappa(4)$	$\kappa(5)$	$\kappa(6)$
$[-\frac{\pi}{6}, \frac{\pi}{6}]$	$[\frac{\pi}{6}, \frac{\pi}{2}]$	$[\frac{\pi}{2}, \frac{5\pi}{6}]$	$[\frac{5\pi}{6}, -\frac{5\pi}{6}]$	$[-\frac{5\pi}{6}, -\frac{\pi}{2}]$	$[-\frac{\pi}{2}, -\frac{\pi}{6}]$

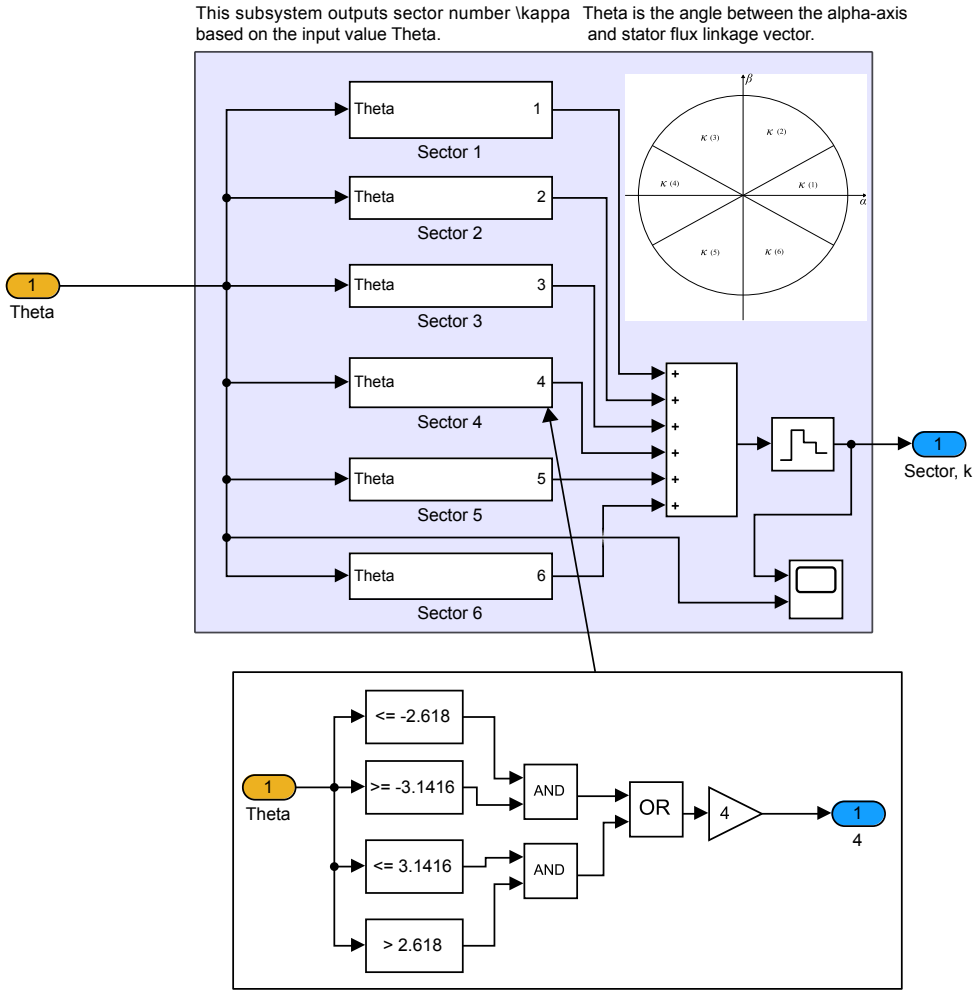

Figure C.6: Sector selector subsystem.

C.6 DTC Optimal switching table and logic

Inputs of the optimal switching table subsystem are the control signals τ, ϕ and κ. Output of the subsystem is the switch states $S_{U,V,W}$. States of the switches shown in table 2.2 were decoupled and implemented in the Simulink with three two-dimensional lookup tables. Every switch has its own lookup table. Each lookup table has six columns, one for each sector, and six rows for the torque τ and stator flux linkage ϕ control signals. Simulink implementation is shown in Fig. C.7.

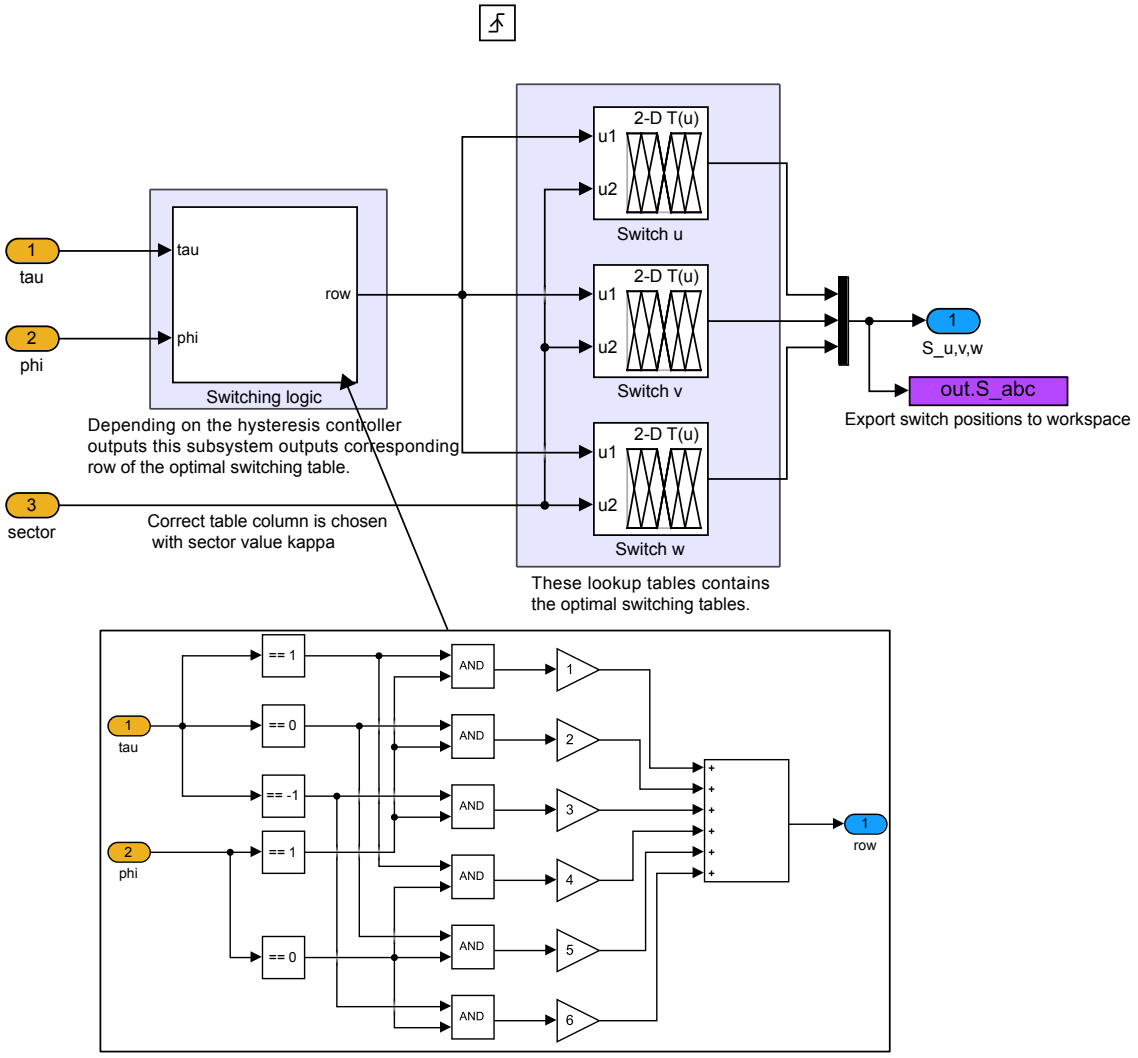

Figure C.7: Optimal switching table subsystem contains the row and three lookup tables, one table for each of the inverter switches.

Simulink lookup table outputs the switch state based on the row and column input signals. Column input signal comes straight from the sector selector subsystem. Row input signal has its own logic based on the states of the torque and stator flux linkage hysteresis controllers. Lookup table used for the switch S_U is shown in table C.2 and lookup tables for switches S_V and S_W were implemented in a similar way.

Table C.2: Optimal switching table for VSI switch S_{U}

ϕ	τ	$\kappa = 1$	$\kappa = 2$	$\kappa = 3$	$\kappa = 4$	$\kappa = 5$	$\kappa = 6$
$\phi = 1$	$\tau = 1$	1	0	0	0	1	1
	$\tau = 0$	0	1	0	1	0	1
	$\tau = -1$	1	1	1	0	0	0
$\phi = 0$	$\tau = 1$	0	0	0	1	1	1
	$\tau = 0$	0	1	0	1	0	1
	$\tau = -1$	0	1	1	1	0	0

C.7 Stator current limiter

Stator current limiter implementation calculates absolute value of the stator current in stator reference frame and compares it to the predetermined maximum current limit. If the stator current is equal or exceeds the maximum current a zero vector is passed to the inverter. Also torque delaying makes sure that constant voltage vector applied until the reference stator flux linkage has been reached during the startup. Stator current limiter is toggled on or off in the m-file by changing the value of Current_limit_enable. Stator current limiter Simulink implementation is shown in Fig. C.8.

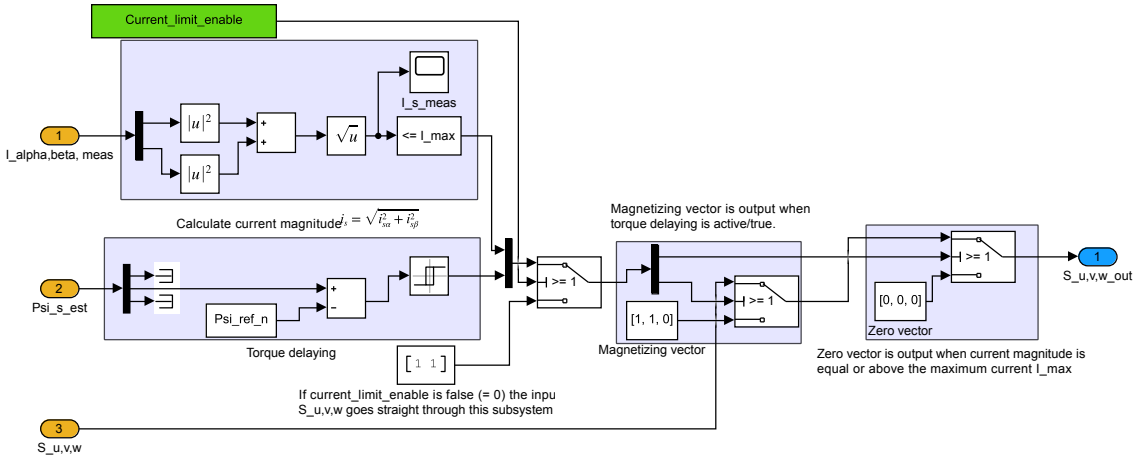

Figure C.8: Stator current limiter subsystem.

C.8 Average switching frequency control

Input of the average switching frequency calculator subsystem is the switch states from the stator current limiter subsystem. Average switching frequency is calculated by comparing the delayed values of the inverter switches to the current switch states. If any of the switch states has changed the counter value is increased by 1. Every 5 ms the counter value is divided with Δt = 5 ms to get the value of the average switching frequency. Counter value is reset every time the average switching frequency has been calculated. Subsystem output $f_{\mathrm{s,average}}$ is held constant until a new value is calculated. Switching frequency calculator Simulink implementation is shown in Fig. C.9.

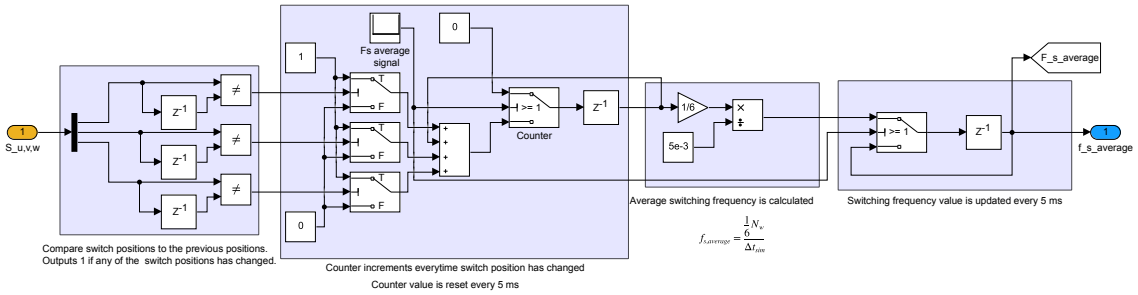

Figure C.9: Average switching frequency calculator subsystem.

Hysteresis limit controller subsystem input is the average switching frequency $f_{\mathrm{s,average}}$. This is fed to the PI-controller which calculates error between the desired switching frequency value and the current switching frequency value. PI-controller output is supplied to an else-if ladder which then increases or decreases the hysteresis band widths by adjusting a coefficient used in the calculation of the hysteresis band widths. Hysteresis limits are adjusted every 5 ms. Hysteresis limit controller Simulink implementation is shown in Fig. C.10.

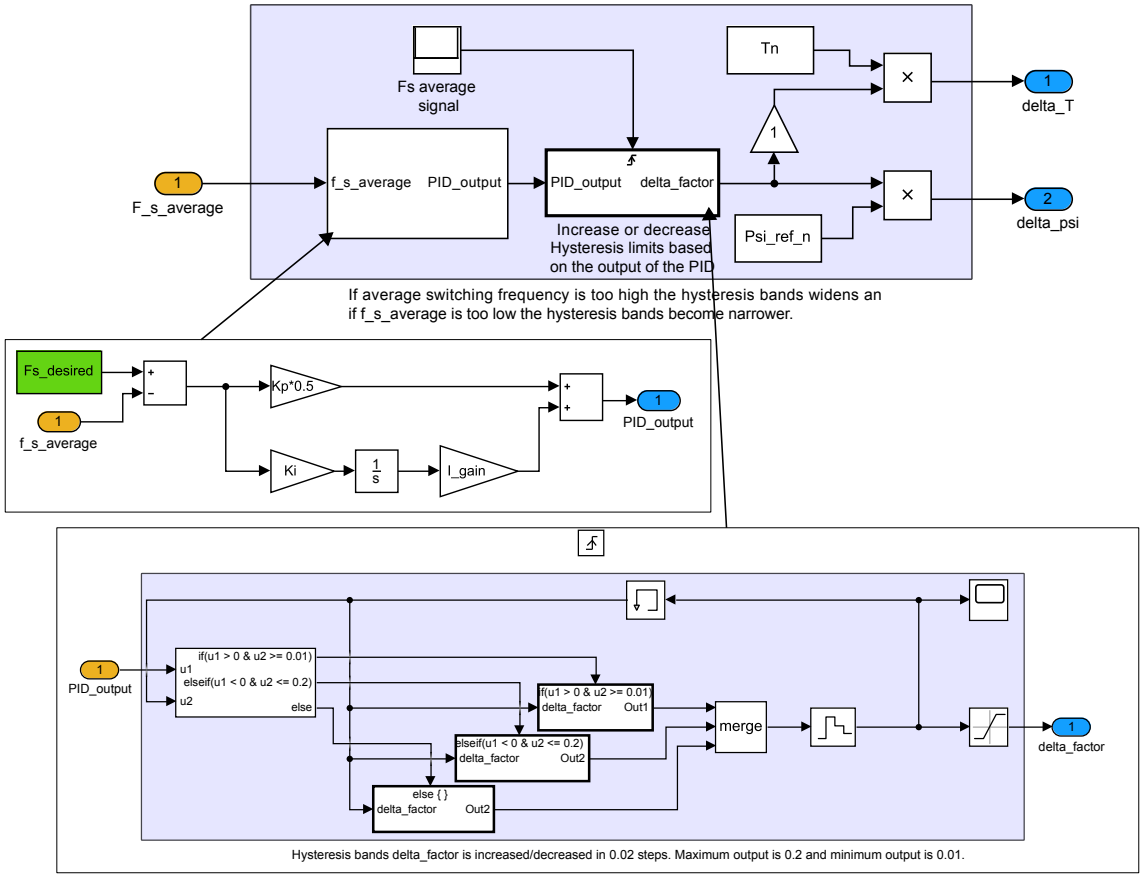

Figure C.10: Hysteresis limits controller subsystem controls the average switching frequency by changing the hysteresis band widths.

C.9 Speed controller feedforward loop

Speed controller feedforward loop increases the torque reference given by the speed PI-controller to ensure the speed reference is reached with different load conditions. Torque saturation limits subsystem creates saturation limits for the torque reference to ensure that the maximum output power stays in somewhat realistic levels and that the breakdown torque is not exceeded with higher speed references. Simulink implementations of these subsystems are shown in Fig. C.11.

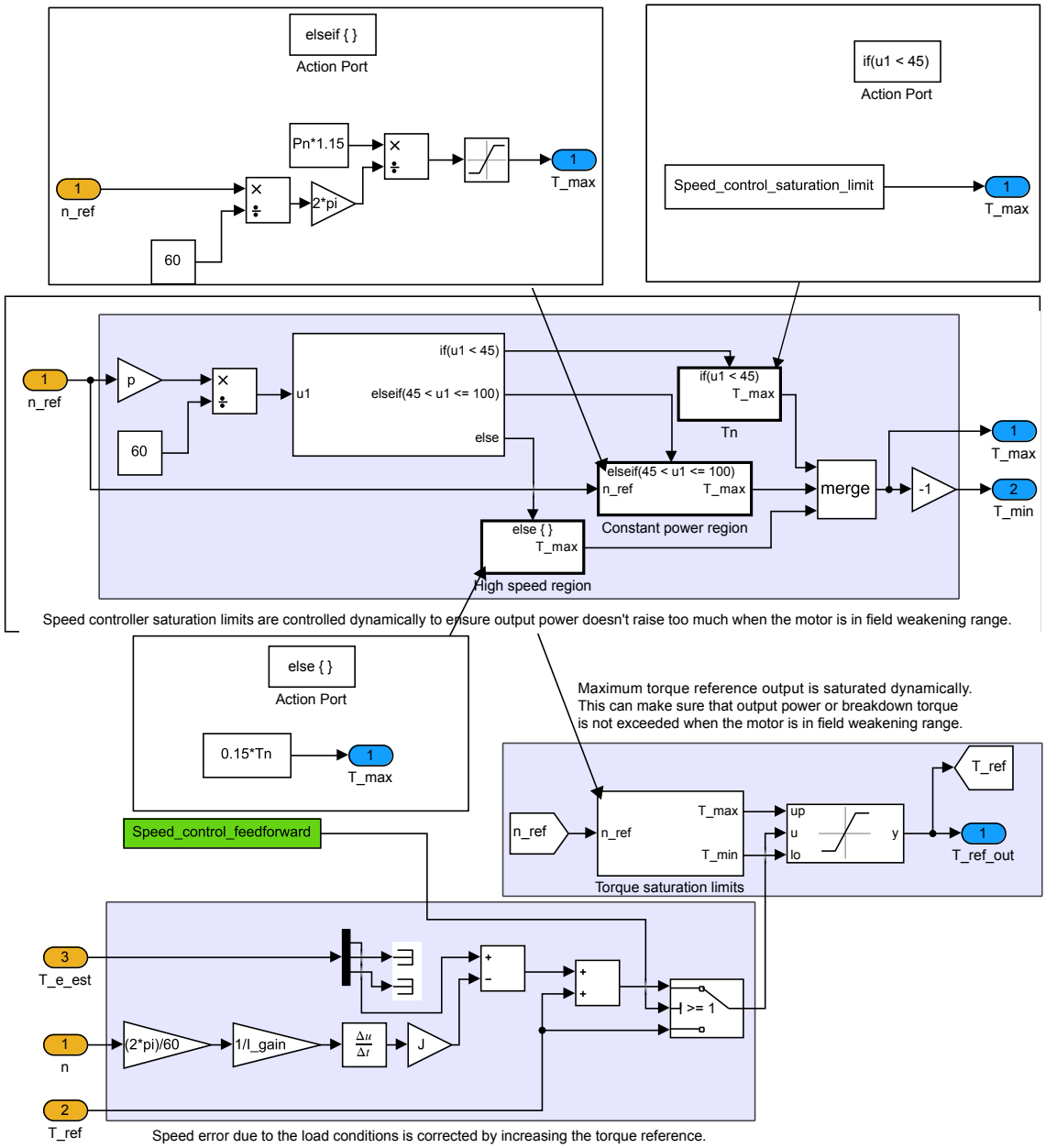

Figure C.11: Load estimation subsystem contains the speed controller feedforward loop and torque reference saturation limits.

D Appendix Reference signals

Simulink implementations of the stator flux linkage and speed reference signals are shown in following subsections.

D.1 Stator flux linkage reference

Stator flux linkage reference subsystem takes the speed reference as an input to create stator flux linkage reference for the stator flux linkage hysteresis controller inside the DTC model subsystem. If-else structure is used to keep the stator flux linkage reference at a constant value when the speed reference is below 45 Hz value. If the field weakening is enabled in the m-file the stator flux linkage reference starts to diminish above the 45 Hz speed. Simulink implementation is shown in Fig. D.1.

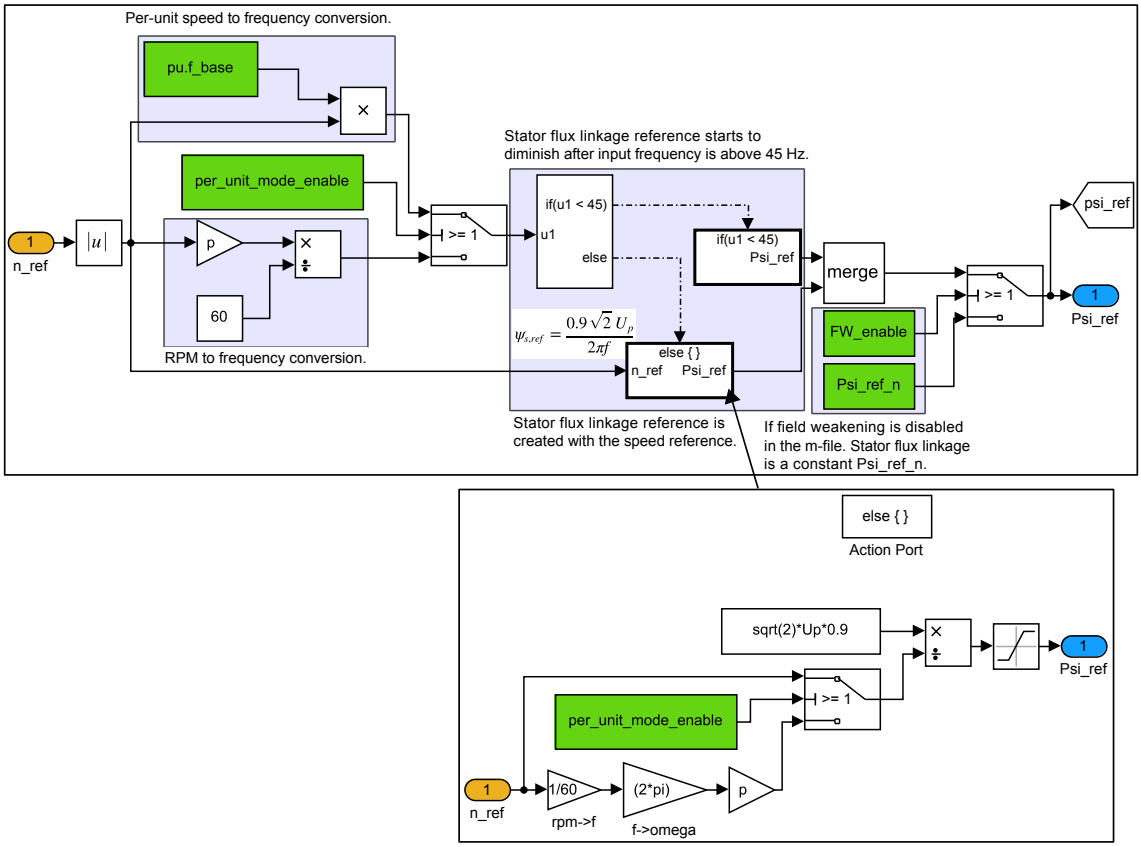

Figure D.1: Stator flux linkage reference subsystem.

D.2 Speed reference and controller

Speed reference is brought from the Matlab workspace with a step function. Else-if ladder creates ramp signal from the step function. With the speed reference ramp the stator flux linkage reference does not drop down abruptly when entering into field weakening region. Speed reference Simulink implementation is shown in Fig. D.2.

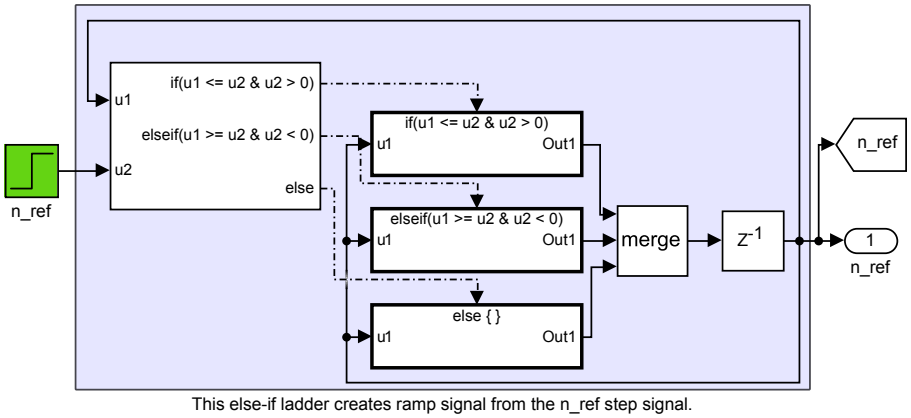

Figure D.2: Speed reference subsystem.

Speed controller takes the speed reference and measured speed from the motor model as inputs and outputs torque reference to the DTC model. Speed PI-controller is shown in Fig. D.3.

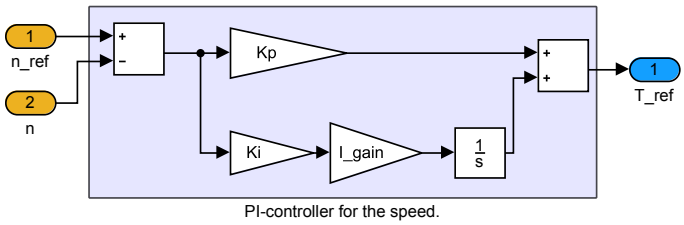

Figure D.3: Speed PI-controller subsystem.